
SNOWFALL IN THE ALPS:

EVALUATION AND PROJECTIONS BASED ON THE EURO-CORDEX REGIONAL
CLIMATE MODELS

MASTER THESIS

IN ATMOSPHERIC AND CLIMATE SCIENCES, ETH ZURICH

Author:

PRISCO FREI

Department of Earth Sciences,
ETH Zurich, Switzerland

Supervisors:

DR. SVEN KOTLARSKI

Federal Office of Meteorology and Climatology, MeteoSwiss, Switzerland

PROF. DR. CHRISTOPH SCHÄR

Institute for Atmospheric and Climate Sciences, ETH Zurich, Switzerland

DR. MARK LINIGER

Federal Office of Meteorology and Climatology, MeteoSwiss, Switzerland

2nd May 2016

Acknowledgements

My biggest thank you goes to Sven Kotlarski. Whenever problems arose, he immediately answered my questions and tried to solve the issues. He always assisted me in tackling my own ideas and tried to push me further by coming up with additional recommendations. Thank you Sven!

I would also like to thank Christoph Schär and Mark Liniger. Christoph made it possible to write this Thesis in his group. His wide expertise on global climate change and its impact on the hydrological water cycle was a very helpful asset to me. At our occasional meetings, he came up with additional explanations and propositions for further analyses without losing sight of my own objectives and ideas. Mark was extremely helpful and gave useful input when I was stuck or was struggling with the data interpretation. Thanks to both of you!

Special thanks go to to Christoph Marty from the Snow and Avalanche Research Institute (SLF) in Davos for the strong support during the setup of the thesis proposal in Spring 2015.

Furthermore I'm very grateful to Jan Rajczak and Elias Zubler in giving me advice regarding technical issues and data pre-processing, as well as Rob Spence and Jeff Welter for commenting language-related flaws in the thesis.

I also acknowledge the climate modelling groups of EURO-CORDEX for producing and making available their model output, as well as Urs Beyerle for keeping the data repository here at ETH up to date.

Last but not least, I'd like to give a special thanks to my friends and family who always supported me in good and in bad times. They always shared my fascination for weather and climate during my studies here at ETH.

Without all these people (and many more), I wouldn't be where I am today.

Abstract

Snow is an important resource for the Alpine region, be it for tourism, hydro power generation or water management. In addition, heavy snowfall events can lead to destructive effects, which range from avalanches and floods to road or rail damage. Future projections of snowfall are highly relevant for federal offices, re-insurances, forest management or for avalanche defence planning. However, global climate simulations at coarse resolution can only partly address this issue over the topographically complex Alpine domain. Therefore, we here exploit the most current set of high resolution regional climate model (RCM) scenarios for the European continent carried out within the EURO-CORDEX initiative at a spatial resolution of 12 km.

We both analyse direct snowfall output of the RCMs and investigate the possibility to derive snowfall amounts based on simulated temperature and total precipitation data only. In addition, a bias correction approach for model-derived snowfall is developed and scale effects on snowfall are quantified. The bias correction leads to a significant reduction in model spread and an appropriate reproduction of seasonal cycles in mean snowfall. However, snowfall indices directly related to snowfall frequency or intensity cannot be adjusted satisfactorily by applying this simple approach.

21st century snowfall scenarios for the Alps show a significant decrease of both mean and heavy snowfall amounts in most regions, in response to increasing temperatures which have a direct effect on snowfall frequency. For both emission scenarios, RCP4.5 and RCP8.5, spatial and vertical change patterns reveal similar distributions and differ only in their magnitude. Emission scenario uncertainties at the end of the 21st century are generally larger than model uncertainties. The analysis of bias-corrected and raw snowfall outputs shows, that relative change signals are not affected by the type of correction.

Domain mean snowfall reductions between September and May 2070 - 2099 for simulations carried out under RCP4.5 and RCP8.5, are as large as -25% and -45%, respectively. At mid elevations, changes of heavy snowfall are less pronounced than for mean snowfall. Snowfall increases in mid-winter are obtained for restricted high-elevation regions only where more intense, rather than more frequent, winter precipitation is able to (partly) offset the temperature effect. Our results indicate the general and physically consistent applicability of RCM output to assess future changes in mean and heavy Alpine snowfall.

Contents

| | | |
|----------|--|-----------|
| 1 | Introduction | 1 |
| 1.1 | Snowfall in the Alps | 1 |
| 1.2 | Climate models | 2 |
| 1.3 | Future snowfall changes: State of knowledge | 4 |
| 1.4 | Objectives | 6 |
| 2 | Data and methods | 7 |
| 2.1 | Observational data | 7 |
| 2.2 | Climate model data | 8 |
| 2.3 | Analysis domain and periods | 10 |
| 2.4 | Overview and workflow | 11 |
| 2.5 | Separating snowfall from total precipitation | 12 |
| 2.6 | Bias correction approach | 16 |
| 2.7 | Analysed snowfall indices and projected change signals | 17 |
| 3 | Grid coarsening effect on snowfall | 21 |
| 3.1 | Scale effect on mean snowfall | 21 |
| 3.2 | Scale effect on heavy snowfall | 22 |
| 3.3 | Discussion | 23 |
| 4 | Bias correction and evaluation | 25 |
| 4.1 | Analysis of adjustment factors | 26 |
| 4.2 | Evaluation of mean snowfall | 27 |
| 4.3 | Evaluation of heavy snowfall | 28 |
| 4.4 | Evaluation of further snowfall indices | 30 |
| 4.5 | Discussion | 32 |
| 5 | Snowfall projections for the late 21st century | 35 |
| 5.1 | Projected changes of mean snowfall | 35 |
| 5.2 | Projected changes of heavy snowfall | 38 |
| 5.3 | Projected changes of further snowfall indices | 41 |
| 5.4 | Scenario and snow fractionation uncertainty | 43 |
| 5.5 | Discussion | 48 |
| 6 | Simulated raw snowfall | 53 |
| 6.1 | Evaluation of simulated raw snowfall | 53 |
| 6.2 | Projections of simulated raw snowfall | 55 |
| 7 | Conclusions and Outlook | 57 |

| | |
|---|--------------|
| References | VII |
| Abbreviations | i |
| Acronyms | iii |
| Appendices | vii |
| A Additional information data and methods | vii |
| B Additional information grid coarsening | xi |
| C Additional information bias correction and evaluation | xii |
| D Additional information snowfall projections | xviii |
| E Additional information simulated raw snowfall | xxxvi |
| Declaration of originality | xxxix |

1 Introduction

1.1 Snowfall in the Alps

Snow is an important component of the climate system. Even small changes in its spatial distribution can heavily affect the surface energy budget or water cycle. With rising temperatures, a decline in snow cover is assumed to amplify regional warming at high latitudes through a positive albedo feedback¹(Vaughan et al., 2013).

In addition, snow is an important resource for the Alpine regions, be it for tourism, hydro power generation, or water management (Abegg et al., 2007). According to the Swiss Federal Office of Energy (SFOE), hydropower generation accounts for approximately 55% of domestic electricity production (SFOE, 2014). In the recent past, a substantial decrease of the mean snow cover and duration in the Alps was observed (e.g Laternser and Schneebeli (2003); Marty (2008); Scherrer et al. (2004)). Between the late 19th and early 21st century, the (annual mean) temperature rose by 2 °C (Voigt et al., 2010). This is twice as much as the average warming of the Northern Hemisphere. In Switzerland, tourism is the third most important export industry with approximately 300'000 employees working full time in this sector. For people living in rural, Alpine regions, it is often by far the most essential income source (Koenig and Abegg, 1997). With rising temperatures and the shift of the snowline towards higher altitudes (Steger et al., 2013), these destinations are coming under strong financial pressure. Especially at lower elevations, the winter season will become shorter, resulting in the need for more investment in artificial snow making to keep ski areas running in a competitive way (Elsasser and Messerli, 2001).

Projected temperature increases will also have an impact on the form of winter precipitation. Even though the snowfall fraction (ratio between solid and total precipitation) is expected to decrease at lower elevations during the 21st century (Serquet et al., 2013), an extraordinary snowfall event can still leave a trail of destruction. The catastrophic effects of heavy snowfalls range from avalanches and floods to road or rail damage. In some extreme cases these events can even result in the collapse of buildings or loss of human life (Marty and Blanchet, 2011). One of the biggest devastations in recent years occurred in 1999. In literature, this winter is often referred to as the "avalanche winter 1999". Between the end of January and the end of February, three successive heavy precipitation events plunged large parts of the Alps into chaos. Within 30 days, fresh snow depths of up to 500 cm were measured along the northern part of the Swiss Alps. The WSL Institute for Snow and Avalanche Research (SLF) in Davos counted 1500 destructive avalanches² - 8.6% of them

¹According to its high albedo of approximately 0.8, snow reflects much more short wave radiation than its underlying surface (with lower albedo values) would do.

²According to Ammann (2013) the term "destructive avalanche" is used if an avalanche endangers people, real estate or transport routes.

affecting transport routes - over the entire winter period (Wiesinger and Adams, 2007). In Switzerland alone, seventeen people lost their lives because of these extreme events and the financial costs totalled to more than 600 million Swiss Francs (SLF, 2000).

The Swiss Federal Office of Meteorology and Climatology (MeteoSwiss) is actually making use of an early warning system for heavy snowfall in the Alps, in order to be better prepared for such worst case scenarios (Haechler and Gerstgrasser, 2009). However, as for every other extreme event, a short range forecast is very difficult. The assessment of future long-term evolutions of heavy snowfall events in the Alps is even more challenging. Climate projections for the full century mostly depend on climate models which are subject to inaccuracies, uncertainties and restrictions in their spatial resolution.

1.2 Climate models

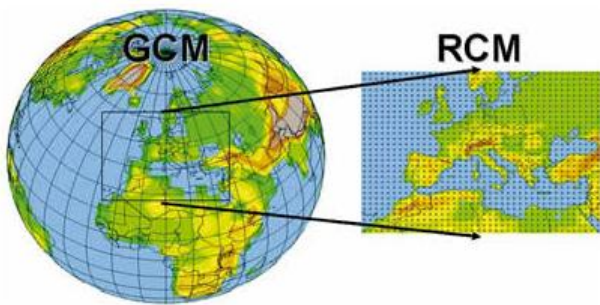


Fig. 1.1: The GCM (left) covers the entire globe whereas the RCM is applied over a limited area only (here: European continent) with a higher resolution (Giorgi, 2006).

Future projections of 21st century climate typically rely on climate models. For large-scale projections, global climate models (GCMs), with a rather coarse spatial resolution of approximately 100 km or more, are used. If one is interested in regional-scale impacts, where a much higher spatial resolution is preferred, a GCM can be dynamically downscaled by nesting a regional climate model (RCM) over the specific domain of interest (Giorgi, 1990). In such a setup, the GCM provides the lateral boundary conditions to the RCM (Fig. 1.1). One advantage of climate models is the ability to estimate climate change under different greenhouse gas (GHG) emission scenarios (e.g., the SRES scenarios; IPCC (2000)). With the Intergovernmental Panel on Climate Change's (IPCC) release of the Fifth Assessment Report (AR5; IPCC (2013)), the representative concentration pathway (RCP) scenarios have been introduced, replacing the former SRES scenarios (Moss et al., 2010). The new scenarios specify GHG concentrations and corresponding emissions for several different pathways. To sample and quantify inherent uncertainties, often a whole ensemble of experiments, employing different models, are analysed. Conclusions can then be drawn on the mean or median of the corresponding model ensemble as well as on its spread. By making use of future projections based on climate models, one should always be aware of their uncertainties. A detailed investigation of possible error sources is well beyond the scope of this thesis. Thus, for more information one should refer to existing literature such as Gobiet et al. (2014), Hawkins and Sutton (2009), Rummukainen (2010) or Soncini and Bocchiola (2011).

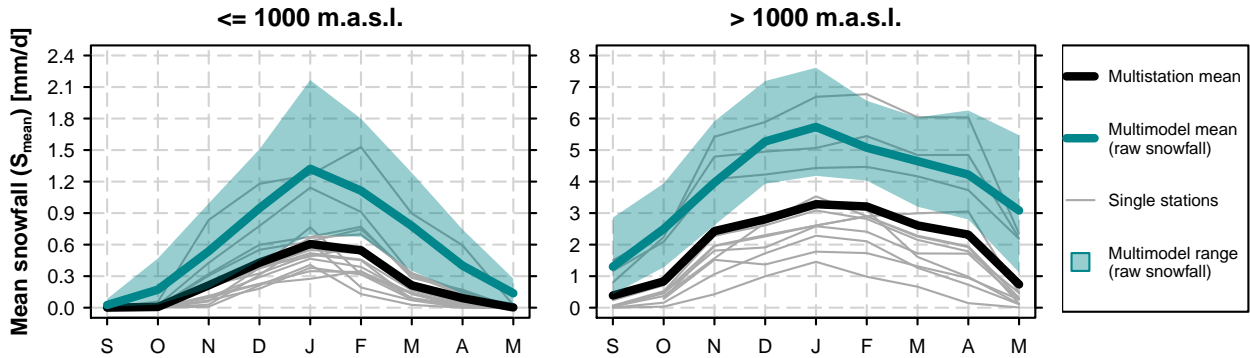


Fig. 1.2: Seasonal cycles (September to May) of mean snowfall in Switzerland in the period 1971 - 2005. The turquoise line represents the multimodel mean for a subset of six GCM-driven RCM simulations (see Ch. 6) spatially averaged over the corresponding elevation interval. The grey lines show the seasonal cycle of snowfall measurements as derived from daily new snow sums at individual Swiss stations (see Tab. A.1) whereas the black line denotes the mean snowfall over all stations in the corresponding elevation interval below 1000 m.a.s.l. (left panel) and above 1000 m.a.s.l. (right panel). Primary station measurements were converted from centimetres per day (cm/d) to millimetres snow water equivalent per day (mm SWE/d) by assuming a ratio of 10:1, i.e., a mean snow density of 100 kg/m^3 .

Apart from the standard variables, for example temperature and total precipitation, some (but not all) RCMs also provide special variables such as snowfall flux, i.e., the amount of solid precipitation reaching the surface. Figure 1.2 indicates that, despite having an offset, RCMs are able to reproduce the seasonal (September to May) cycle of mean snowfall over the Swiss domain and its elevation dependency reasonably well. At elevations both below and above 1000 m.a.s.l., the multimodel mean, based on a subset of six EURO-CORDEX simulations (see Sec. 2.2 and Ch. 6), is generally higher than for single station measurements. For the period 1971 - 2005, a set of 29 stations of MeteoSwiss with a data availability of more than 80% were used. To allow a comparison against raw model output, the new snow sum, measured in cm, has been converted to mm snow water equivalent (mm SWE, always noted mm hereafter), by assuming a ratio of 10:1 (1 cm snow = 1 mm SWE, i.e., a snow density of 100 kg/m^3). More information about the geographical distribution

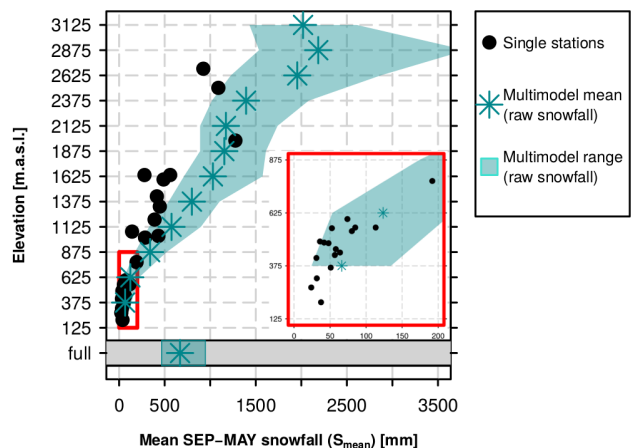


Fig. 1.3: Seasonal (September to May) mean snowfall in the period 1971 - 2005 vs. elevation for the Swiss domain. Same data sets as in Fig. 1.2. Black circles represent mean September to May snowfall at specific Swiss stations. The turquoise asterisks (shading) show the multimodel mean (multimodel range) of six GCM-driven RCMs. The simulation data is based on the spatio-temporal mean of 250 m elevation ranges and plotted at the mean height of the corresponding interval.

of the stations is given in Table A.1. Comparing the observed mean September to May snowfall with simulations at 250 m elevation intervals emphasises our findings (Fig. 1.3). RCMs generally tend to overestimate solid precipitation, especially at mid-range altitudes. Given these preliminary results, we conclude that raw model results can be used for future projections. However, a bias correction might be necessary to get more robust results.

1.3 Future snowfall changes: State of knowledge

Within the last few years several studies investigated the future evolution of mean, heavy and extreme snowfall events. O’Gorman (2014) analysed the northern hemispheric changes of mean and extreme snowfall by the end of this century using 20 GCMs. Corresponding results show stronger signs of change in mean than in extreme snowfall. This can be explained by the fact that snowfall extremes usually occur near a fixed optimal temperature, which appears to be insensitive to climate warming. Because of the low spatial GCM resolution, O’Gorman (2014) mainly focused on elevations below 1000 m.a.s.l. and no conclusions about the Alpine region were drawn. A more local study for the Western United States was carried out by Lute et al. (2015). As in O’Gorman (2014), they estimated changes in snowfall extremes based on GCMs. Climatologically cooler locations, e.g. in the Rocky Mountains, appear to experience an increase in snowfall extremes whereas at warmer stations, the magnitudes tend to decrease. Nevertheless, for both warm and cold stations, a larger fraction of annual SWE from snowfall extremes is projected. Piazza et al. (2014) discuss projections for 21st century snowfall changes over the French Alps. They compare two different methods: 1) Statistical downscaling of GCMs and 2) Dynamical downscaling, i.e., RCM scenarios used in the ENSEMBLES project (Van der Linden and Mitchell, 2009). For both approaches, large changes - with winter snowfall decreases of about -25% - are expected by the mid of this century. The projections were established under the A1B greenhouse scenario, which describes a future world of very rapid economic growth, a global population that peaks in mid-century and declines thereafter (IPCC, 2000).

Regarding the present thesis, a further relevant study was written by de Vries et al. (2014). For the first time, the newest generation of GCMs and RCMs, as also applied in the EURO-CORDEX framework (see Sec. 2.2), was used to assess future snowfall extremes. One RCM, KNMI-RACMO2, was driven with different GCM simulations, resulting in an eight-member ensemble. For large parts of the Western and Central European continent, decreases of snowfall intensities are projected. Locally they might be as large as -30% per degree of warming. This is in strong contrast to future trends of total winter precipitation intensities which tend to increase for locations north of about 45 °N (Jacob et al., 2013). For the Alps, a qualitative, general intensification of winter precipitation, due to an increase in extreme events rather than a frequency change, is supported by robust RCM results (e.g. Deller (2015); Rajczak et al. (2013)). The results of Rajczak et al. (2013) are based on RCM ensembles from the

former ENSEMBLES project while the latter used a similar set of EURO-CORDEX simulations as those used in this work. Despite reductions of snowfall extremes for most of Europe, the analysis of de Vries et al. (2014) expects an increasing trend for high-elevation regions in the Alps, with changes of about +10% per degree of warming under an RCP8.5 scenario. A possible explanation might be, that with global warming, temperatures at high-elevation sites start approaching the freezing point, thus, sliding more and more towards the ideal extreme snowfall condition range (O’Gorman, 2014). However, one needs to keep in mind that the results of de Vries et al. (2014) are only based on one individual RCM experiment. When they did the same analysis with another driving GCM, they found that Alpine trends were not statistically significant.

In summary, the recent focus was mainly based on mean snowfall projections rather than heavy and extreme snowfall changes which are predominantly related to small scale flow settings (Plaut et al., 2001). GCMs and RCMs running at low spatial resolution are not able to resolve such heavy and extreme events over regions with strong topography, e.g. the Alps. New generations of high resolution RCMs are a first step toward an improvement on this issue. This is necessary because an accurate estimation of future extreme events is in high demand for federal offices, re-insurances, forest management, avalanche defence planning etc. To assess and prevent related socio-economic impacts and costs, robust results are essential. The de Vries et al. (2014) study presents the first highly resolved trend estimates for extreme snowfall events in the Alpine region. To get more convincing results, however, an evaluation of several RCMs is still required.

1.4 Objectives

By analysing observational-based data and a set of 14 GCM-driven RCM simulations of the EURO-CORDEX initiative (see Sec. 2.1 and 2.2), this study aims to achieve the following three main objectives:

1. Snowfall separation and scale effect

Due to the non-availability of snowfall flux for all simulations, an adequate derivation of snowfall based on daily temperature and precipitation data is crucial for evaluating the RCM performance and estimating future changes. As the observation and simulation variables are not available on the same horizontal resolution, the scale effect on snowfall will be quantified as well.

2. Employment of a bias correction approach and comparison of observation-based and simulated snowfall indices

To remove systematic model biases in temperature and precipitation, a model bias correction will be employed. Then, different snowfall indices in the bias-corrected output will be compared against observational estimates.

3. Projections of different snowfall indices for the late 21st century

Change signals for various snowfall indices over the Alpine domain, derived by a comparison of 30-year control and scenario periods, will be analysed under the assumption of the two representative concentration pathways RCP4.5 and RCP8.5. Furthermore, we will assess the scenario and snow fractionation uncertainty in detail.

2 Data and methods

2.1 Observational data

The observation-based snowfall is derived from two gridded data sets provided by MeteoSwiss. Both the precipitation (RhiresD) and temperature (TabsD) data sets are available on a daily basis, with a horizontal resolution of 2 km for the entire Swiss domain.

RhiresD was interpolated by incorporating a high-resolution rain-gauge network of approximately 420 MeteoSwiss stations (MeteoSwiss, 2013a). Only quality-checked measurements for a particular day were considered. Nevertheless, the accuracy depends on several factors, such as the preciseness of underlying rain-gauge measurements or the interpolation technique itself. Precipitation undercatch, especially during episodes with strong winds or snowfall, is a widely known issue. The systematic error for such events during winter might be as high as 40% (e.g. Neff (1977); Sevruk (1985); Yang et al. (1999)). The high density network has a balanced distribution in the horizontal direction, but high altitudes are significantly under-represented (Frei and Schär (1998); Isotta et al. (2014); Konzelmann et al. (2007)). Despite the data set's resolution of 2 km, the effective grid resolution, i.e., the mean inter-station distance, is about 15 - 20 km and thus comparable to the available climate model data (see Sec. 2.2). Due to measurement uncertainties, daily precipitation values smaller than or equal to 0.1 mm were set to zero within the present study.

TabsD utilises a set of approximately 90 homogeneous long-term station series (MeteoSwiss, 2013b). All measurements were taken 2 meters above ground, according to the standards of the World Meteorological Organisation (WMO). Errors might be introduced by unresolved scales and interpolation uncertainty (Frei, 2014). Small-scale effects on the temperature distribution are not accounted for in this analysis. Thus, the unresolved effects of land cover or local topography probably lead to an underestimation of spatial variability. An analysis of the interpolation accuracy, calculated by a leave-one-out cross-validation, quantified the standard error (SE) to be highest during winter. Over the Alps, deviations might be as high as 1.7 °C. Another problem arises in inner Alpine valleys, where cold air pool environments are systematically overestimated (SE = 4 °C).

2.2 Climate model data

One of the World Climate Research Program's (WCRP) main targets is to produce improved regional climate change projections. The initiative, which operates under the name of Coordinated Regional Downscaling Experiment (CORDEX), intends to cover all land regions world-wide. For this purpose EURO-CORDEX - the European branch - provides experiments at both 50 km (EUR-44) and 12.5 km (EUR-11) resolution on a European domain (Kotlarski et al., 2014). For evaluating the model performance, most RCMs employed, carried out both a hindcast (reanalysis driven) and a control (GCM driven) run for the recent past (Jacob et al., 2013).

Future projections are based on the new RCP scenarios defined for the AR5 of the IPCC. These scenarios describe different anthropogenic radiative forcings at the end of the 21st century. For instance, the most frequently used pathways within the EURO-CORDEX framework, namely RCP4.5 and RCP8.5, assume forcing increases of about 4.5 Wm^{-2} and 8.5 Wm^{-2} , respectively, by 2100 (Cubasch et al. (2013); Collins et al. (2013)).

Within this project, we focus on all available EUR-11 simulations for which control, RCP4.5 and RCP8.5 runs are available within our periods of interest (see Sec. 2.3). Hence, a total set of 14 simulations, combining five driving GCMs with six different RCMs, has been selected. The experiments were carried out at different European institutes (Tab.2.1).

Each of the six RCMs uses its own individual topography field for its simulation. Model topographies might therefore considerably differ from each other, and also from the observation-based orography (Fig. A.2). Hence, it is not meaningful to compare single grid-point snowfall values since they might be situated at completely different elevations. Therefore, most analyses of the present work were carried out by averaging over distinct elevation intervals, i.e., results for a given (model or RCM) data set are interpreted with respect to the respective data set's orography.

Tab. 2.1: Available RCM simulation chains of this study

Table showing the 14 EURO-CORDEX simulations available for this study. The whole model set consists of six RCMs driven by five different GCMs which were carried out at six institutions (Institute ID). All experiments were realized on a grid, covering the European domain, with a horizontal resolution of approximately 12.5 km (EUR-11) and are available for control, RCP4.5 and RCP8.5 within the considered time periods of interest.

| RCM | GCM | Acronym | Institute ID |
|------------|-----------------------|-------------------|--|
| ALADIN53 | CNRM-CERFACS-CNRM-CM5 | CNRM - ALADIN | CNRM ^a |
| CCLM4-8-17 | CNRM-CERFACS-CNRM-CM5 | CNRM - CCLM | CLMcom ^b |
| CCLM4-8-17 | ICHEC-EC-EARTH | EC-EARTH - CCLM | CLMcom |
| CCLM4-8-17 | MOHC-HadGEM2-ES | HadGEM2 - CCLM | CLMcom |
| CCLM4-8-17 | MPI-M-MPI-ESM-LR | MPI-ESM - CCLM | CLMcom |
| HIRHAM5 | ICHEC-EC-EARTH | EC-EARTH - HIRHAM | DMI ^c |
| RACMO22E | ICHEC-EC-EARTH | EC-EARTH - RACMO | KNMI ^d |
| RACMO22E | MOHC-HadGEM2-ES | HadGEM2 - RACMO | KNMI |
| RCA4 | CNRM-CERFACS-CNRM-CM5 | CNRM RCA | SMHI ^e |
| RCA4 | ICHEC-EC-EARTH | EC-EARTH - RCA | SMHI |
| RCA4 | IPSL-IPSL-CM5A-MR | IPSL - RCA | SMHI |
| RCA4 | MOHC-HadGEM2-ES | HadGEM2 - RCA | SMHI |
| RCA4 | MPI-M-MPI-ESM-LR | MPI-ESM - RCA | SMHI |
| WRF331F | IPSL-IPSL-CM5A-MR | IPSL - WRF | INERIS ^f , IPSL ^g |

^aCentre National de Recherches Météorologiques France

^bClimate Limited area Modelling community, here: btu Brandenburg University of Technology (CNRM, EC-EARTH and MPI-ESM forcing) and ETH Zurich (HadGEM2 forcing).

^cDanish Meteorological Institute

^dRoyal Netherlands Meteorological Insitute

^eSwedish Meteorological and Hydrological Institute

^fInstitute National de l'Environnement industriel et des Risques, France

^gLaboratoire des Sciences du Climate et de l'Environnement

2.3 Analysis domain and periods

2.3.1 The Alpine domain

The arc-shaped European Alps, with a length of roughly 1200 km stretching from Nice to Vienna, are home to more than 15 million people. With a total area of 190,000 km², it is the highest and most extensive mountain range which is situated entirely in Europe. The river Rhine divides the mountain chain in two parts. The higher Western Alps span the area from South-Eastern France up to Western Switzerland. The Eastern Alps cover Eastern Switzerland and parts of Italy, Germany, Liechtenstein, Austria and Slovenia (Agrawala, 2007). For this project, two different analysis domains were used: The investigation of the

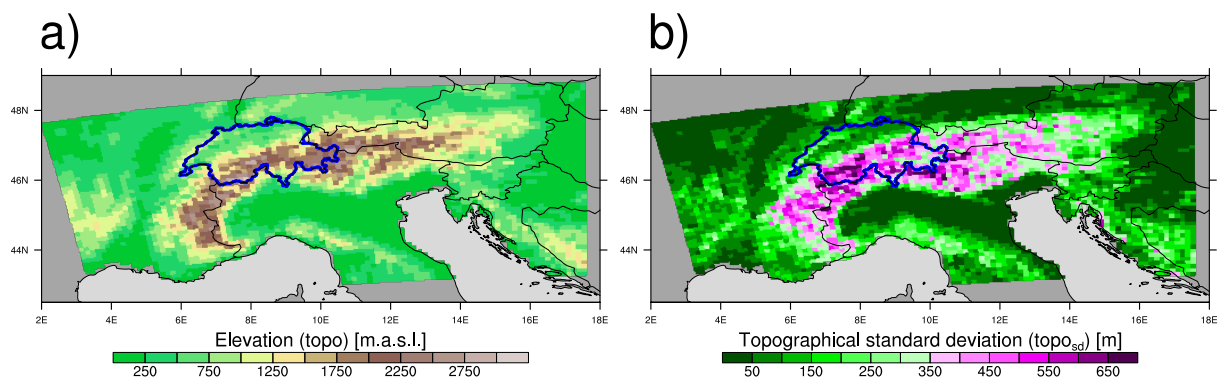


Fig. 2.1: **a)** Topography (topo) of analysed domain. **b)** Topographical standard deviation (topo_{sd}) of analysed domain. The topo_{sd} strongly depends on the horizontal resolution of the final coarse grid as well as the underlying subgrid data (see Eq. 2.8). The blue outline marks the domain used for the grid coarsening and bias correction analysis (see Ch. 3 and 4) as well as the evaluation of simulated raw snowfall (see Sec. 6.1). The coloured domain is used for the assessment of snowfall projections (see Ch. 5 and Sec. 6.2).

scale effect on snowfall (see Ch. 3) and the evaluation of the bias correction approach (see Ch. 4) and simulated raw snowfall (see Sec. 6.1), respectively, depend on the observational data provided by MeteoSwiss (see Sec. 2.1). As these cover just a fraction of the entire Alpine area, this part of the study was constrained to the Swiss domain (Fig. 2.1 a), blue outline). For projected changes of different snowfall indices (see Ch. 5 and Sec. 6.2), the domain was widened to an area including the entire Alpine crest with its forelands (Fig. 2.1 a), colored domain). The area, including large parts of South-Eastern France, Northern Italy and Austria, enables a suitable comparison to results from a previous Master Thesis written by Deller (2015). In his project, Deller focused on the analysis of extreme precipitation projections based on a similar set of EURO-CORDEX simulations as those used here.

2.3.2 Analysed time periods and seasons

Throughout chapters 3 to 6, different time periods and seasons will be taken into account. For analysing the effect of the grid resolution on snowfall (see Ch. 3), all days in the period 1971 - 2005 were considered. The assessment of the bias correction approach is based on the evaluation period (EVAL) 1971 - 2005 (see Ch. 4 and Sec. 6.1). To estimate future changes of different snowfall indices (see Ch. 5 and Sec. 6.2), two 30-year periods were defined: The control period (CTRL) is equal to the current climate normal period 1981 - 2010 whereas the scenario period (SCEN) covers the last three decades of the 21st century from 2070 - 2099. For the EVAL, CTRL and SCEN periods, the summer months June, July and August (JJA) are left out from any statistical analysis while these months are included in the grid coarsening analysis (see Ch. 3). In addition to mean snowfall conditions during the 9 month period from September to May, we also analyse the seasonal cycle at monthly resolution.

2.4 Overview and workflow

Figure 2.2 presents a schematic overview on this study's workflow. More details are provided in the following chapters. A complete overview of all analysed data sets within this thesis is given in Figure A.1. In a first step (grey; see Ch. 3 and 4), observation-based and simulated daily temperature and precipitation fields over Switzerland are employed to develop a temperature-based procedure that separates snowfall from total precipitation and to bias-correct the simulated and separated snowfall amounts. The developed separation and bias correction procedure accounts for subgrid variability of the snowfall fraction and is then used to separate and bias-correct RCM-based snowfall amounts for both the CTRL and the SCEN period for each individual RCM (red; see Ch. 5). Based on this product, our primary estimate for 21st century changes of different snowfall indices over the entire Alps is derived. Afterwards also the raw RCM snowfall output, which is only available for a subset of the EURO-CORDEX ensemble, is analysed with respect to 21st century changes of the same snowfall indices (turquoise; see Ch. 6). Both approaches to derive snowfall projections are finally compared to each other.

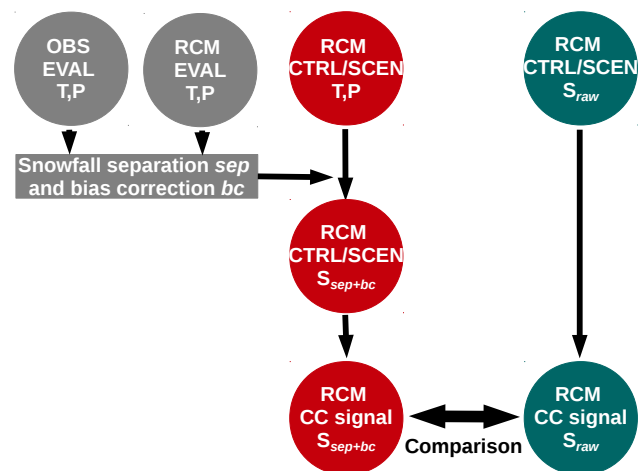


Fig. 2.2: Schematic overview on the study's workflow. From left to right: Snowfall separation and bias correction (grey; see Ch. 3 and 4); analysis of separated and bias-corrected snowfall climate change signals (red; see Ch. 5); analysis of raw RCM snowfall climate change signals (turquoise; see Ch. 6). OBS: observation-based data; RCM: RCM-based data; EVAL/CTRL/SCEN: the analysis periods introduced in Section 2.3; T: temperature; P: precipitation; S: snowfall; CC signal: climate change signal.

2.5 Separating snowfall from total precipitation

There are some advantages in separating snowfall from total precipitation through temperature rather than taking the simulated raw snowfall output from the models. First of all, not all models provide snowfall as an output variable, i.e., we would be left with a smaller set of simulations. On the other hand, due to the temperature dependency of snowfall occurrence, snowfall biases of a given climate model cannot be expected to remain the same under current and future climate conditions. For instance, a climate model with a given temperature bias might pass the snow-rain temperature threshold earlier or later than reality during the general warming process. Hence, traditional bias correction approaches based only on snowfall amounts would possibly fail due to a non-stationary bias structure.

By using daily temperature and total precipitation rather than real measured snowfall amounts, the temperature at which the transition from solid to liquid precipitation occurs (snow fractionation temperature hereafter) must be determined. The simplest approach is to fractionate the two phases binarily by applying a snow fractionation temperature threshold. In literature, different values between 0 - 2.5 °C are commonly used (e.g. de Vries et al. (2014); Schmucki et al. (2015); Zubler et al. (2015)). More sophisticated methods estimate the snow fraction (sf) dependence on temperature with the help of linear or logistic curves (e.g. Kienzle (2008); McAfee et al. (2014)).

In our case, the different horizontal resolutions of the observational (high resolution, 2 km) and simulation (coarse resolution, 12.5 km) data sets also impede a proper comparison of the snowfall outputs and the physical consistency between variables. Thus, we analyse the snowfall amount dependency on the grid resolution and exploit possibilities for including subgrid-scale variability in analyses based on coarse grid information. This approach is important as especially in Alpine terrain, a strong subgrid variability of near-surface temperatures due to orographic variability has to be expected, with corresponding effects on the subgrid snowfall fraction.

2.5.1 Determination of snowfall based on information from a high resolution grid

To analyse the grid coarsening effect on snowfall, a reference dataset (obtained by the so called Subgrid method; see below) was introduced. The daily snowfall at each high resolution grid point was derived by applying the same snow fractionation temperature (T^*) of 2 °C as in Zubler et al. (2015). Whenever the daily mean temperature (T') was lower as or equal to the snow fractionation temperature, i.e., $T' \leq T^*$, the whole daily precipitation amount (P') was accounted for as snow (S'). For days with $T' > T^*$, the daily snowfall amount was set to zero and P' was attributed as rain.

The coarse-grid reference snowfall amount (S_{SG}) was determined by summing up the separated daily high resolution snowfall amount S' at each grid point (i) which will account for the new coarse grid point (k):

$$S_{SG}(k) = \frac{1}{n} \cdot \sum_{i_k=1}^n P'(i_k)[T'(i_k) \leq T^*] = \frac{1}{n} \cdot \sum_{i_k=1}^n S'(i_k) \quad (2.1)$$

Total precipitation and daily mean temperature for each coarse grid box (P , resp. T) were estimated by a simple conservative regridding method:

$$P(k) = \frac{1}{n} \cdot \sum_{i_k=1}^n P'(i_k) \quad (2.2)$$

$$T(k) = \frac{1}{n} \cdot \sum_{i_k=1}^n T'(i_k) \quad (2.3)$$

The whole calculation was made under the assumption, that all high resolution grid cells have the same surface area. Last but not least, the reference snowfall fraction (sf_{SG}) was calculated by dividing Equations 2.1 and 2.2 :

$$sf_{SG}(k) = S_{SG}(k)/P(k) \quad (2.4)$$

2.5.2 Determination of snowfall based on information from a low resolution grid

For data sets with a coarse resolution such as the RCM simulations of the EURO-CORDEX initiative, three different snow fractionation methods were employed to separate the snowfall amount. In Chapter 3 they will be compared against the Subgrid method. For all coarse grid methods, total precipitation and temperature are exactly the same as for the reference method (see Eq. 2.2 and 2.3).

Binary method

The easiest approach would be to implement the so called Binary method. The snowfall fraction (sf_{BI}) is simply derived by applying the same constant snow fractionation temperature as for the high resolution grid on the coarse grid variables:

$$sf_{BI}(k) = \begin{cases} 1 & \text{if } T(k) \leq T^* = 2^\circ C \\ 0 & \text{if } T(k) > T^* = 2^\circ C \end{cases} \quad (2.5)$$

Multiplying it by the total precipitation leads to the snowfall amount S_{BI} :

$$S_{BI}(k) = sf_{BI}(k) \cdot P(k) \quad (2.6)$$

The Binary method results in a sharp transition between rain and snow at 2 °C, which is only a very rough approximation of the actual snowfall - temperature relationship.

Slope method

To overcome the drawback of having an abrupt change from 100% snowfall to 100% rainfall, the Slope method was developed. This scheme accounts for a linear (subgrid-based) snow fraction dependence on temperature. For each grid point, the relationship between daily temperature and subgrid snow fraction has been derived by the following linear regression:

$$sf_{SG}(k) = intercept(k) + slope(k) \cdot T(k) \quad (2.7)$$

In a second step, The slope parameters of all individual grid points were found to be expressible by a global function which depends only on the topographical standard deviation ($topo_{sd}$) of the coarse grid point, k :

$$topo_{sd}(k) = \sqrt{\frac{(\sum_{i_k}^n topo(i_k) - \overline{topo}(k))^2}{n - 1}} \quad (2.8)$$

$$slope(k) = A \cdot topo_{sd}(k)^B = -15.093 \cdot topo_{sd}(k)^{-0.822} \quad (2.9)$$

The $topo_{sd}$ is a measure for the uniformity of the underlying topography. Small values indicate a low subgrid topographic variability. A good example is the Swiss plateau (see Fig. 2.1 b). High values result from non-uniform elevation distributions. In the Canton of Valais for instance, a fractional part of a coarse grid box might be at the valley floor whereas the other part contains mountainous regions.

The two parameters A and B of Equation 2.9 were determined with the R function "nls" which iteratively reduces the non-linear least-squares.

By placing the grid point-dependent slopes at a fixed point, with $T = T^* = 2$ °C; $sf = 0.5$ in the temperature - snow fraction system, the snow fraction (sf_{SL}) for each day and coarse grid point could be parametrized as a function of $T(k)$ and $slope(k)$:

$$sf_{SL}(k) = 0.5 - slope(k) \cdot (\underbrace{2 \text{ } ^\circ\text{C}}_{=T^*} - T(k)) \quad (2.10)$$

Finally, the daily snowfall amount (S_{SL}) for each coarse grid box was inferred by considering the following constraints:

$$S_{SL}(k) = \begin{cases} 0 & \text{if } sf_{SL}(k) \leq 0 \\ sf_{SL}(k) \cdot P(k) & \text{if } 0 < sf_{SL}(k) < 1 \\ P(k) & \text{if } sf_{SL}(k) \geq 1 \end{cases} \quad (2.11)$$

Richards method

A short pre-analysis of the relationship between snow fraction and temperature in the Sub-grid method led to the indication that for temperatures close to the freezing point, the snow fractions might be overestimated by the Binary method and underestimated by the Slope method, respectively (Fig. B.1). To prevent this, especially regarding extreme snowfall events which often occur in the aforementioned temperature interval, a third snowfall fractionation method has been introduced.

The Richards method (Richards, 1959) is a type of logistic regression which accounts for asymmetry of the curve¹. The snow fraction (sf_{RI}) has been calculated by using the following formula:

$$sf_{RI}(k) = 1 / [(1 + C(k) \cdot \exp(D(k) \cdot (T(k) - \underbrace{2^\circ C}_{=T^*}))^{1/C(k)}] \quad (2.12)$$

with C as the point of inflexion and the growth rate D. First, the two parameters C and D were fitted locally for each grid point separately. In an additional procedure, C and D were turned into global parameters by expressing them as a function of $topo_{sd}$, i.e., we again used the "nls" function for the curve fitting approach. For the point of inflexion the Equation reads:

$$C(k) = 1 / (E + topo_{sd}(k) \cdot F) = 1 / (1.1477 + topo_{sd}(k) \cdot -0.000968) \quad (2.13)$$

The growth rate D has the same form as the slope parameter of the Slope method (see Eq. 2.9) but with different values for A and B, denoted G and H:

$$D(K) = G \cdot topo_{sd}(k)^H = 143.89 \cdot topo_{sd}(k)^{-0.877} \quad (2.14)$$

The snowfall amount (S_{RI}) was again obtained by multiplying the snow fraction with the total precipitation:

$$S_{RI}(k) = sf_{RI}(k) \cdot P(k) \quad (2.15)$$

¹In contrast to general logistic curves which are symmetrical about the point of inflexion, this type deals with situations where the growth curve is asymmetrical

A schematic illustration of the snow fraction dependence on temperature is shown in Figure 2.3. On the left side, the curves of the Binary, Slope and Richards snow fractionation methods are plotted for a coarse grid box with a topo_{sd} of 50 m. The snow fraction distributions appear to be pretty similar. For boxes having a more complex topography ,i.e., higher topo_{sd} (Fig. 2.3, right panel), the differences among the three coarse grid snow fractionation methods become clearly visible. Here, daily mean temperatures close to the freezing point lead to a snow fraction of 100% for the Binary method, however, the Slope and Richards methods would account for just 60% - 70% of total precipitation as snow.

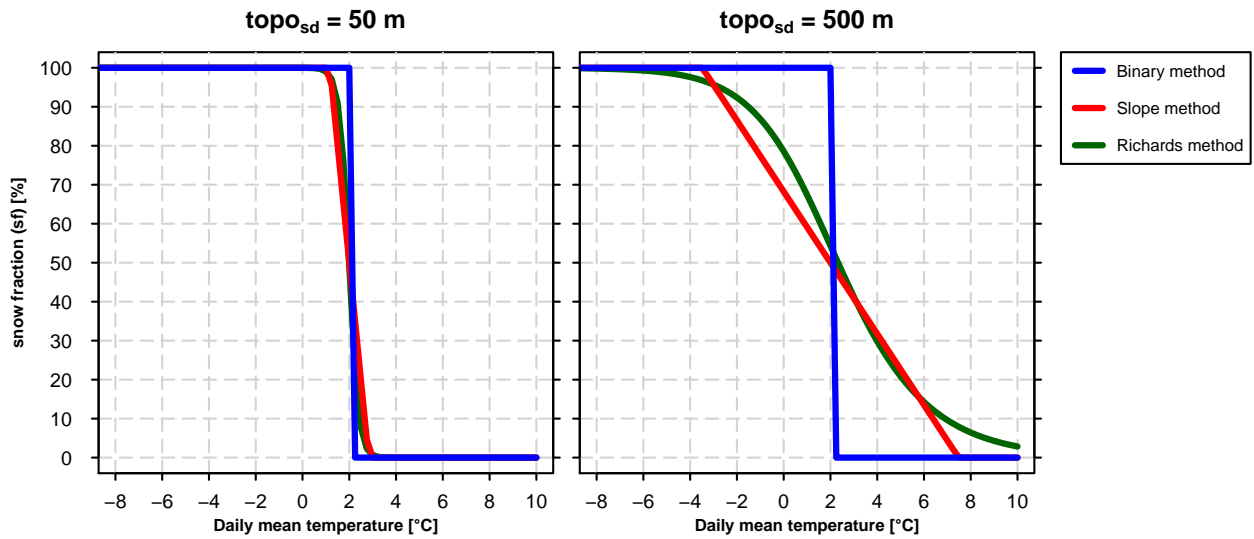


Fig. 2.3: Schematic illustration of snow fraction dependence on daily mean temperature for the Binary (blue), Slope (red) and Richards (green) snow fractionation methods. **a)** Snow fraction curves for a coarse grid box with a topographical standard deviation (topo_{sd}) of 50 m. **b)** Snow fractionation curves for a coarse gridbox with a topo_{sd} of 500 m.

2.6 Bias correction approach

For assessing the GCM-RCM simulation performance in terms of snowfall, all days from September to May within the period 1971 - 2005 were considered. As climate models tend to produce a lot of drizzle, daily precipitation values smaller or equal to 0.1 mm were set to zero. Initially, the 14 RCM simulations were bias-corrected in two steps: Total precipitation was adjusted by introducing an elevation-dependent correction factor which corrects for total simulated precipitation biases regardless of temperature. To account for remaining snowfall deviations, driven by remaining temperature biases, the snow fractionation temperature, T^* , was shifted up to the point at which simulation outputs match the observation-based results.

2.6.1 Total precipitation adjustment

First, the total precipitation of the observation and each RCM was added up. By deriving total mean precipitation ratios (RCM simulation wrt. observation) for 250 m elevation intervals, an almost linear relationship between the total precipitation ratios with altitude was found for most simulations (Fig. C.1). As a result, it was decided to fit a linear regression line through the mean total precipitation ratios between the intervals from 250 m.a.s.l. to 2750 m.a.s.l.. The reason for not fitting data at higher altitudes is the sparse number of grid points and measurement stations which were used to interpolate the observations on to a grid (see Sec. 2.1). A lack of confidence in the reference data means that including the corresponding total precipitation would not be justified.

In each RCM, the total precipitation adjustment factor (P_{AF}) for each grid point was calculated by the following formula:

$$P_{AF}(k) = slope / (topo(k) - intercept) \quad (2.16)$$

with slope and intercept being the fitted parameters of the linear regression (Tab. C.1). $Topo(k)$ is the altitude of the RCM topography at grid point k . The corrected precipitation (P_{corr}) was obtained by multiplying P_{AF} with the daily precipitation, P :

$$P_{corr}(k) = P_{AF}(k) \cdot P(k) \quad (2.17)$$

2.6.2 Snow fractionation temperature adjustment

After applying the RCM-dependent P_{AF} to the daily precipitation fields of the different simulations, the snow fractionation temperature needed to be "tuned". This was achieved by finding T^* at which differences in the spatio-temporal snowfall sums between the observational analysis and the RCMs are minimized. Compared to the adjustment of the total precipitation, the adjusted snow fractionation temperature (T_a^*) has been chosen as a global value and independent of topography.

2.7 Analysed snowfall indices and projected change signals

2.7.1 Snowfall indices

Mean snowfall (S_{mean})

Mean snowfall (S_{mean}) refers to the (spatio-) temporally-averaged snowfall amount in mm SWE (from this point we will use the term "mm" as a synonym for "mm SWE" for simplicity). For the grid coarsening analysis (see Ch. 3), S_{mean} corresponds to the mean annual snowfall amount whereas for the evaluation (see Ch. 4) and the projections (see

Ch. 5) only days between September and May were taken into account. Whenever seasonal cycles are discussed, S_{mean} is determined in mm/d.

Heavy snowfall (S_{q99} , $S_{q99,\text{month}}$)

We define heavy snowfall (S_{q99}) as the grid point-based 99% all-day snowfall percentile of the probability density function (PDF). Therefore, the statistics are based on all days within a specific period:

Grid coarsening analysis period:

1971-2005 (JAN-DEC) \approx 12775 days $\rightarrow S_{q99}$ = daily snowfall amount which is exceeded by the 128 heaviest snowfall events

EVAL period:

1971-2005 (SEP-MAY) \approx 9555 days $\rightarrow S_{q99}$ = daily snowfall amount which is exceeded by the 96 heaviest snowfall events

CTRL/SCEN period:

1981-2010/2070-2099 (SEP-MAY) \approx 8190 days $\rightarrow S_{q99}$ = daily snowfall amount which is exceeded by the 82 heaviest snowfall events

For monthly statistics, the heavy snowfall ($S_{q99,\text{month}}$) depends on number of days within the considered period and month, respectively. Thus, a comparison between S_{q99} and $S_{q99,\text{month}}$ is not straight forward.

As the number of wet days might change over time, using all-day percentiles rather than wet-day percentiles substantially simplifies the data interpretation (Schär et al., 2016).

Snowfall frequency (S_{freq})

The snowfall frequency (S_{freq}) is derived by dividing the total number of days with snowfall > 1 mm by the total number of days within the analysed time period.

Snowfall intensity (S_{int})

The snowfall intensity (S_{int}) is a measure of the daily mean snowfall during days with snowfall > 1 mm.

Maximal 3-day and 10-day snowfall amount (S_{3d} , S_{10d})

The maximum consecutive 3-day (S_{3d}) and 10-day (S_{10d}) snowfall amounts, are obtained by averaging the maximum values of each (September to May) season within the considered period of interest.

Consecutive snowfall days (CSD)

The determination of consecutive snowfall days (CSD) follows the concept of S_{3d} and S_{10d} : First, the longest period with days at which snowfall > 1 mm/d are extracted for each single (September to May) season; Second, values are averaged.

Heavy snowfall fraction ($S_{q99frac}$)

The heavy snowfall fraction ($S_{q99frac}$) is a measure of the heavy snowfall sum (sum of $S > S_{q99}$) percentage of total snowfall (S_{tot}).

2.7.2 Projected signals of change

Two different methods are used to assess the projected signals of change between the SCEN and CTRL period:

Absolute change signal

The absolute change signal (Δ) quantifies the difference of a particular snowfall index X (see Subsection above) between SCEN and CTRL:

$$\Delta X = X_{SCEN} - X_{CTRL} \quad (2.18)$$

Relative signal of change

The relative change signal (δ) describes the mean snow index value X of the SCEN period as a percentage of the CTRL period:

$$\delta X = \left(\frac{X_{SCEN}}{X_{CTRL}} - 1 \right) \cdot 100\% \quad (2.19)$$

To prevent erroneous data interpretation due to possible large relative changes of small values, certain grid boxes were masked out before calculating the signal of change. The filtering was done by setting threshold values for individual snowfall indices and types of statistics. For more information, we refer to the Appendix (see Sec. A).

3 Grid coarsening effect on snowfall

This Chapter analyses the results of the three coarse grid snow fractionation methods Binary, Slope and Richards against the high resolution Subgrid method as they have been introduced in Section 2.5. The Swiss domain consists of 304 12 km x 12 km coarse-grid boxes, all of which are located entirely within the country’s borders. For the analysis, all days between 1971 and 2005 were considered. During this period, a spatial mean precipitation of 1381 mm/y was observed. According to the Subgrid method, i.e., our reference, approximately a third of this amount, namely 467 mm/y, fell as snow (Tab. 3.1).

Tab. 3.1: Overview of derived snowfall characteristics for the Swiss domain during the period 1971 - 2005: the spatio-temporal mean snowfall (S_{mean}); the interquartile range of the temporal mean snowfall over all grid points (S_{IQR}); the spatial heavy snowfall mean ($S_{\text{q99,mean}}$) and the interquartile range of heavy snowfall over all grid points ($S_{\text{q99,IQR}}$). For the Binary, Slope and Richards methods, the yearly snowfall which was wrongfully attributed as rain (wrong rain) and the yearly rainfall which was wrongfully attributed as snow (wrong snow) has been estimated by a comparison to the Subgrid method.

| Method | S_{mean} [mm/y] | S_{IQR} [mm/y] | wrong rain [mm/y] | wrong snow [mm/y] | $S_{\text{q99,mean}}$ [mm/d] | $S_{\text{q99,IQR}}$ [mm/d] |
|----------|-----------------------------|----------------------------|-------------------------|-------------------------|---------------------------------|--------------------------------|
| Subgrid | 467 | 152 - 652 | - | - | 19.8 | 9.4 - 27.2 |
| Binary | 450 | 146 - 628 | 60 | 43 | 21.6 | 10.0 - 29.8 |
| Slope | 449 | 150 - 620 | 31 | 13 | 18.7 | 9.1 - 25.6 |
| Richards | 468 | 148 - 655 | 19 | 20 | 19.4 | 9.2 - 26.6 |

3.1 Scale effect on mean snowfall

By taking the snowfall data based on the Subgrid method, one can quantify the introduced errors by applying the simple Binary method. On average, 60 mm/y are accounted for as rainfall even though it has fallen as solid precipitation. On the other hand, 43 mm/y are attributed as snow while it is actually rain. These errors are relatively small when compared with the mean precipitation of 1381 mm/y (3.1% to 4.3%) and they approximately balance each other out. The ratio of total snowfall between the Binary and Subgrid methods, with $S_{\text{mean,BI}}/S_{\text{mean,SG}} = 0.96$, is close to 1. The lowest mean snowfall ratios are observed between altitudes of 750 m.a.s.l and 1500 m.a.s.l. (Fig. 3.1 a)).

The Slope method produces a yearly S_{mean} amount of 449 mm. In general, the approach leads to a slight underestimation of mean snowfall across most elevation ranges. 31 mm of the yearly precipitation are wrongfully attributed as rain and 13 mm as snow . However,

the absolute daily grid point-based snowfall differences are much smaller than for the Binary method (not shown).

The smallest deviations are found for the Richards method. With a yearly S_{mean} of 468 mm, an almost perfect match to the reference is obtained. 19 mm/y are wrongfully attributed as rain and 20 mm/y as snow. In addition, the mean snowfall ratios, in contrast to the Binary and Slope methods, are nearly independent of altitude.

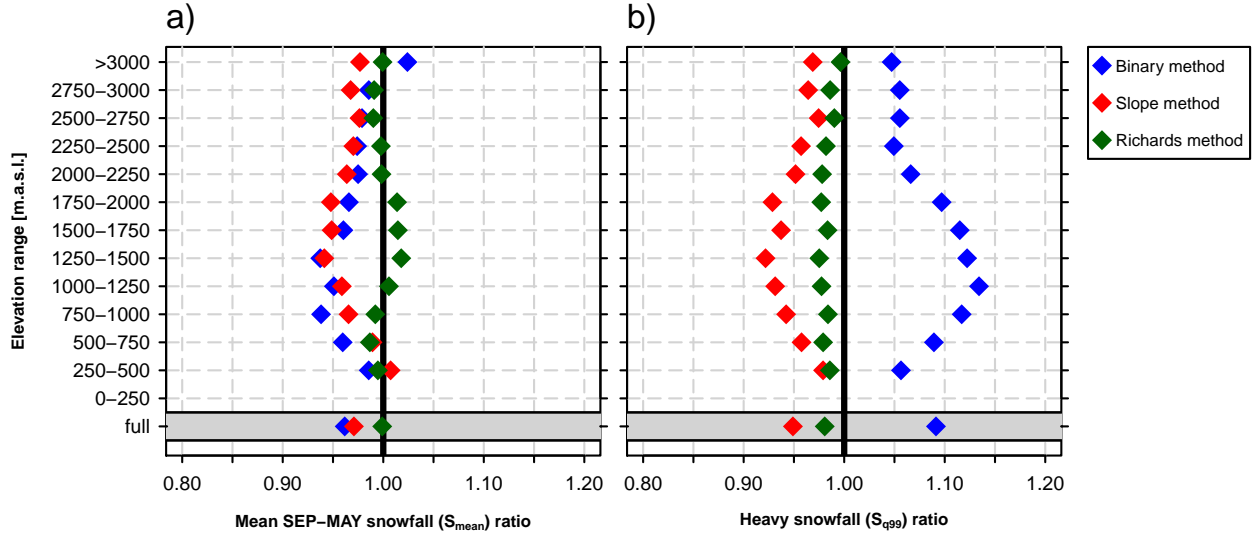


Fig. 3.1: Snowfall ratios for the coarse grid fractionation methods Binary (blue), Slope (red) and Richards (green) with respect to the reference (Subgrid method) for the Swiss domain during the period 1971 - 2005. Ratios were derived after averaging the values for 250 m elevation intervals. **a)** Ratios for mean snowfall (S_{mean}). **b)** Ratios for Heavy snowfall (S_{q99}).

3.2 Scale effect on heavy snowfall

For S_{q99} the three methods diverge more than for S_{mean} . $S_{q99,\text{mean}}$ of the Subgrid method shows a value of 19.8 mm/d with an interquartile range (IQR) of 9.4 - 27.2 mm/d.

The Binary method results in S_{q99} values which are too high across all elevation ranges (Fig. 3.1 b). The largest (elevation-range mean) ratios are obtained for altitude intervals around 1250 m.a.s.l., with values greater than 1.1. This is in strong contrast to the method's S_{mean} , for which the ratios are generally lower than 1. A good reproduction at highest elevation intervals is achieved by the Slope method. Nevertheless, compared to the Subgrid method, S_{q99} is generally too low, i.e., S_{q99} ratios < 1 . As for S_{mean} , the Richards method shows the best performance. Similarly to the Slope method, the S_{q99} ratios are slightly too low, but much closer to 1. $S_{q99,\text{mean}}$ almost matches the reference with $S_{q99,\text{IQR}}$ covering a similar interval (Tab. 3.1).

3.3 Discussion

In terms of effort, an implementation of the Binary method on the coarse grid might be favoured. However, this method can lead to large errors. Let's assume a coarse grid box with a daily mean temperature of $T = 2.5 \text{ }^\circ\text{C}$. By definition, the snowfall fraction, according to the Binary method, would be zero. But it might well be that, on the high resolution grid, there are grid points with temperatures $T' \leq T^*$ and precipitation $P' > 0 \text{ mm}$. In such a case, a part of the snowfall would be "lost" when applying this type of snow fractionation. The other case with $T \leq T^*$ and only precipitation in grid boxes with $T' > T^*$, i.e., rain, is also possible. However this scenario seems to be less likely due to the general underestimation of S_{mean} (see Fig. 3.1 a). The higher probability for wrongfully attributing too much rain, rather than too much snow might arise due to the general precipitation dependency on elevation. Additionally, a PDF of the temperature at snowfall, i.e., daily mean temperature at days with $S > 1 \text{ mm}$, points out that snowfall still occurs at temperatures well above the freezing point (Fig. 3.2 a). While the probability of the Binary method drops to zero at $2 \text{ }^\circ\text{C}$, the distributions of the Slope and Richards methods are in good agreement with the Subgrid method. On the other hand, S_{q99} is overestimated by the Binary method. Following O'Gorman (2014), heavy snowfall events should be expected to occur in a narrow temperature range below the rain-snow transition. According to his physically-based argumentation, heavy snowfall at colder temperatures is unlikely due to low saturation-specific humidities. Our own investigation of the temperature distribution at heavy snowfall, i.e.,

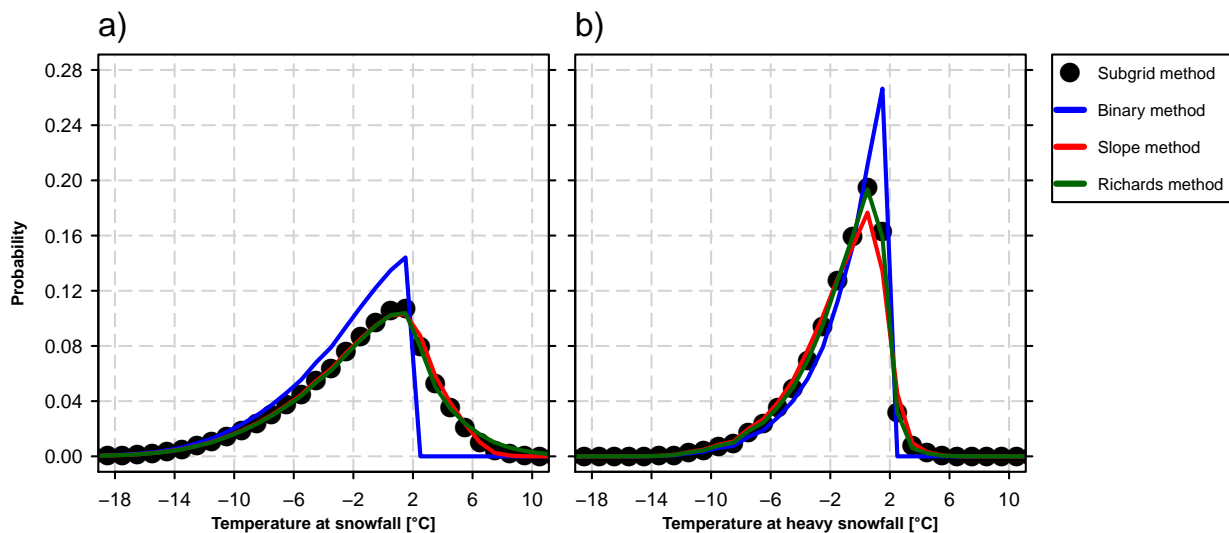


Fig. 3.2: Daily temperature distribution at snowfall for the Swiss domain in the period 1971 - 2005. Black circles denote the Subgrid method (reference). The lines show the distributions of the three introduced coarse-grid snow fractionation methods: Binary (blue), Slope (red) and Richards (green). **a)** PDF of daily temperature at snowfall days (days at which the snowfall exceeds 1mm). **b)** PDF of daily temperature at heavy snowfall days (days at which the snowfall exceeds the grid-point-based 99% all day snowfall percentile (S_{q99})). The PDFs are generated by creating daily temperature bins of width $1 \text{ }^\circ\text{C}$.

daily mean temperature for days with $S \geq S_{q99}$, confirms the theory: Highest probabilities for heavy snowfall to occur are observed in a temperature interval between $-2\text{ }^{\circ}\text{C}$ and $+2\text{ }^{\circ}\text{C}$ (Fig. 3.2 b). In this range, the Binary method assigns the whole precipitation as snowfall, which most likely leads to the overestimation. On the other hand, the probabilities of the Slope method are slightly too low.

Based on all these conclusions, it has been decided to derive the snowfall amounts according to both the Richards and Binary methods. The Richards method clearly shows the best results, however, the Binary method is simpler and less computationally expensive to implement, also for future studies.

4 Bias correction and evaluation

At this point, it is important to mention, that we did not carry out a "classical" evaluation of the RCMs in terms of simulated snowfall amounts. We primarily compare separated + bias-corrected snowfall with observation-based data, and separated + not bias-corrected snowfall is not investigated in detail. Hence, we evaluate the performance of the bias correction rather than the performance of the climate models themselves. Furthermore, no cross-validation is carried out and the validation period equals the calibration period of the bias correction. This leads - by definition - to zero biases for certain features, e.g. for the domain mean snowfall. If not stated otherwise, the terms "simulated" and "modelled" used in Sections 4.2 - 4.4 refer to the separated + bias-corrected data outputs.

The bias correction itself was carried out in two steps:

1. Adjustment of total precipitation, such that the total sum between September to May in the period 1971 - 2005 approximately matches the observational analysis for each 250 m elevation interval.
2. Adjustment of the snow fractionation temperature, such that the difference in the total (domain) snowfall amount between the observational analysis and each RCM simulation is minimized.

While the first step corrects for RCM precipitation biases independent of temperature, the second step accounts for potential RCM temperature biases and corresponding biases in the snowfall fraction. This two-step procedure is considered superior to a standard bias correction of simulated and separated snowfall amounts as it presumably avoids non-stationarities in the correction function: Due to the temperature dependency of snowfall occurrence, snowfall biases of a given climate model cannot be expected to remain the same under current and future climate conditions. For instance, a climate model with a given temperature bias might pass the 0 °C melting/freezing point earlier or later than reality during the general warming with corresponding effects on the snowfall bias structure.

To be consistent in terms of horizontal grid spacing, the observational data sets Rhires and TabsD (see Sec. 2.1) were conservatively regridded to the RCM resolution before deriving the snowfall according to the Richards and Binary method with initial $T^* = 2$ °C (see Eq. 2.5 and 2.12). As the former approach performed better in the grid coarsening analysis (see Ch. 3), emphasis is laid on this type of snow fractionation throughout the following chapters.

4.1 Analysis of adjustment factors

A comparison of the total precipitation ratios (simulations wrt. observation) for September to May in the period 1971 - 2005, reveals substantial differences. All simulations tend to overestimate total precipitation, especially at high elevations (Fig. C.1). However, as the precipitation ratios between simulations and observations seem to follow a linear trend with elevation, the calculation of P_{AF} via a linear regression of the ratios against elevation (see Sec. 2.6) seems to be reasonable. The regression parameters for the 14 simulations are listed in Table C.1. By plugging them into Equation 2.16, P_{AF} for every model and elevation can be derived. For the CCLM and RACMO simulations, P_{AF} does not vary much with height, while P_{AF} of EC-EARTH - HIRHAM is much larger than 1 in low lying areas (Fig. 4.1 a). However, for most elevations and simulations, P_{AF} is generally smaller than 1.

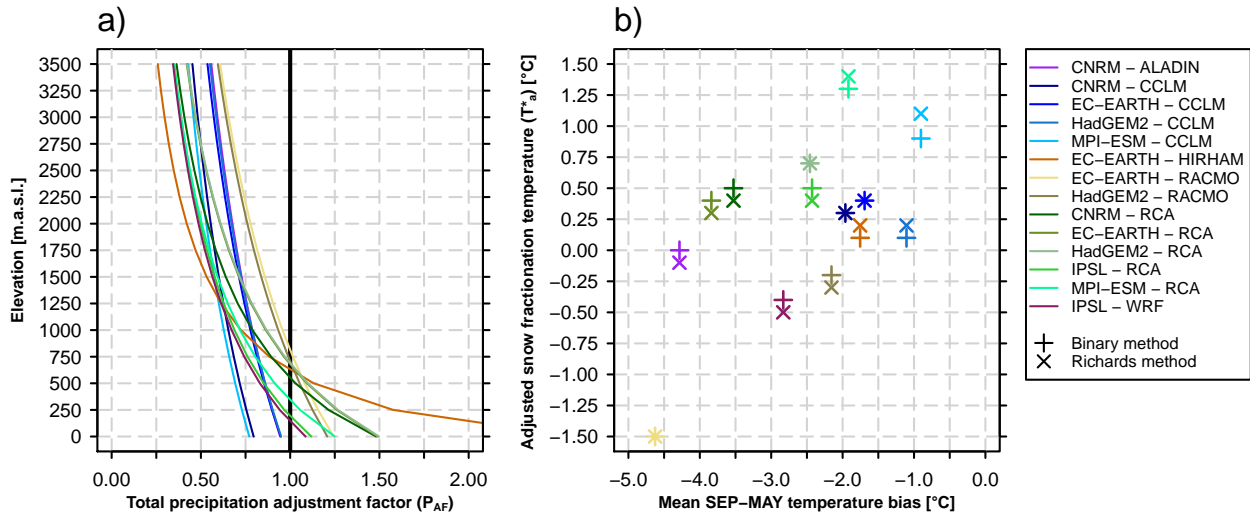


Fig. 4.1: **a)** Elevation-dependent total precipitation adjustment factors (P_{AF}) for the 14 RCM simulations (see Eq. 2.16). **b)** Scatterplot of mean September to May temperature biases (RCM simulation wrt. observational analysis) vs. adjusted snow fractionation temperatures (T_a^*).

After applying P_{AF} to the daily fields, a snowfall fractionation at the initial T^* of 2°C (see Eq. 2.5 and 2.12) would lead to a snowfall excess in all 14 simulations as models typically experience a cold temperature bias between spring and autumn. To match the observation-based spatio-temporally averaged S_{tot} , T^* for all models needed to be decreased, resulting in $T_a^* < T^* = 2^\circ\text{C}$ (Fig 4.1 b). T_a^* values indicate a weak positive relation with the mean temperature bias from September to May in the period 1971 - 2005. Furthermore, the applied snow fractionation method type does not seem to influence the model specific T_a^* (Tab. C.1, cf. $T_{a,BI}^*$ and $T_{a,RI}^*$). While EC-EARTH - RACMO shows one of the best performances in terms of total precipitation, its temperature bias of close to -5°C is the highest deviation in our model set. This might be related to this model's unrealistic accumulation of snow at the ground (personal discussion with S. Kotlarski and E. Zubler).

4.2 Evaluation of mean snowfall

Spatial patterns of S_{mean} for the 14 RCMs from September to May, after implementing the bias correction, are presented in Figure 4.2. The observational analysis in the lower right panel visualises the snowfall distribution as it would be expected: The highest values are observed along the Alpine main ridge, whereas the Swiss plateau, Southern Ticino and main valleys, such as the Rhône and Rhine valley, experience less snowfall between September and May. Almost all models are able to represent the overall picture with snow-poor lowlands and snow-rich Alpine regions.

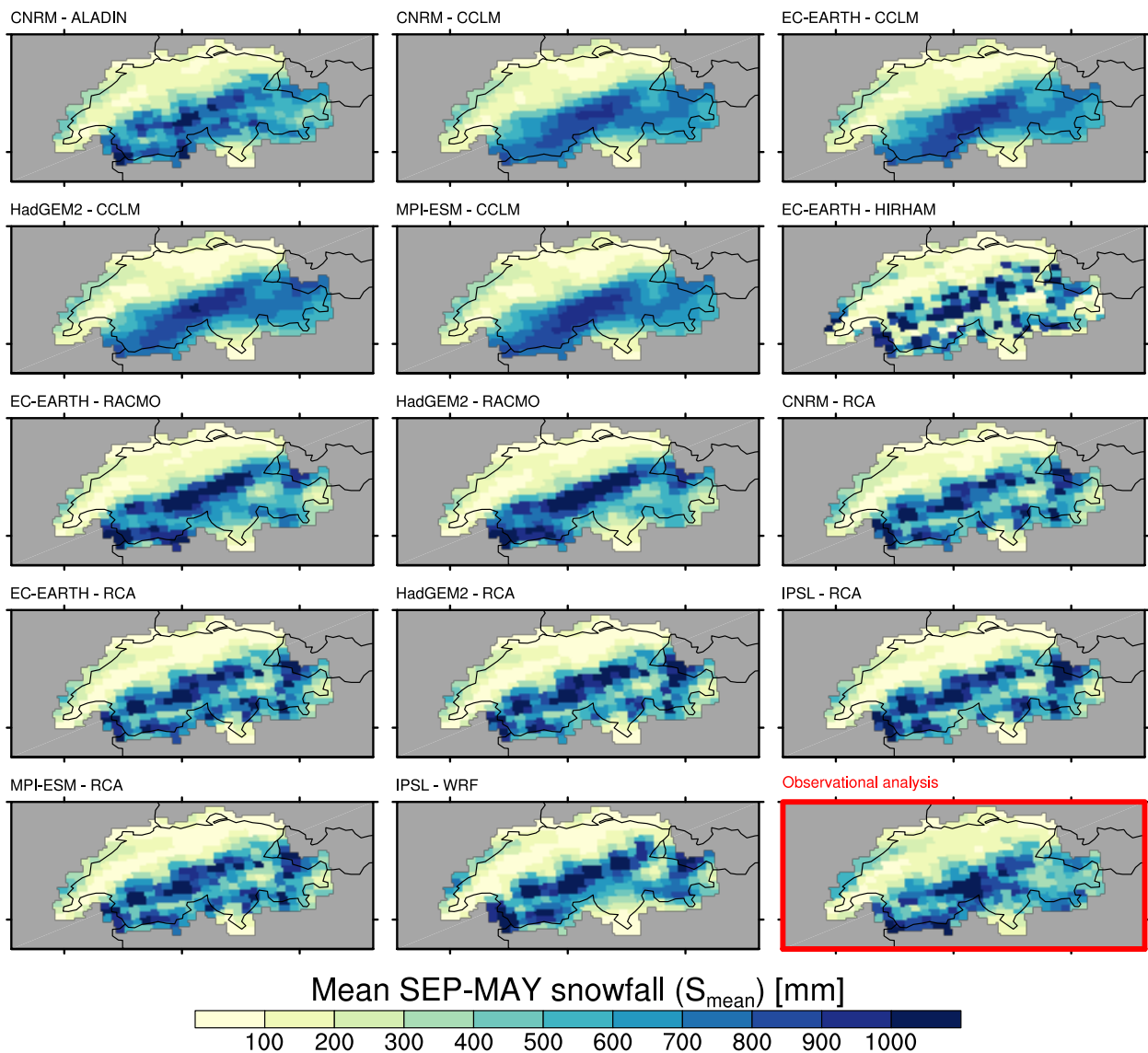


Fig. 4.2: Spatial distribution of mean September to May snowfall (S_{mean}) in the period 1971 - 2005 and for the 14 RCM simulations after applying the bias correction and fractionating the snowfall with the Richards method. In the lower right panel, the horizontal map of the observation-based estimate is shown (snow fractionation with Richards method at $T^* = 2^\circ\text{C}$, see Eq. 2.12). For the Binary snow fractionation method, see Fig. C.2.

Nevertheless, by taking a closer look, substantial differences compared to the observational analysis arise. EC-EARTH - HIRHAM, for example, has a very "pixelated" structure. This can be the result of frequent "grid-cell storms" connected to parametrisations struggling with complex topographies (personal discussion S. Kotlarski and E. Zubler). It is important to indicate that our simple bias correction approach only takes S_{tot} over the entire domain into account. Hence, simulated spatial patterns are only slightly modified by the adjustment of T^* . These patterns reveal a strong similarity among RCMs and obviously don't directly depend on the driving GCM. The CCLMs and RCAs are a good example. However, the bias-corrected spatio-temporal mean snowfall is by definition identical for all simulations.

An analysis of S_{mean} , averaged over 250 m elevation ranges, confirms that bias-corrected RCMs are able to reproduce the observational analysis (Fig. 4.4 a). Even the shift, from strong dependencies of snowfall amounts on elevation at lower regions (< 1250 m.a.s.l.) to minor dependencies aloft, is well captured. Highest deviations between the multimodel mean and the observational analysis occur in the interval 2750 m.a.s.l. - 3000 m.a.s.l. As already mentioned in Section 2.1, observational values above 2500 m.a.s.l. should be treated cautiously as the available number of stations used for the grid interpolations and the number of total grid points is very sparse. Here, most of the observational grid boxes in this interval are located over the Jungfrau region in the Bernese Alps where some precipitation devices are assumed to measure unrealistically high values. These measurements are unfortunately incorporated into our observational data set to estimate the elevation dependent precipitation rates for the data interpolation on a grid (personal communication C. Frei). Second, in most of our simulations, the grid boxes over this area contribute to another elevation interval (not shown). Over the full domain, the individual simulations match the observation-based analysis by definition.

4.3 Evaluation of heavy snowfall

Problems emerge when evaluating S_{q99} . While simulations fairly well reflect the low observational values over large parts of the Swiss plateau and the Jura mountains, heavy snowfalls over the Alpine ridge are underestimated (Fig. 4.3). In particular, CNRM - ALADIN, IPSL - WRF and all CCLM experiments show a substantial underestimation of the spatial S_{q99} variability. The performance of the two RACMO simulations in the Valais region looks reasonable while observational analyses in the Ticino region are adequately captured by the RCA simulations. Note that in contrast to S_{mean} , domain mean values of S_{q99} are not identical among models and between the observational analysis and models, respectively. Thus, despite bias correcting for domain mean snowfall, the daily snowfall distribution might still differ among simulations. The right tail of the snowfall distribution for HadGEM2 - RACMO is for example more pronounced than the one for EC-EARTH - RACMO which leads to higher S_{q99} .

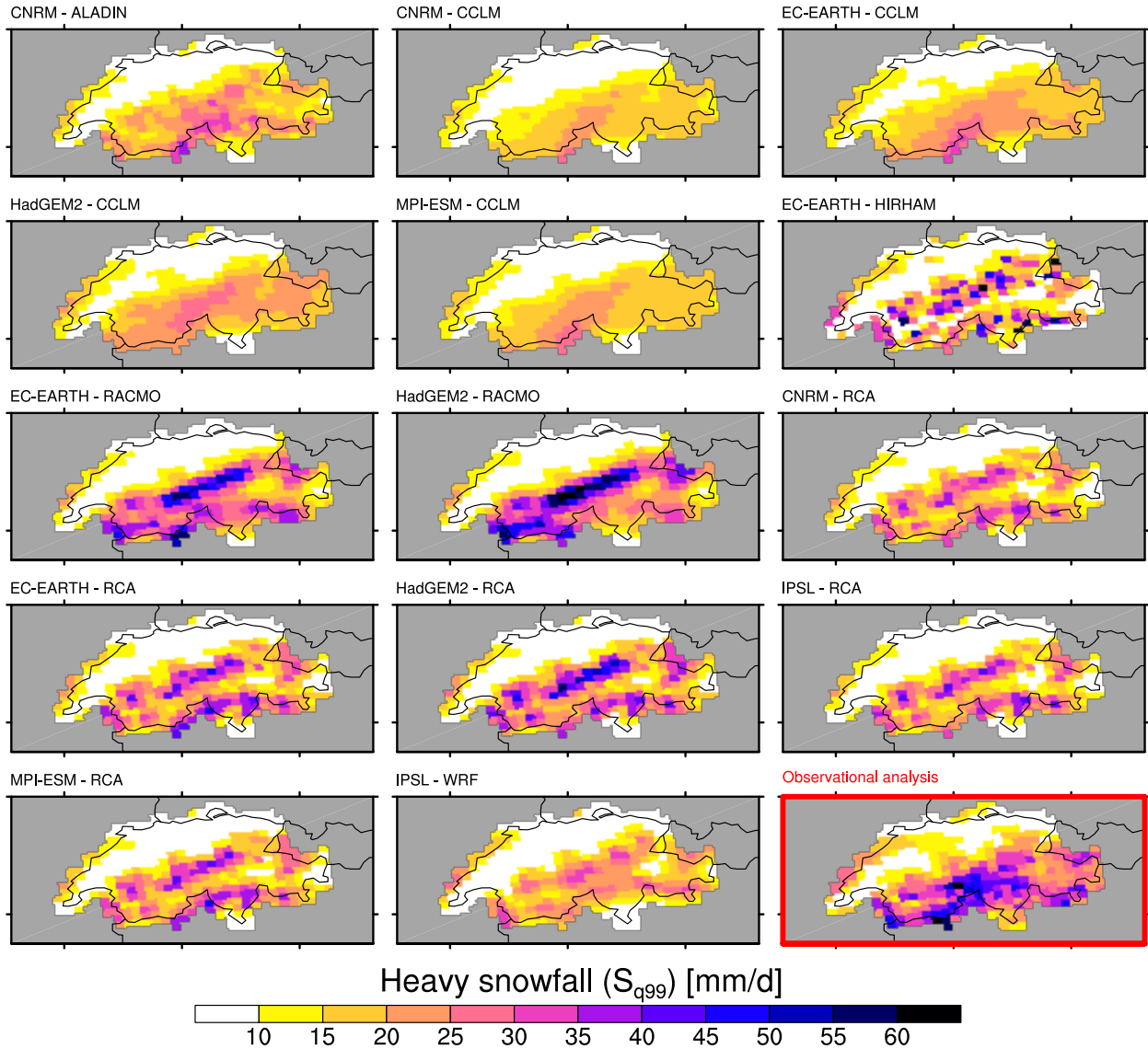


Fig. 4.3: Spatial distribution of heavy snowfall (S_{q99}) between September and May in the period 1971 - 2005 and for the 14 RCM simulations after applying the bias correction and fractionating the snowfall with the Richards method. In the lower right panel, the horizontal map of the observation-based estimate is shown (snow fractionation with Richards method at $T^* = 2^\circ\text{C}$, see. Eq. 2.12). For the Binary snow fractionation method, see Fig. C.3.

In general, S_{q99} is slightly larger for RCMs driven by the HadGEM2 GCM than by the EC-EARTH GCM. This might arise due to warmer mean temperatures of the HadGEM2 which could cause higher specific humidities and support stronger snowfalls (personal communication S. Kotlarski). The vertical profile of S_{q99} in Figure 4.4 b) confirms the first impressions. At low elevations, models approximately reproduce S_{q99} . From 1500 m.a.s.l. to 3000 m.a.s.l. the multimodel mean is nearly constant at around 25 mm/d whereas observation-based S_{q99} rise linearly from 30 mm/d to 40 mm/d. As a result, over the full domain, S_{q99} is (largely) underestimated by most simulations. The two RACMO simulations, for which the total precipitation adjustment are smallest (see Fig. 4.1, a)), clearly show the best performance.

4.4 Evaluation of further snowfall indices

RCMs are able to pick up the general exponential decrease of $S_{q99frac}$ with altitude (Fig. 4.4 c). Despite a large model spread below 1000 m.a.s.l., multimodel means match the observations quite well. Above 1500 m.a.s.l., constant $S_{q99frac}$ with elevation are captured accurately. However, the multimodel means are too low. Observation-based S_{freq} show a strong increase from 5% to 20% for the lowermost elevation ranges (Fig. 4.4 d). At higher altitudes snowfall is, on average, expected to occur every 3 - 4 days, i.e., $S_{freq} = 30\%$. In these regions, none of the RCM simulations is able to reproduce the climatology. The multimodel means gradually increase with altitude, resulting in an overestimation of S_{freq} . Additionally, the disagreement between models might be as large as 20%. Complementary, modelled S_{int} is underestimated (Fig. 4.4 e). Especially in elevated areas, differences are close to 3 mm/d. Over the entire domain, compared to the observational analysis, multimodel mean S_{freq} is too high whereas S_{int} is too low. CSD shows a strong increase from three to eight days across the lowermost four elevation intervals (Fig. 4.4 f). Above 1250 m.a.s.l., it is independent of altitude. Simulations reflect these characteristics quite well. Hence, an offset of roughly three days at higher regions is found. For both S_{3d} and S_{10d} , the snowfall amount increases with altitude (Fig. 4.4 g) and h). S_{10d} is generally 1.5 - 2 times higher than S_{3d} . RCMs struggle in reproducing these tendencies above 1500 m.a.s.l.. Instead of a further rise of snowfall levels, most of the models indicate a slight decrease with altitude.

Similar to the spatial distributions, a general clustering of simulations carried out with the same RCM is detected. For most of the discussed snowfall indices the RACMO simulations are the most accurate, while CCLM experiments show highest discrepancies. The RCA model, which has the strongest influence on the multimodel mean by providing 5 of the total 14 simulations, has a medium accuracy. Separating snowfall with the Binary method results in very similar characteristics (Fig. C.4).

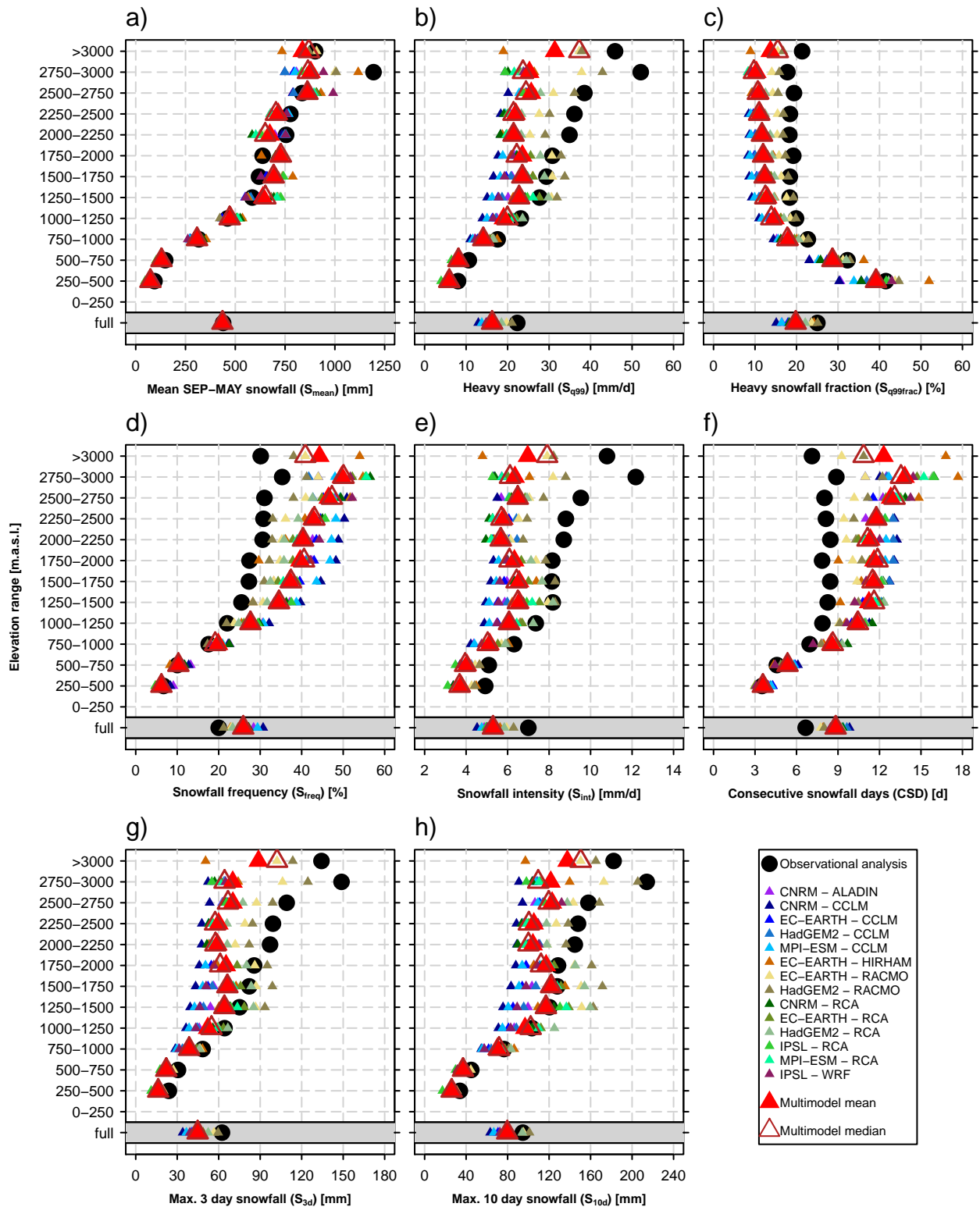


Fig. 4.4: Evaluation of seasonal (September to May) snowfall indices in the period 1971 - 2005 after applying the bias correction and separating the snowfall with the Richards method. The black circles represent the values of the observation-based analysis. Small triangles show the individual RCM simulations whereas the large triangles denote the multimodel mean (red, filled) and multimodel median (brown, open). For the Binary snow fractionation, method see Fig. C.4.

4.5 Discussion

Many simulations show on average up to two times more precipitation than the observations. These characteristics have already been detected in previous studies. Deller (2015) found the errors to be largest during spring and winter. Especially at high elevations, these apparent positive precipitation biases could be related to observational undercatch, i.e., an underestimation of true precipitation sums by the observational analysis. Frei et al. (2003) estimated seasonal Alpine precipitation undercatches for three elevation intervals. Results show that measurement biases are highest in winter and increase with altitude. However, these measured undercatches just partly explain the overestimation of precipitation. Another known issue is the systematic underestimation of dry days in RCMs and GCMs which is reflected in the general overestimation of simulated precipitation frequencies (Dai (2006); Kendon et al. (2012)).

Simulated snowfall excesses with initial snow fractionation at $T^* = 2 \text{ }^\circ\text{C}$ emerge due to underestimated mean September to May temperatures in all models. In a study by Kotlarski et al. (2014), similar temperature biases, as shown in Fig. 4.1 b) are discovered. For the winter months December, January and February (DJF), all of their nine EURO-CORDEX simulations reveal biases of up to $-5 \text{ }^\circ\text{C}$ across the Alpine main ridge. Note, however, that the latter evaluated the reanalysis-driven EURO-CORDEX ensemble, while we here exclusively analyse GCM-driven experiments.

After applying the bias correction to the simulations, most snowfall indices are fairly well represented at elevations below 1000 m.a.s.l.. With increasing altitude and smaller sample sizes, observational analyses and models diverge. This might be caused by the remaining simulated overestimation of S_{freq} and underestimation of S_{int} . While the bias correction approach leads to a reduction of S_{int} due to the total precipitation adjustment, S_{freq} is only slightly modified by T^*_a . Nevertheless, these two parameters strongly influence the other indices. The counteracting effects of overestimated S_{freq} and underestimated S_{int} result in appropriate amounts of S_{mean} . Discrepancies in S_{q99} , S_{q99frac} , S_{3d} and S_{10d} are mainly driven by too low S_{int} , while CSD heavily depends on S_{freq} .

Figure 4.5 denotes the seasonal cycles for S_{mean} , $S_{\text{q99,month}}$, S_{freq} and S_{int} of separated + bias-corrected and separated + not bias-corrected simulations. In separated + not bias-corrected simulations, raw precipitation has been separated with the Richards method at the initial snow fractionation temperature of $T^* = 2 \text{ }^\circ\text{C}$ (see Eq. 2.12). Despite the snowfall bias correction approach which is only based spatio-temporally averaged S_{tot} , RCMs are able to resolve the seasonal cycle of S_{mean} at all three elevation intervals. S_{mean} amounts of separated + not bias-corrected simulations are up to two times higher.

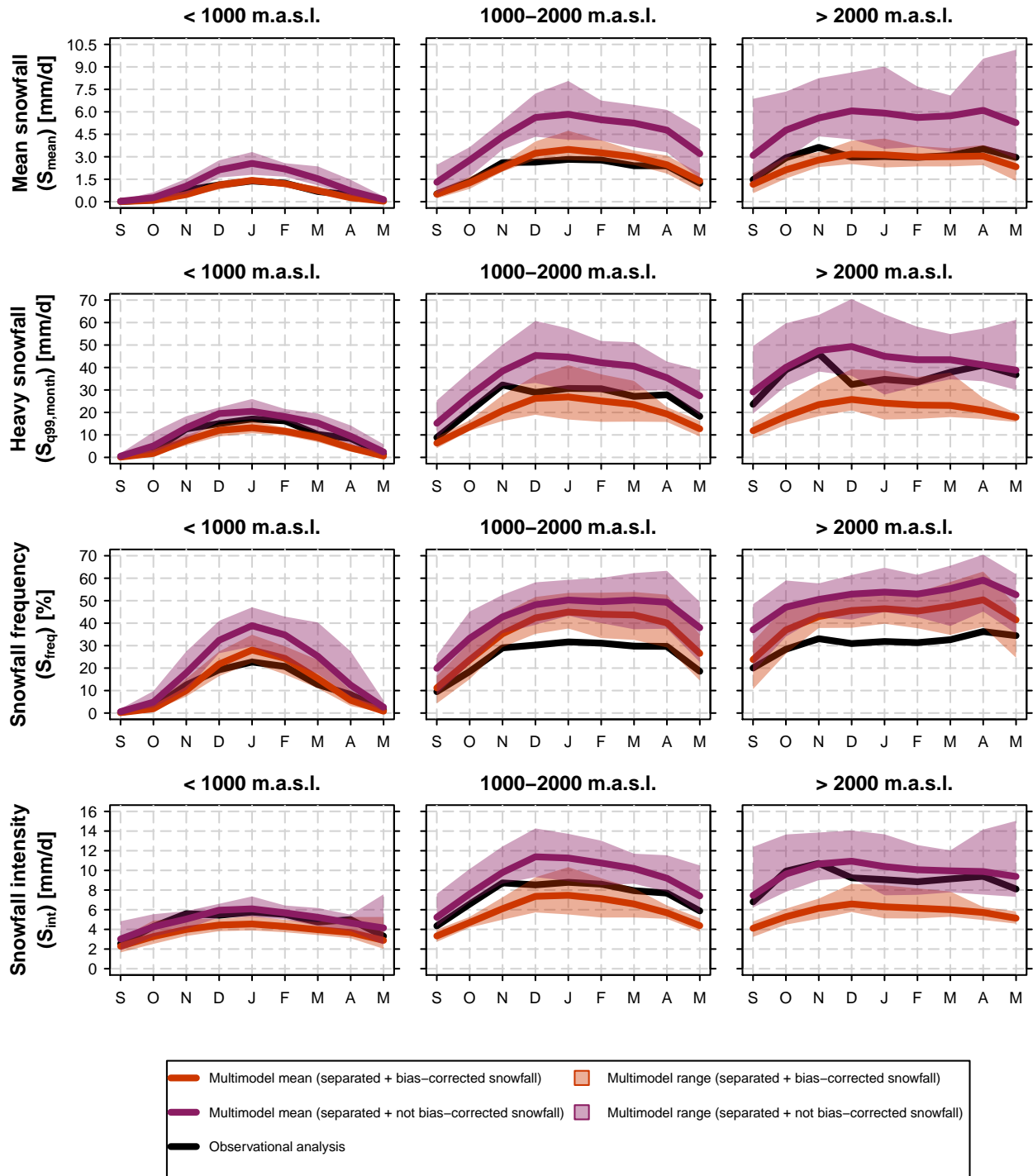


Fig. 4.5: Evaluation of monthly (September to May) snowfall indices in the period 1971 - 2005. Black lines depict the observation-based analysis (snow fractionation with Richards method at $T^* = 2^\circ\text{C}$, see Eq. 2.12). The red line displays the seasonal cycle of the multimodel mean based on the separated + bias-corrected snowfall of the 14 RCM simulations (snow fractionation with Richards method at $T_{a,RI}^*$, see Tab. C.1). Seasonal cycles of the multimodel mean based on the separated + not bias-corrected snowfall are shown in violet (snow fractionation with Richards method at $T^* = 2^\circ\text{C}$). The shading represents the corresponding multimodel range. The columns represent the three elevation intervals below 1000 m.a.s.l., between 1000 m.a.s.l. and 2000 m.a.s.l. and above 2000 m.a.s.l.. For the Binary snow fractionation method, see Fig. C.5.

For $S_{q99,month}$ at highest elevations, the performance of the separated + not bias-corrected simulations is better than the bias-corrected outputs, especially in autumn and spring. The same feature is detected for S_{int} . This can partly be explained by the insufficient total precipitation adjustment in these regions. At high altitudes, most of the RCMs have precipitation ratios close to 1 (see Fig. C.1). With our linear correction approach (see Sec. 2.6) these ratios are increased by a factor of 1.5 - 3 resulting in too low P_{AF} , i.e. a too strong correction of positive precipitation biases. S_{freq} is clearly overestimated by both the bias-corrected and not bias-corrected simulations. As already discussed before, the bias correction method is not capable of adjusting the frequencies to the observational analyses. The improvements, compared to the not bias-corrected snowfall frequencies, are small.

The here presented bias correction approach for snowfall significantly reduces the model spread for all snowfall indices. At lower elevations the adjustments lead to more realistic outcomes, while substantial deviations remain aloft. This, of course, has some implications for the snowfall projection analysis in the following chapter. In our opinion, the insufficient correction of certain snowfall indices should not have a substantial impact on relative change signals (see also Ch. 6). In terms of absolute changes, much more caution is required. For separated and bias-corrected indices which still lack to reproduce observational analyses, it is not reasonable to rely on absolute changes.

5 Snowfall projections for the late 21st century

For the study of climate change signals, the analysis domain was extended to the entire Alps (see Sec. 2.3). Simulated drizzle was removed from the data set by setting daily precipitation amounts ≤ 0.1 mm to zero and the the summer months JJA were excluded from any analysis. After applying the bias correction according to the procedures described in Section 2.6, snowfall indices were temporally averaged. Signals of change are derived by comparing the SCEN period 2070 - 2099 to the CTRL period 1981 - 2010. Due to identified difficulties of bias correcting certain snowfall indices (see Ch. 4), emphasis is laid upon relative signals of change. This type of change is less dependent on the remaining inaccuracies after the correction. If not stated otherwise, all graphics are based on the RCP8.5 scenario and the Richards snow fractionation method.

5.1 Projected changes of mean snowfall

Projections of S_{mean} show a significant decrease over the entire Alpine domain (Fig. 5.1). Most of the 14 simulations project largest percental changes across the Alpine forelands such as the Po Valley or Western France. Over the Alpine main ridge, reductions are smaller but still mostly negative. Elevated regions between Souteastern Switzerland, Northern Italy and Austria seem to be least affected. Some simulations, e.g. CNRM - RCA or MPI-ESM - RCA project no significant changes. Experiments employing the same RCM but different driving GCMs can disagree in regional-scale change patterns and especially in the general magnitude of changes. The former is in contrast to the almost identical spatial distributions of S_{mean} for the EVAL period (see Fig. 4.2). Regarding absolute changes, simulations are generally in good agreement (Fig. D.6). Largest decreases of S_{mean} are projected in mid- to high-elevated areas in Southwestern France, Switzerland, Northern Italy and Eastern Austria.

Figure 5.2 provides more insight into absolute and relative changes of the seasonal cycle between September and May. For completeness, monthly values for the CTRL period are displayed as well. Below 1000 m.a.s.l., ΔS_{mean} is largest during December and April. With a multimodel mean of -60%, δS_{mean} is smallest in winter but still substantial. At mid-elevations, largest absolute changes are predicted for the months before and after the DJF period. δS_{mean} is strongest during autumn and spring. This feature is obtained across all three elevation ranges. Above 2000 m.a.s.l., models indicate two slight peaks during the transition seasons from autumn into winter and winter into spring, respectively, for S_{mean} in the CTRL period. These details are also noticed in the observational analysis (see Fig. 4.5). Furthermore, almost no negative changes in S_{mean} are expected between January and March.

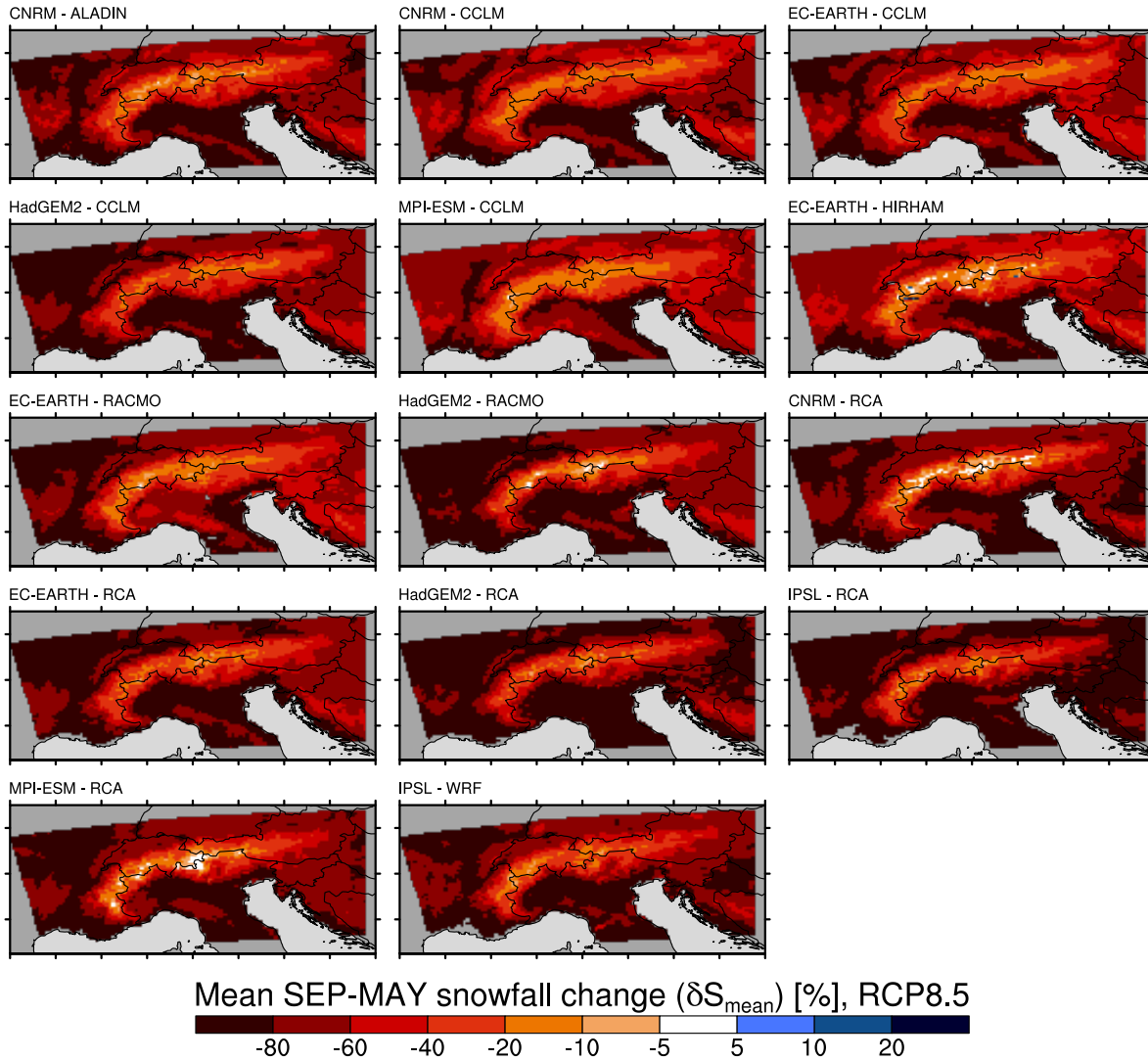


Fig. 5.1: Spatial distribution of relative changes (SCEN 2070 - 2099 wrt. CTRL 1981 - 2010) in mean September to May snowfall (δS_{mean}) for RCP8.5 and for the 14 RCM simulations after applying the bias correction and fractionating the snowfall with the Richards method. Relative changes for RCP4.5 are shown in Fig. D.1. For the Binary snow fractionation method, see Fig. D.8 (RCP4.5) and Fig. D.13 (RCP8.5).

The multimodel mean even hints to a slight increase in snowfall. HadGEM2-driven simulations, for which comparable spatial patterns were detected in Figure 5.1, also follow a very similar seasonal change cycle. This might be featured by comparable warming rates which have a strong influence on the corresponding RCM. Relative (seasonal) changes of S_{mean} appear to be strongly dependent on elevation (Fig. 5.5 a). The multimodel mean ranges from -80% at lowest altitudes to -10% at 3000 m.a.s.l.. Largest differences between elevation intervals are obtained from 750 m.a.s.l. to 1500 m.a.s.l.. Over the entire Alps, our results show a reduction of S_{mean} by -35% to -55% with a multimodel mean of -45%. The elevation independent multimodel spread is comparably small and goes well along with the similar spatial distribution of the 14 simulations.

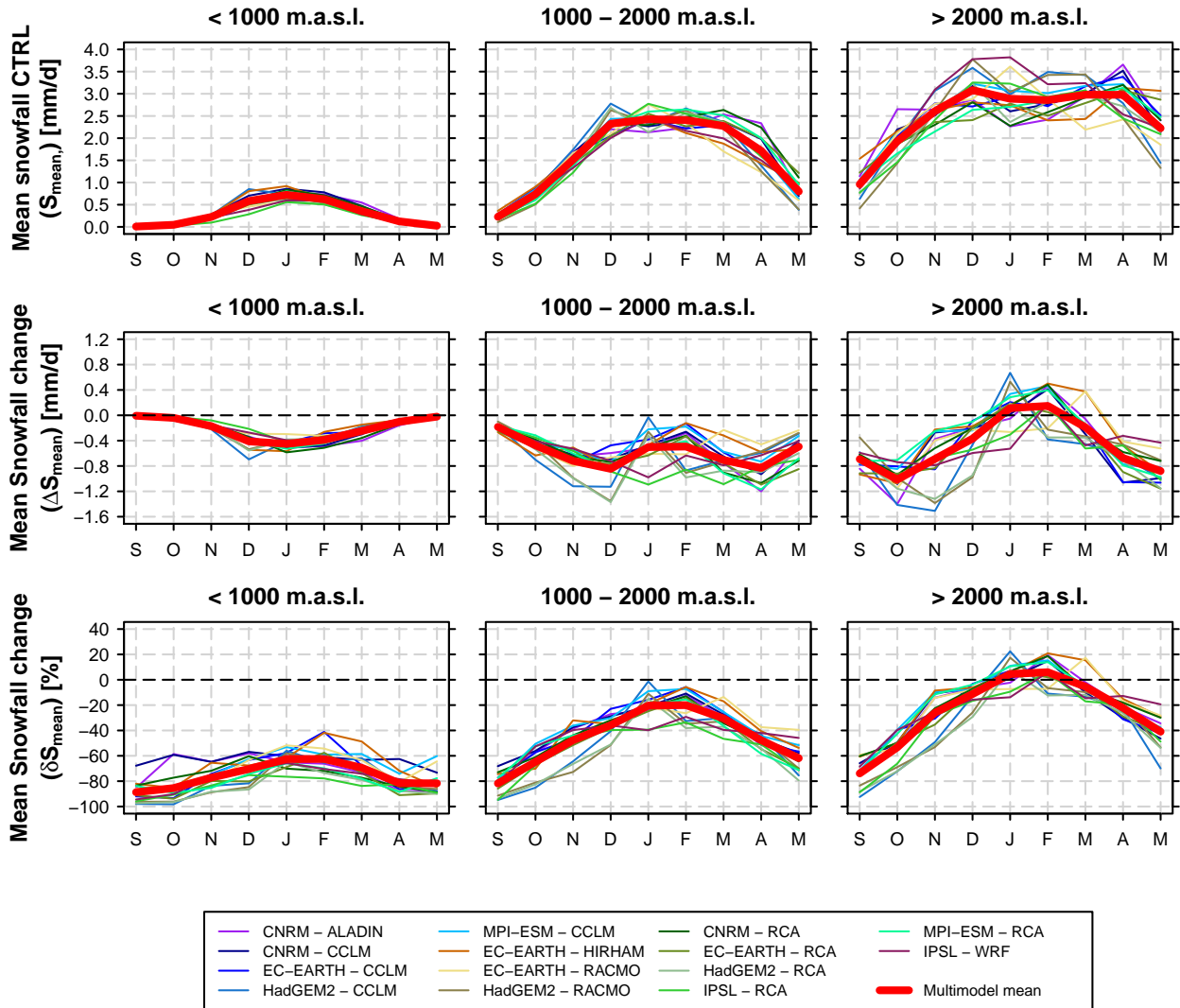


Fig. 5.2: Seasonal cycles (September to May) of mean snowfall (S_{mean}) at three different elevation intervals after applying the bias correction and fractionating the snowfall with the Richards method. Upper row: Mean snowfall during CTRL period 1981 - 2010. Middle row: Absolute changes of mean snowfall (SCEN 2070 - 2099 wrt. CTRL 1981 - 2010). Bottom row: Relative changes of mean snowfall (SCEN 2070 - 2099 wrt. CTRL 1981 - 2010). The columns represent the three elevation intervals below 1000 m.a.s.l., between 1000 m.a.s.l. and 2000 m.a.s.l. and above 2000 m.a.s.l..

5.2 Projected changes of heavy snowfall

For regions close to mean sea level, such as the Po Valley, Burgundy, Central France, Western Slovenia or Northern Croatia, S_{q99} is projected to decline by more than -80% (Fig. 5.3). Across the Alpine ridge, changes are less negative, while some individual simulations even project slight increases. Despite this general pattern agreement, no general similarities among GCMs or RCMs are found. Even though the HadGEM2 - RCA and HadGEM2 - RACMO are in close analogy, the third HadGEM2-driven simulation, i.e., HadGEM2 - CCLM, indicates less variations in Western Austria. This is also obtained for the EC-EARTH- and MPI-ESM driven CCLMs whereas CNRM - CCLM projects additional S_{q99} increases in the Valais region. Similar to spatial changes of S_{mean} , reductions for simulations driven by the HadGEM2 GCM are usually stronger than for other driving GCMs. This is also evident in the spatial patterns of absolute changes (Fig. D.7).

Monthly changes within the seasonal cycle of $S_{q99,\text{month}}$ are depicted in Figure 5.4. The shape of the curves reveal close similarities to S_{mean} and monthly changes in ΔS_{mean} and δS_{mean} , respectively. At low lying areas, $\Delta S_{q99,\text{month}}$ is strongest in the DJF period while above 2000 m.a.s.l. individual simulations and also the multimodel mean indicate a minor increase. For mid-elevations, we again note strongest absolute changes during the transition seasons and smallest relative shifts in winter. Despite the substantial underestimation of spatial variability of S_{q99} in the EVAL period, monthly changes simulated by the CCLM experiments are the most moderates (cf. to Fig. 4.3). Largest $\Delta S_{q99,\text{month}}$ decreases in late autumn are obtained for HAdGEM2 - RACMO. Whether this is related to this model's high $S_{q99,\text{month}}$ in the CTRL period remains unclear. However, model agreement in terms of relative changes is quite good and smallest in early spring.

Many of the previously discussed features can also be detected in the vertical profile of δS_{q99} (Fig. 5.5 b). Largest model uncertainties are found at lower elevations. While the CCLM simulations indicate smallest reductions of S_{q99} , the signals of the RCA experiments are up to 30% larger. Above 500 m.a.s.l., relative reductions in S_{q99} are less pronounced than for S_{mean} . At highest elevations no significant changes are obtained. However, due to the large fractional area of our domain being situated at lower altitudes and indicating large decreases in S_{q99} , domain mean reductions are in the order of -45%. This is comparable to δS_{mean} (see Fig. 5.5 a).

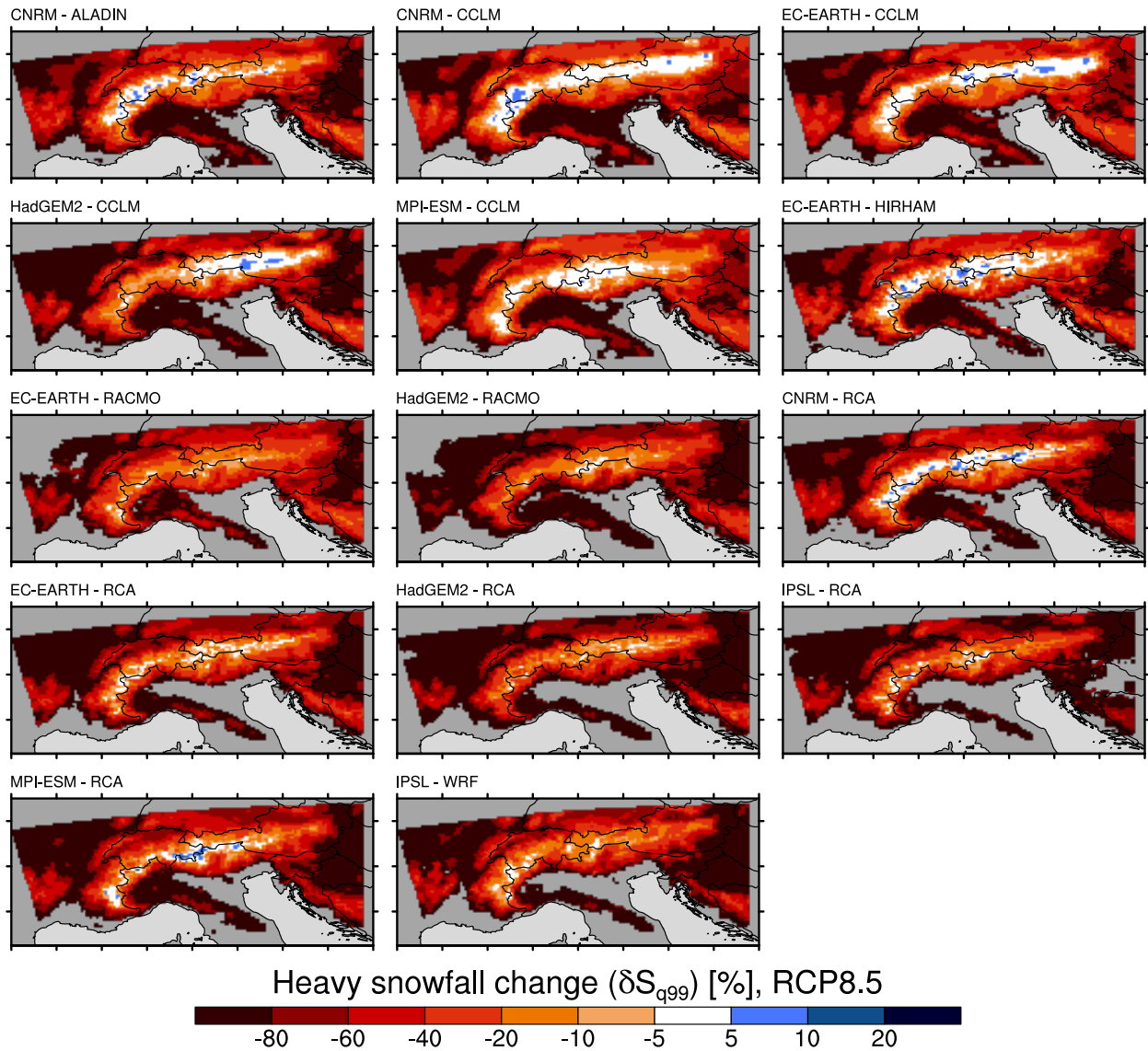


Fig. 5.3: Spatial distribution of relative changes (September to May, SCEN 2070 - 2099 wrt. CTRL 1981 - 2010) in heavy snowfall (δS_{q99}) for RCP8.5 and for the 14 RCM simulations after applying the bias correction and fractionating the snowfall with the Richards method. Relative changes for RCP4.5 are shown in Fig. D.3. For the Binary snow fractionation method, see Fig. D.10 (RCP4.5) and Fig. D.15 (RCP8.5).

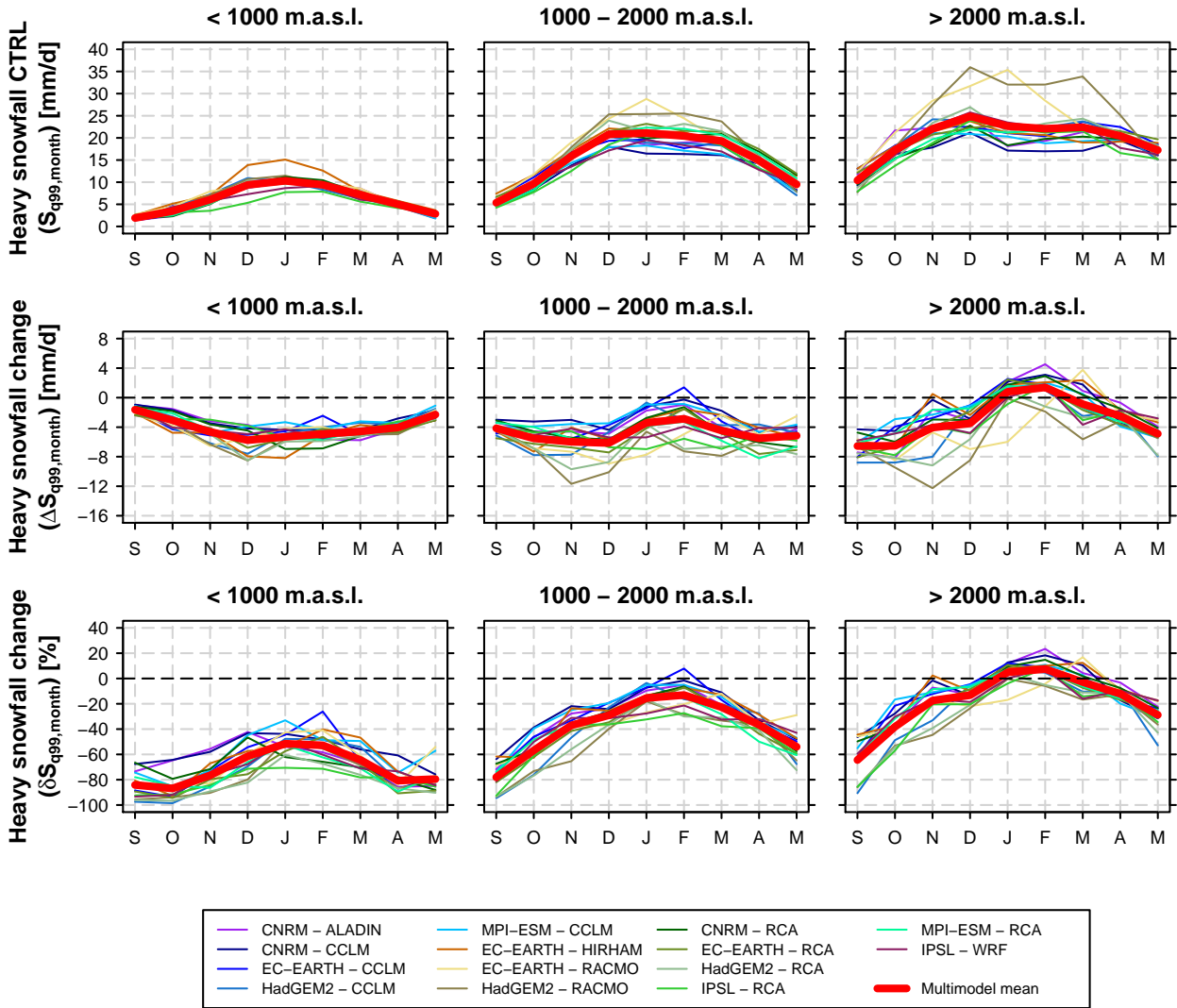


Fig. 5.4: Seasonal cycles (September to May) of heavy snowfall ($S_{q99, \text{month}}$) at three different elevation intervals after applying the bias correction and fractionating the snowfall with the Richards method. Upper row: Heavy snowfall during CTRL period 1981 - 2010. Middle row: Absolute changes of heavy snowfall (SCEN 2070 - 2099 wrt. CTRL 1981 - 2010). Bottom row: Relative changes of heavy snowfall (SCEN 2070 - 2099 wrt. CTRL 1981 - 2010). The columns represent the three elevation intervals below 1000 m.a.s.l., between 1000 m.a.s.l. and 2000 m.a.s.l. and above 2000 m.a.s.l..

5.3 Projected changes of further snowfall indices

Relative (seasonal) changes of the remaining snowfall indices are depicted in Figure 5.5 c) - h). The individual experiments project an increase of $\delta S_{q99frac}$ across all elevations. Largest changes of +60% to +75% are predicted in the lower third of the altitude range (Fig. 5.5 c)). Similar evolutions were obtained in a study by Lute et al. (2015). For the Western US, they analysed future changes of extreme snowfall events by using GCM data output. However, a direct interpretation of this behaviour is very difficult as this index is influenced by variations in S_{tot} as well as fluctuations of the snowfall amount exceeding S_{q99} (see Sec. 2.7). These two dependencies might also cause the large model uncertainty for this parameter. Decreases of S_{freq} are comparable to δS_{mean} : Below 1000 m.a.s.l. the relative changes are largest while differences among elevation intervals become smaller in the upper part. In-between is a "transition" zone with rather strong changes between elevation intervals (Fig. 5.5 d)). Individual simulations with large δS_{mean} , such as the RCA experiments also project strongest declines in S_{freq} . In Section 5.5 we will further discuss this relationship. S_{int} seems to be subject to smallest percental variations in our set of snowfall indices. Apart from mid-elevations, with decreases of roughly -10%, mean intensities from September to May are projected to remain stable by the end of the century (Fig. 5.5, e)). Hence, model agreement is best for high elevations while the multimodel spread is largest for lowlands. At the lowermost elevation interval from 0 m.a.s.l. - 250 m.a.s.l., MPI-ESM - RCA hints to a strong increase in S_{int} of more than +80%. This is not obtained in the RCP4.5-driven simulation (Fig. D.5 e)). There are two possible explanations for this "outlier": The large δS_{int} is either caused by internal model variability or by the small number of grid points used for the data sampling. CSD shrinks on average by -35% (Fig. 5.5 f)). Strongest signals are detected below 1500 m.a.s.l.. Aloft, changes are independent of altitude and roughly -10%. Similar features are observed for S_{3d} and S_{10d} . (Fig. 5.5 g) and h)). δS_{10d} is marginally more negative than δS_{3d} .

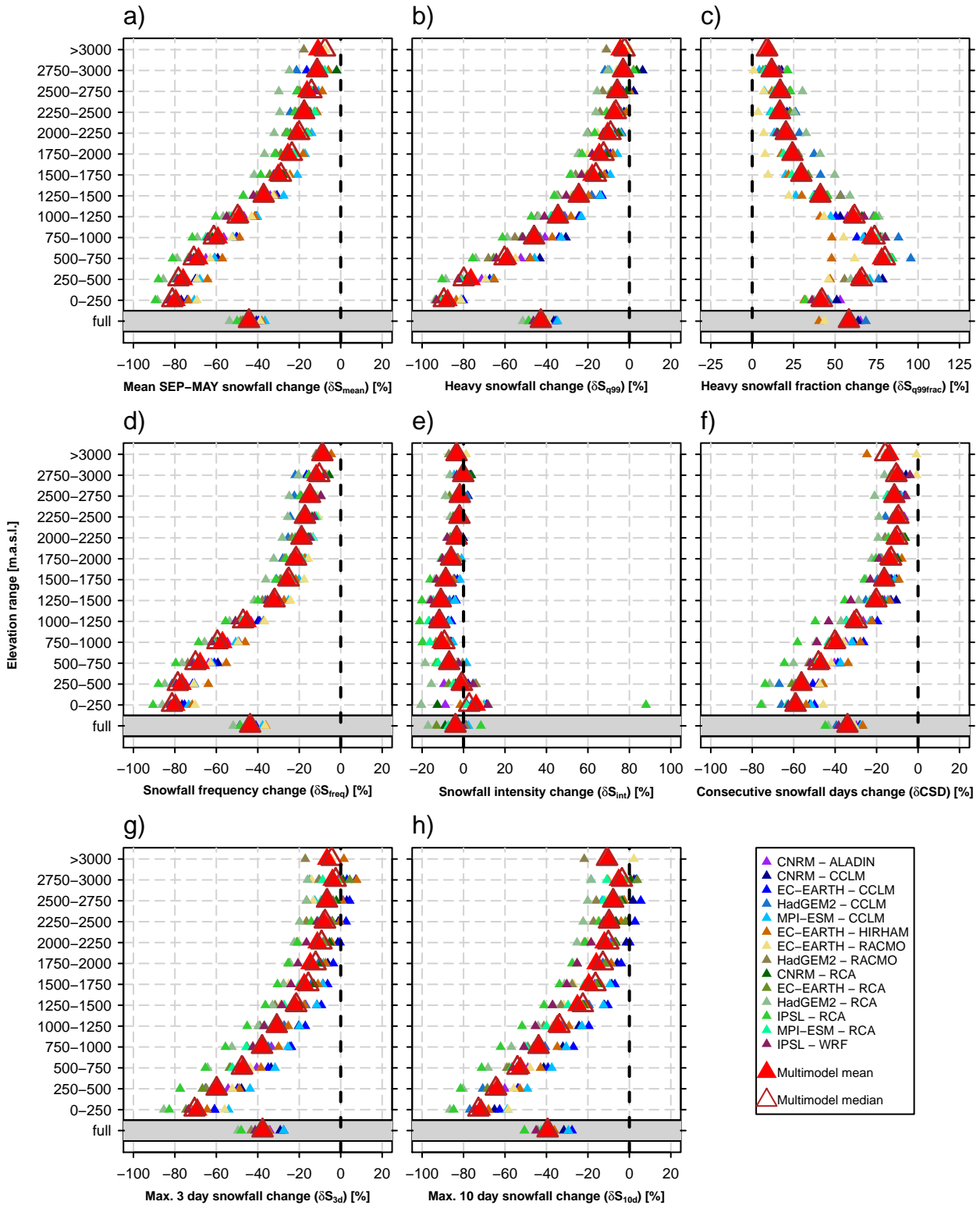


Fig. 5.5: Relative changes (SCEN 2070 - 2099 wrt. CTRL 1981 - 2010) of seasonal (September to May) snowfall indices for RCP8.5 after applying the bias correction to the 14 RCM simulations and separating the snowfall with the Richards method. Small triangles show the individual RCM simulations whereas the large triangles denote the multimodel mean (red, filled) and multimodel median (brown, open). Relative changes for RCP4.5 are shown in Fig. D.5. For the Binary snow fractionation method, see Fig. D.12 (RCP4.5) and Fig. D.17 (RCP8.5).

5.4 Scenario and snow fractionation uncertainty

The climate projection results presented in the sections before, can be assumed to highly depend on the considered emission scenario. Thus, if resources and time permits, simulations are usually carried out with a set of different RCP scenarios in order to quantify emission scenario uncertainty. To get a better feeling of how this type of uncertainty translates into our snowfall projections, we investigate the model results based on a comparison of RCP4.5- and RCP8.5-driven simulations. Figure 5.6 shows the relative changes of various seasonal snowfall indices for both emission scenarios.

Differences in δS_{mean} are most pronounced below 1000 m.a.s.l. (Fig. 5.6 a)). Percental changes under RCP4.5 are approximately 25% smaller than for RCP8.5. At higher elevations, multimodel means are closer together and the multimodel ranges start overlapping. Over the entire Alpine domain, a quarter of current snowfall is expected to be lost under a more moderate emission scenario while a reduction of approximately -50% is projected for RCP8.5. For seasonal cycles, the shift of δS_{mean} between RCP4.5 and RCP8.5 is constant across all months and slightly decreases with altitude (Fig. 5.7). Above 2000 m.a.s.l., multimodel mean changes reveal a different shape. In January and February, the magnitude of δS_{mean} is independent of the chosen RCP simulation, while negative changes before and after mid-winter are more pronounced for RCP8.5 experiments.

Alpine domain mean δS_{q99} almost doubles under the assumption of stronger GHG emissions. (Fig. 5.6 b)). This is due to different projections at lower altitudes whereas above 2000 m.a.s.l. δS_{q99} does not seem to be affected by increases in radiative forcing. Differences in monthly changes are in close analogy to δS_{mean} (Fig. 5.7). Higher emissions lead to a further negative shift in $\delta S_{\text{q99,month}}$. Up to mid-elevations differences are independent of season. At highest elevations, no differences between RCP4.5 and RCP8.5 are detected during the first three months of the year.

Highest RCP scenario discrepancies for $\delta S_{\text{q99frac}}$ are obtained between 250 m.a.s.l. and 1500 m.a.s.l. (Fig. 5.6). While changes in S_{q99frac} are only weakly elevation dependent in RCP4.5, a strong peak evolves under an RCP8.5 scenario at elevations between 500 m.a.s.l. and 1000 m.a.s.l..

September to May δS_{freq} are very similar to δS_{mean} . The RCP4.5-based decrease is generally 5% to 25% lower than for RCP8.5 with declining differences at high regions (Fig. 5.6 d)). The same applies for the monthly statistics (Fig. 5.7). The higher the elevation, the smaller the scenario discrepancies.

δS_{int} differences are of minor nature (Fig. 5.6 e)). Largest emission scenario uncertainties show up at mid-elevations where RCP8.5 simulations tend to produce larger negative changes of S_{int} (Fig. 5.7).

For δCSD , $\delta S_{3\text{d}}$ and $\delta S_{10\text{d}}$ the two emission scenarios differ most at areas below 1000 m.a.s.l. (Fig. 5.6 f), g) and h)). Thus, domain mean changes under RCP8.5 are projected to be two times larger than for the more moderate RCP4.5.

A second projection uncertainty is introduced by the applied snow fractionation method. Binary and Richards snow fraction could potentially lead to different signals. However, a comparison of these two methods does not show significant differences for relative changes of most seasonal snowfall indices (Fig. 5.8). Highest inconsistencies are detected for $\delta S_{\text{q99frac}}$, δS_{freq} and δS_{int} . The Binary method results in a stronger increase of S_{q99frac} at mid-elevations (Fig. 5.8 c)) while the sign of δS_{freq} is more negative (Fig. 5.8 d)) compared to the Richards method. A sizeable offset is identified for changes in S_{int} . In contrast to the mainly negative δS_{int} of the Richards method, δS_{int} derived with the Binary snow fractionation method is generally positive, especially at high elevations.

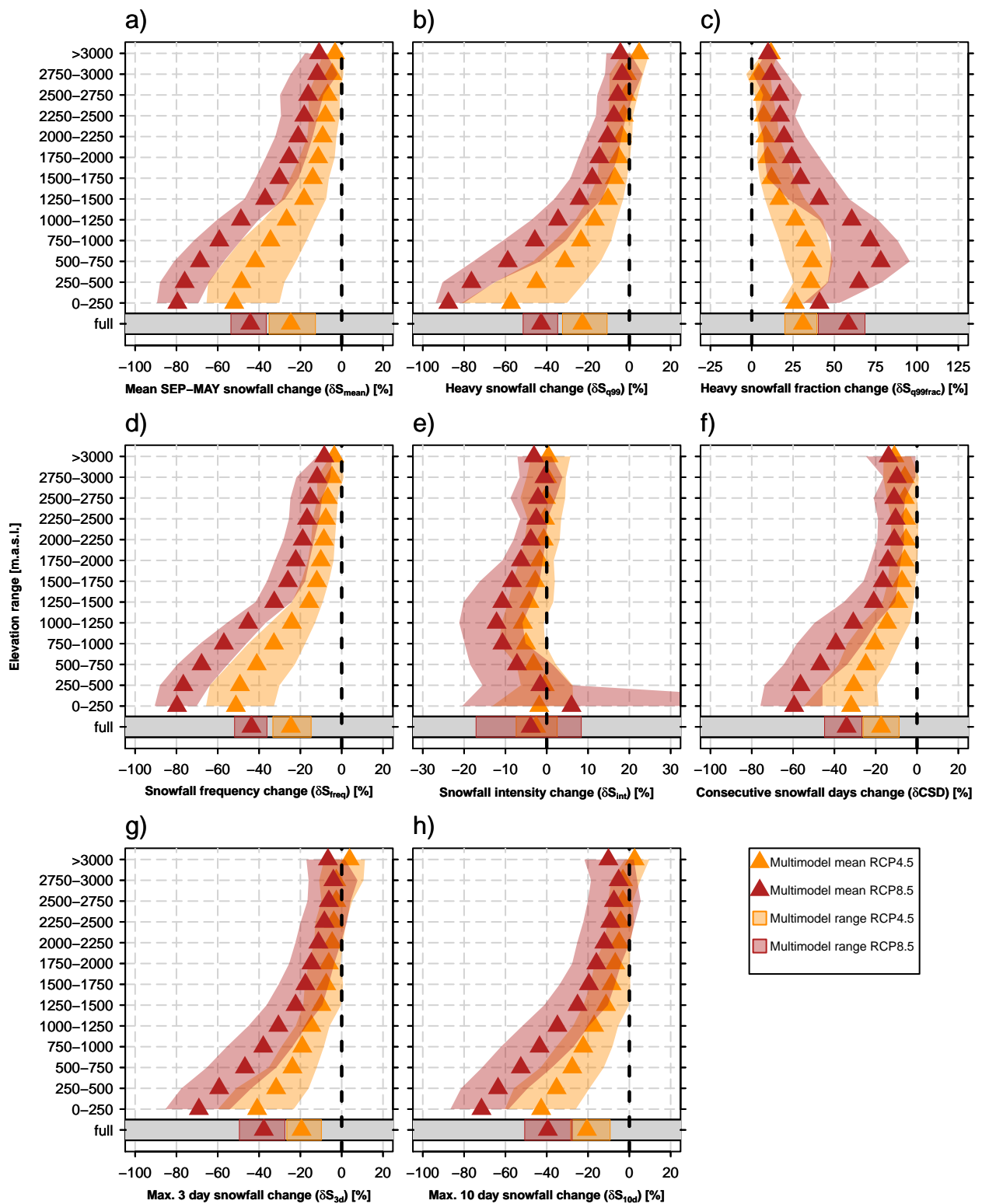


Fig. 5.6: Relative changes (SCEN 2070 - 2099 wrt. CTRL 1981 - 2010) of seasonal (September to May) snowfall indices for RCP4.5 (orange) and RCP8.5 (red) after applying the bias correction to the 14 RCM simulations and separating the snowfall with the Richards Method. The triangles show the multimodel mean according to the respective RCP scenario. The shading represents the multimodel range.

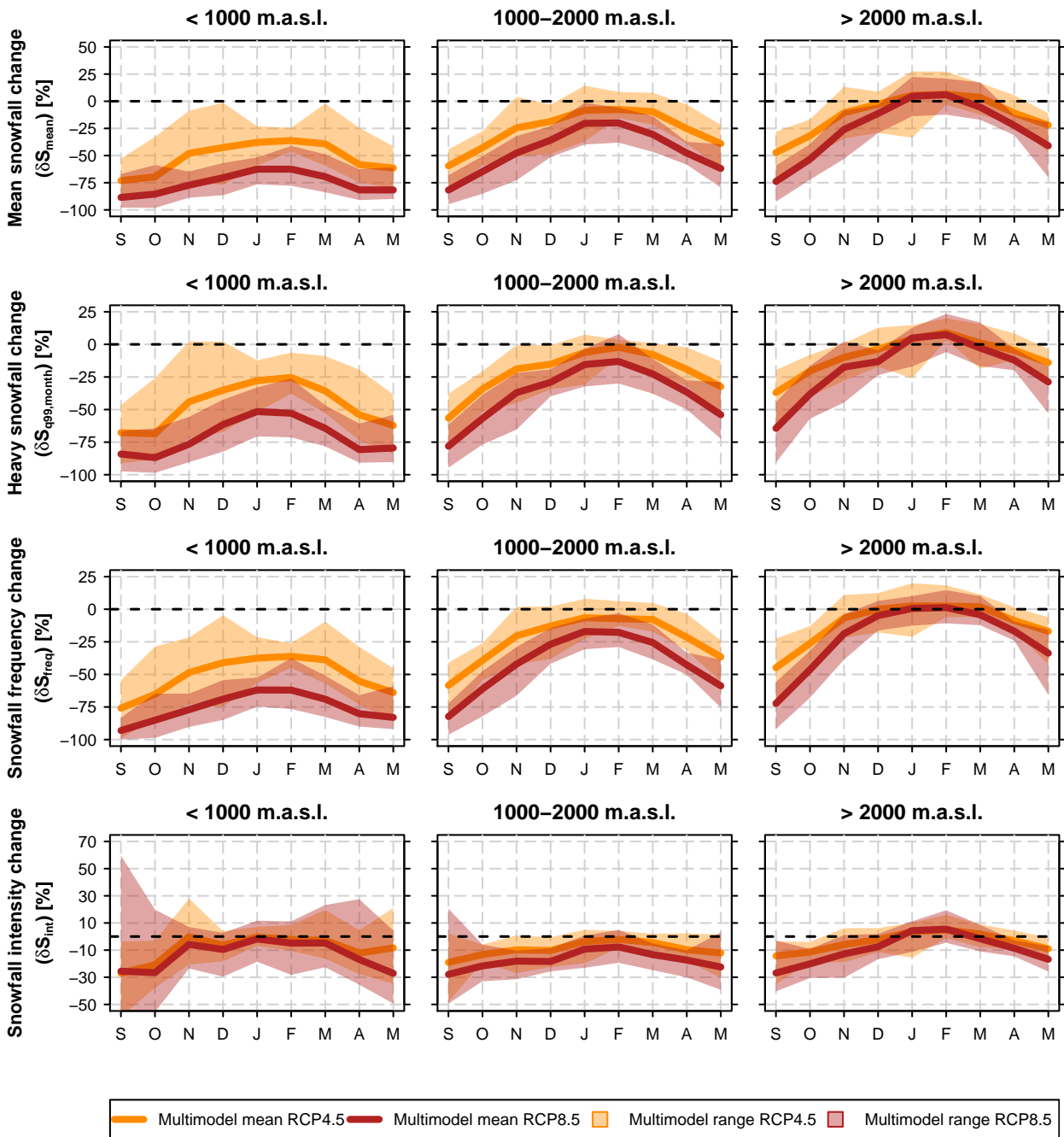


Fig. 5.7: Relative changes (SCEN 2070 - 2099 wrt. CTRL 1981 - 2010) of monthly (September to May) snowfall indices for RCP4.5 (orange) and RCP8.5 (red) after applying the bias correction to the 14 RCM simulations and separating the snowfall with the Richards Method. The lines show the seasonal cycle of the multimodel mean according to the respective RCP scenario. The shading represents the multimodel range. The columns represent the three elevations intervals below 1000 m.a.s.l., between 1000 m.a.s.l. and 2000 m.a.s.l. and above 2000 m.a.s.l.. For the Binary snow fractionation method, see Fig. D.18.

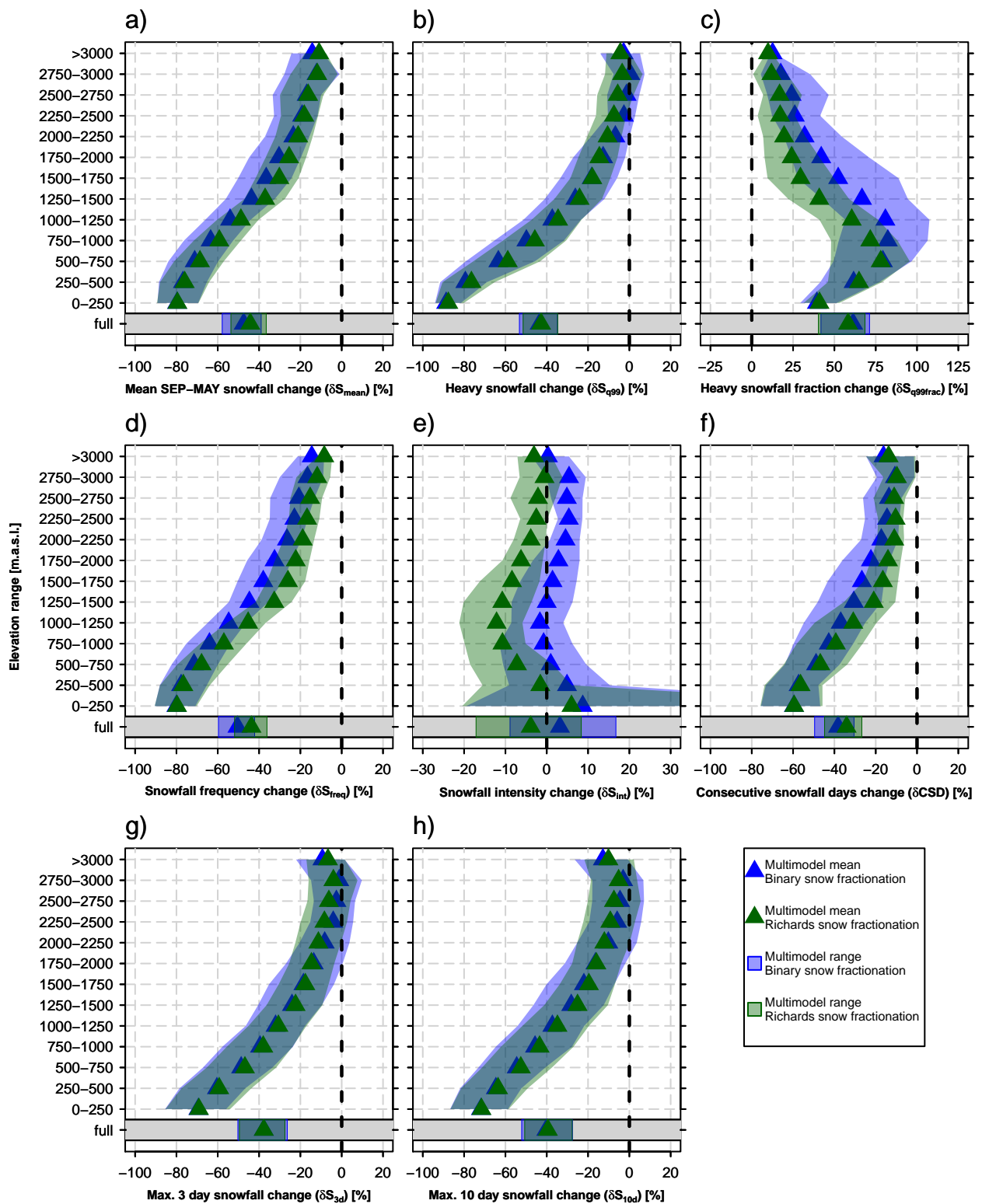


Fig. 5.8: Relative changes (SCEN 2070 - 2099 wrt. CTRL 1981 - 2010) of seasonal (September to May) snowfall indices for RCP8.5 after applying the bias correction to the 14 RCM simulations and separating the snowfall with the Binary (blue) and Richards (green) method. The triangles show the multimodel mean according to the respective snow fractionation method. The shading represents the multimodel range.

5.5 Discussion

The analyses presented on the previous pages indicate substantial changes of snowfall indices over the European Alps in regional climate projections. Most importantly S_{mean} , S_{q99} as well as S_{freq} show substantial decreases. However, in mid-winter, no changes or even slight increases of S_{mean} and $S_{\text{q99,month}}$ at high elevations are expected for both RCP4.5 and RCP8.5. These increases are driven by positive changes of S_{int} while S_{freq} remains constant (see Fig. 5.7). This result is supported by additional analyses given in Figure 5.9. Panels c) and f) indicate, that for elevation intervals and months with positive signs in δS_{mean} and $\delta S_{\text{q99,month}}$, δS_{freq} is nearly constant and close to zero. On the other hand, for these points, a quite linear relationship with δS_{int} is obtained (Fig. 5.9, h) and i). In his study, Deller (2015) came to a similar conclusion for changes in mean precipitation. Nevertheless, the high-elevation mid-winter growth in S_{mean} is smaller than the identified increases of mean winter precipitation by Deller (2015). Additionally, high-elevation S_{mean} peaks in the CTRL climate during early and late winter, $S_{\text{q99,month}}$ during early winter, respectively (see Fig. 5.2 and 5.4). These features might be caused by temperature. As already discussed in Section 3.3, probabilities for (heavy) snowfall are highest in a temperature band slightly below the rain - snow transition. During DJF, temperatures at these elevated regions are too low to carry enough moisture while the transition seasons appear to have many days in the favoured temperature interval under current conditions. With climate change, however, this regime is moving towards January and February resulting in highest S_{mean} and $S_{\text{q99,month}}$ during mid winter in the future. At lower altitudes this is already the case in today's climate.

For elevation intervals with simulated monthly temperatures between $-6\text{ }^{\circ}\text{C}$ and $0\text{ }^{\circ}\text{C}$ in the CTRL period, S_{mean} appears to decrease stronger than $S_{\text{q99,month}}$ (Fig. 5.9 b), e) and l). O'Gorman (2014) found a very similar behaviour while analysing mean and extreme snowfall projections over the Northern Hemisphere with a set of GCMs. He explains these two unequal evolutions with the insensitivity of the temperature interval, at which extreme snowfalls occur, to climate warming. An evaluation of our climate simulations sustains this theory: Mean S_{int} in a given temperature interval is not expected to vary in the future, i.e., highest (mean) intensities will still occur at temperatures slightly below the freezing point by the end of this century (Fig. 5.10, bottom row). Following this line of arguments, the detected relationship between δS_{mean} and δS_{q99} could also partly be influenced by a purely statistical feature introduced by changes in S_{freq} . Frei et al. (2006) estimated frequency and intensity effects on moderate and heavy precipitation percentiles by employing stipulated scaling scenarios. For simplicity, an exponential distribution as an example for a frequency distribution of daily precipitation was assumed. By solely changing the wet-day frequency, they were able to proof that relative decreases in light or moderate percentiles are more pronounced than for large percentiles. I.e., for a given intensity distribution, reductions in S_{freq} lead to stronger relative changes in S_{mean} than in S_{q99} by definition.

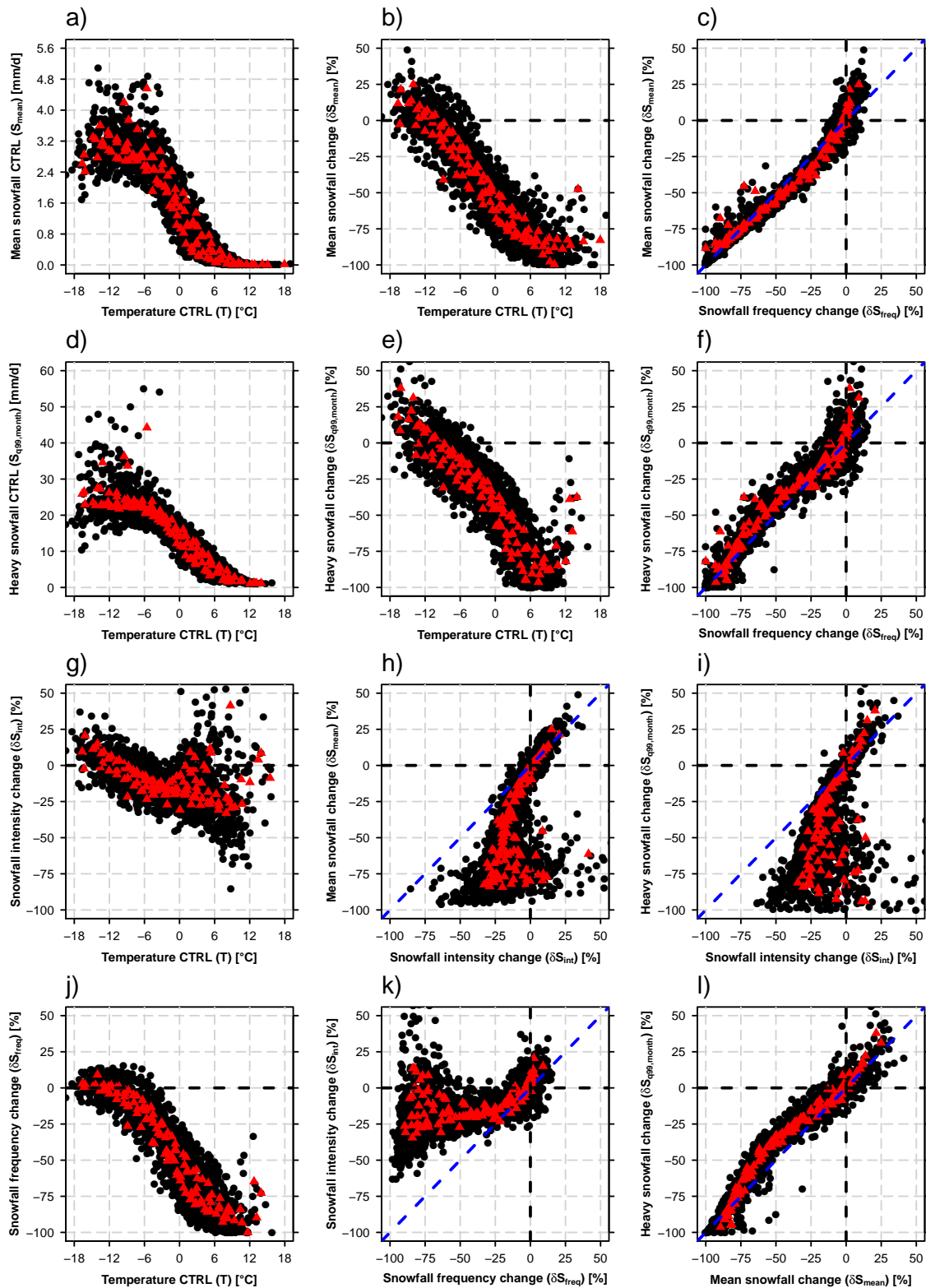


Fig. 5.9: Intercomparison of various snowfall indices and relationship with monthly mean temperature in CTRL. For each panel, the monthly mean statistics over 250 m elevation intervals for the 14 individual RCMs was derived (black circles). Red triangles denote the multimodel mean for a specific month and elevation interval. The monthly statistics is calculated by just considering grid points of the specific elevation intervals which are available for both variables in the corresponding scatterplot (area consistency). The data is taken from the 14 RCM simulations after they were bias-corrected and separated with the Richards method. Relative changes are based on the RCP8.5 driven simulations (SCEN 2070 - 2099 wrt. CTRL 1981 - 2010).

The significant differences for δS_{int} between the Binary and Richards methods (see Fig. 5.8 e)) might arise due to different snow fraction dependencies on temperature. Future temperature increases at mid-elevations are expected to occur in the range of highest snow fraction decreases per degree warming in the Richards snow fractionation method (see Fig. B.1, lower right panel). Thus, a small temperature shift leads to a large change of the snow fraction and lower S_{int} . In the Binary snow fractionation method, snowfalls contributing to S_{int} always have $\text{sf} = 100\%$, i.e. no "snowfall fraction effect" on S_{int} emerges. The two snow fractionation methods also result in very different relative changes in the seasonal cycle of S_{int} (cf. Fig. 5.7 and D.18, bottom row). The large model differences in autumn and spring at lower elevations presumably arise from a small number of analysed grid cells in these seasons and hence from sampling effects.

Nevertheless, the "snowfall fraction effect" does not explain positive monthly variations in δS_{int} (see Fig. 5.7 and 5.9, g)). We guess, that positive changes of S_{int} at high-elevated and cold regions are forced by the higher water holding capacity of the atmosphere in a warmer climate. According to the Clausius-Clapeyron relation, saturation vapour pressure increases by about 7% per degree warming (Held and Soden, 2006). Previous studies show, that simulated changes of heavy and extreme precipitations are consistent with this theory (Allen and Ingram, 2002). However, at mid-elevations this effect might partly be offset by a lower probability of having days in the aforementioned ideal temperature range for snowfall. Besides, at high altitudes, this probability potentially increases, supporting an additional positive shift of S_{int} (Fig. 5.10, top row).

According to Schmucki et al. (2015), who investigated projections of various snowfall indices at station level, biggest absolute changes of S_{freq} by the end of this century are found to occur at high-elevation stations. Conversely, within this project, largest seasonal ΔS_{freq} is obtained at mid-elevations (not shown). One reason for these unequal projections might be, that we left out JJA in our analysis whereas Schmucki considers the whole year. Nevertheless, relative changes for RCP8.5 are in good agreement with station-based results.

Changes of CSD are closely related to reductions in seasonal S_{freq} (see Fig. 5.5 d) and f)). The offset between the fractional changes among these two parameters arise because CSD occurs during longer cold periods in winter. At this time of the year, relative changes in monthly S_{freq} are smaller than the overall seasonal changes (see Fig. 5.7). The same theory can be applied to δS_{3d} and δS_{10d} . Furthermore, δS_{10d} is slightly more negative than δS_{3d} due to the reduction of S_{freq} and CSD which have a stronger impact on the longer time period considered.

Future snowfalls are expected to occur in a narrower temperature interval due to the "loss" of cold days. The fixed upper bound of the snowfall temperature PDF at the snow-rain transition temperature, together with the decrease in the number of cold days, leads to an increase of relative probabilities for snowfall to occur at 0 °C (Fig. 5.10, middle row). Thus, in first approximation, the magnitude of future warming strongly influences the reduction of S_{mean} and S_{q99} by altering S_{freq} . This direct effect becomes clearly visible by comparing the projections of RCP4.5 and RCP8.5 simulations with each other (see Fig. 5.8). For all three indices, domain mean changes reveal similar magnitudes in both emission scenarios. However, for monthly variations with positive signs in δS_{mean} and $\delta S_{\text{q99,month}}$ secondary effects on snowfall need to be taken into account. In these regions, S_{int} , which appears to be tightly linked to temperature changes, is considered to be the main driver of snowfall increases.

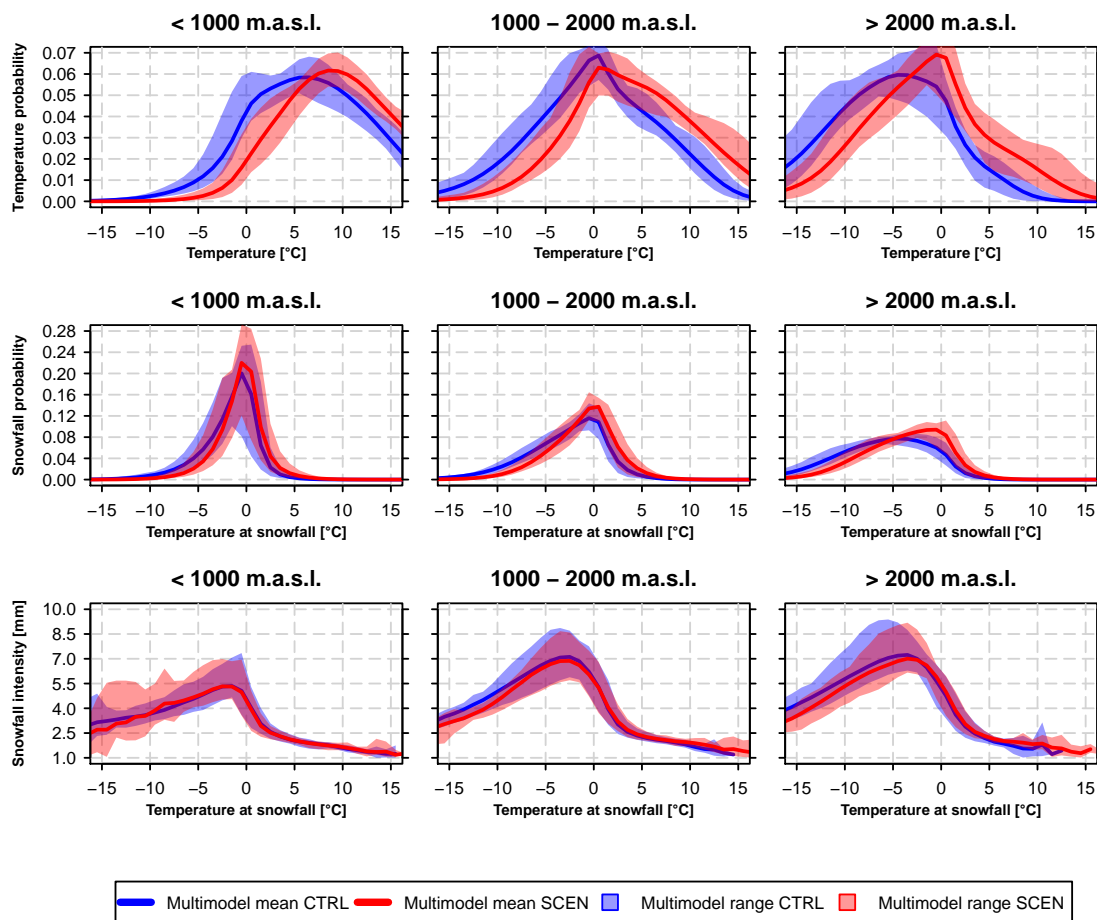


Fig. 5.10: Comparison of temperature probabilities and snowfall intensities for the CTRL period 1981 - 2010 (blue) and SCEN period 2070 - 2099 (red) for RCP8.5. The first row depicts the PDF of the daily temperature distribution, while in the second row only snowfall days, i.e. days with $S > 1$ mm/d, were considered. The third row represents the mean snowfall intensity (S_{int}) for a given snowfall temperature. The lines represent the multimodel mean while the shading represents the multimodel ranges. The PDFs and mean snowfall intensities are calculated by creating daily temperature bins of width 1 °C. The data is taken from the 14 RCM simulations after they were bias-corrected and separated with the Richards method.

6 Simulated raw snowfall

To close the circle, we return back to simulated raw snowfall which has already shortly been introduced in Section 1.2. A subset of six EURO-CORDEX simulations, namely EC-EARTH - HIRHAM, EC-EARTH - RACMO, CNRM - RCA, EC-EARTH - RCA, HadGEM2 - RCA, and IPSL - WRF, provide snowfall as output variable.

In climate models, precipitation is parametrised by using microphysic schemes that might differ from model to model. Thereby both solid and liquid phases need to be accounted for (e.g. Seifert and Beheng (2005)). Compared to solely liquid schemes (e.g. Kessler (1969)), further processes, such as melting, freezing, ice particle initiation or sedimentation need to be implemented for solid phases. Due to a wide variety of ice particle characteristics, ice microphysics is significantly more complicated than liquid microphysics. This leads to larger uncertainties in the parameter estimations and the corresponding simulated snowfall (Morrison (2010); Rutledge and Hobbs (1984); Straka and Mansell (2005)).

6.1 Evaluation of simulated raw snowfall

Figure 6.1 presents the various seasonal (September to May, 1971-2005) snowfall indices based on the separated + bias corrected, separated + not bias corrected and raw snowfall for the six mentioned simulations above. For convenience, only multimodel means are shown. The observational analysis is denoted by black circles. Raw multimodel means of S_{q99} , $S_{q99frac}$, S_{int} and S_{3d} are able to outperform the separated + bias-corrected snowfall indices by considering domain mean results only. Furthermore, a close similarity between raw and separated + not bias corrected snowfall indices is detected.

A comparison for individual models shows that not applying any bias correction and using the introduced Richards snow fractionation method at initial $T^* = 2 \text{ }^\circ\text{C}$ (see Eq. 2.12) generally leads to a good approximation of simulated raw snowfall for EC-EARTH HIRHAM, EC-EARTH - RACMO and IPS-WRF (Fig. E.1). The RCA RCMs have larger discrepancies between the separated + not bias corrected approach and raw snowfall outputs. It might be, that the parametrisation of the temperature 2 m above ground (T_{2m}) in this RCM is flawed (cold biased) relative to the prognostic layer temperatures. Thus, raw snowfall, which depends on prognostic temperatures but not on the diagnostic T_{2m} , results in higher amounts (personal discussion S. Kotlarski). Separating not bias-corrected precipitation data with the Binary method at initial $T^* = 2 \text{ }^\circ\text{C}$ (see Eq. 2.5) results in a (further) overestimation of S_{q99} compared to the raw-based values (not shown). This is in accordance with the differences of the two snow fractionation methods as already discussed in Section 3.3.

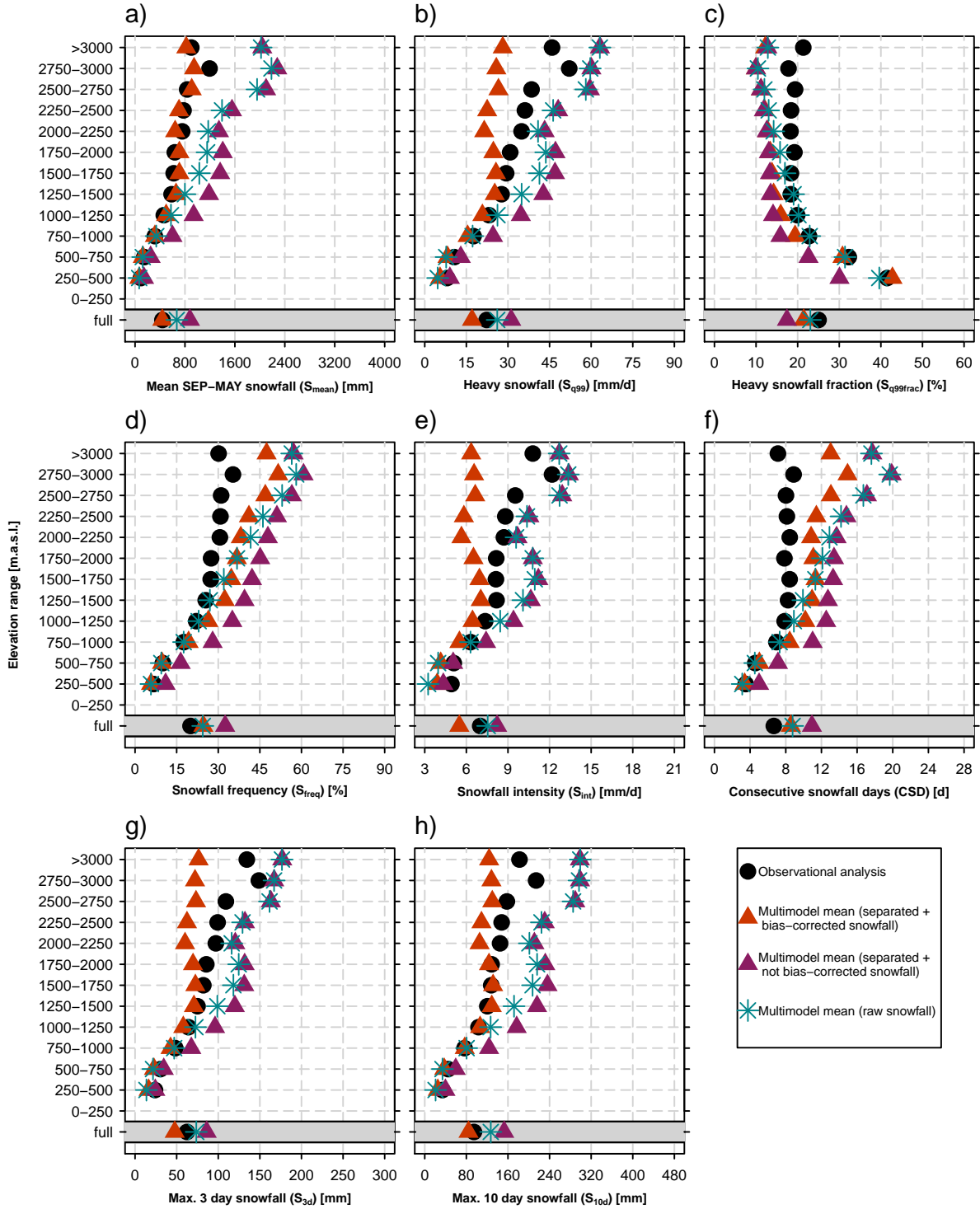


Fig. 6.1: Evaluation of seasonal (September to May) snowfall indices in the period 1971 - 2005 for a subset of six EURO-CORDEX simulations (EC-EARTH - HIRHAM, EC-EARTH - RACMO, CNRM - RCA, EC-EARTH - RCA, HadGEM2 - RCA, IPSL - WRF). The black circles represent the observation-based analysis (snow fractionation with Richards method at $T^* = 2^\circ\text{C}$, see Eq. 2.12). Red triangles denote the multimodel mean based on the separated + bias-corrected snowfall (snow fractionation with Richards method at $T^*_{a,RI}$, see Tab. C.1). The multimodel mean determined by the separated + not bias-corrected snowfall is shown in violet (snow fractionation with Richards method at $T^* = 2^\circ\text{C}$). The multimodel mean of the simulated raw snowfall output is represented by turquoise asterisks. The Evaluation is constrained to the Swiss domain (see Sec. 2.3).

6.2 Projections of simulated raw snowfall

Results in Figure 6.2 support the assumptions we already made in Section 4.5. Whether we correct the separated snowfall or not, or we simply use raw model results, relative change signals don't differ much. Hence, the separated + bias corrected simulations reveal largest reductions for the indices S_{mean} , S_{q99} , S_{3d} and S_{10d} . Separated + not bias corrected and raw snowfall projections result in similar variations. By snow fractionating the separated + bias corrected data with the Richards method, δS_{int} of all three data sets are in very good agreement. Separation with the Binary method has a less negative effect of δS_{int} at mid-elevations (see Fig. 5.8 e). Thus, the separated + bias-corrected and separated + not bias-corrected δS_{int} would diverge more from raw S_{int} (not shown).

In view of this short analysis we're able to take the following conclusions: 1) For certain RCMs, such as HIRHAM, RACMO and WRF, separation of the biased precipitation with the Richards snow fractionation method at initial $T^* = 2 \text{ }^\circ\text{C}$ can be used as a proxy for the simulated raw snowfall and related indices. However, it is tenuous to adopt this approach to other simulations without having additional information on possible biases. 2) If the main interest focuses on analysing relative change signals rather than absolute ones, one can abstain from a time consuming and error prone bias correction approach.

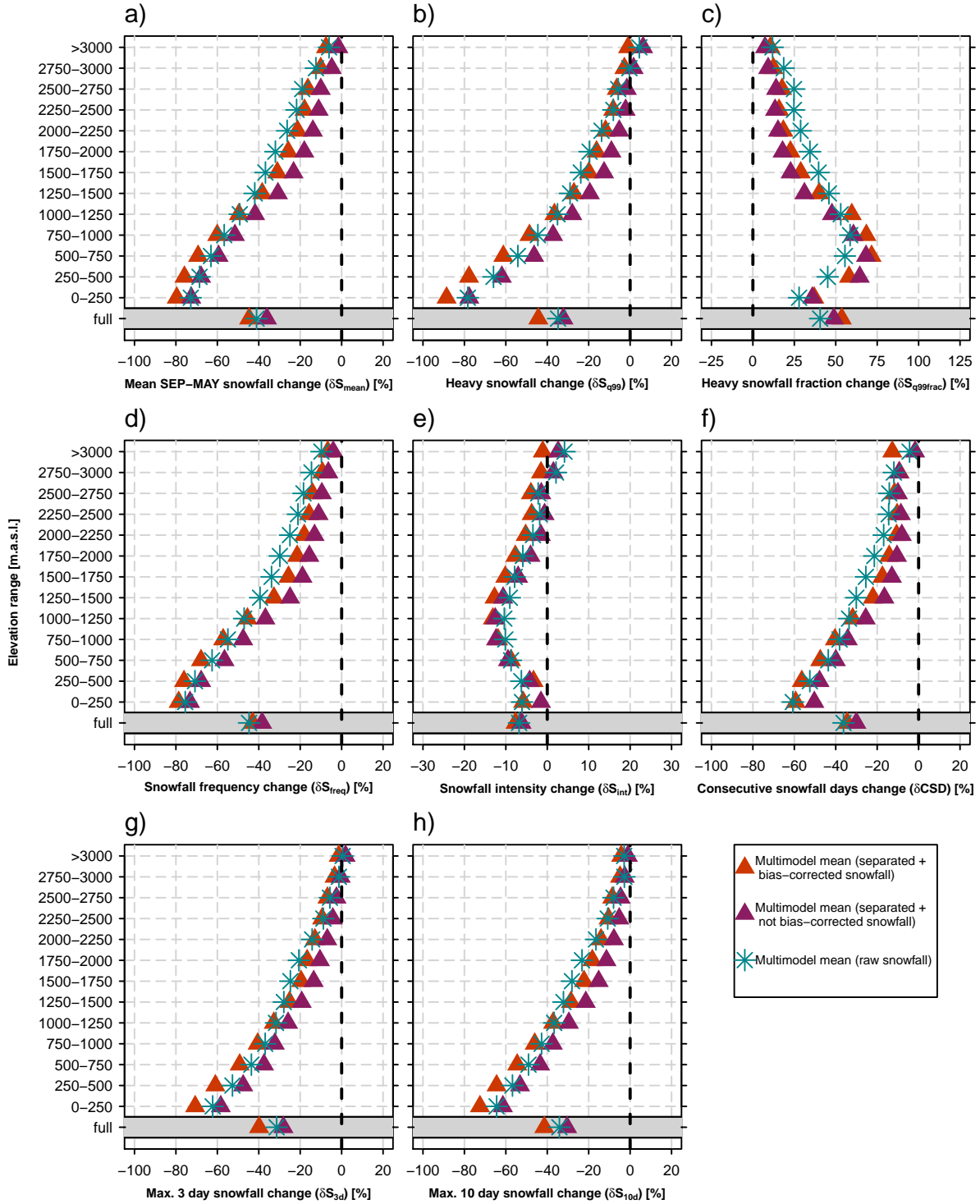


Fig. 6.2: Relative changes (SCEN 2070 - 2099 wrt. CTRL 1981 - 2010) of seasonal (September to May) snowfall indices for RCP8.5 and for a subset of six EURO-CORDEX Simulations (EC-EARTH - HIRHAM, EC-EARTH - RACMO, CNRM - RCA, EC-EARTH - RCA, HadGEM2 - RCA, IPSL - WRF). The black circles represent the observation-based analysis (snow fractionation with Richards method at $T^* = 2 \text{ }^\circ\text{C}$, see Eq. 2.12). Red triangles denote the multimodel mean based on the separated + bias-corrected snowfall (snow fractionation with Richards method at $T^*_{a,RI}$, see Tab. C.1). The multimodel mean determined by the separated + not bias-corrected snowfall is shown in violet (snow fractionation with Richards method at $T^* = 2 \text{ }^\circ\text{C}$). The multimodel mean of the simulated raw snowfall output is represented by turquoise asterisks. The projected change signals are based on the entire Alpine domain (see Sec. 2.3).

7 Conclusions and Outlook

Within this thesis, we were able to analyse scale effects on snowfall and to work out a simple bias correction for separated snowfall. Furthermore, future changes of snowfall over the Alps have been assessed and brought in connection with previous studies. In the following we summarise the most important findings in terms of the scientific objectives we defined in Section 1.4.

1. Objective: Snowfall separation and scale effect

Binary snow fractionation with a fixed temperature threshold on two grids containing the same data information but having different spatial resolution leads to an underestimation of mean snowfall and overestimation of heavy snowfall on the coarser grid (see Fig. 3.1). The effect on heavy snowfall is larger due to its occurrence close to the rain - snow transition. Thus, the Binary method assigns a snow fraction of 100% which does not hold for all heavy snowfall events (see Fig. B.1). To overcome the problematic issue of having a sharp boundary transition between snow and rain, the Richards method was implemented. This approach expresses the snow fraction dependence on daily mean temperature as a function of the topographical standard deviation. Hence, we account for the altitudinal variability which results in better estimates for mean and heavy snowfall in coarse grid boxes.

Parameters used for the Richards snow fractionation method (see Eq. 2.13 and 2.14) were fitted for the Swiss domain only and then applied to the entire Alpine domain. Whether this relationship is robust and practicable could be further investigated by using observational data sets which cover the full domain of interest. Furthermore, the initial binary snowfall separation on the high resolution grid with a snow fractionation temperature of 2 °C might be compared to real station measurements.

2. Objective: Employment of a bias correction approach and comparison of observation-based and simulated snowfall indices.

Many simulations of the current EURO-CORDEX ensemble are still subject to significant biases in precipitation as well as in temperature. In our evaluation period from 1971 to 2005 (with removed summer months JJA), simulated precipitation is largely overestimated, with increasing biases toward higher altitudes. On the other hand, near surface temperatures are generally too low with largest deviations over mountainous regions. These findings have already been found in previous RCM ensemble studies (e.g. Frei et al. (2003); Rajczak et al. (2013)).

By implementing a simple bias correction approach we are partly able to address these errors in order to reduce model spread which finally results in more robust change estimates. Seasonal cycles of mean snowfall can be reproduced fairly well. Nevertheless, for better es-

timations of heavy snowfall-related indices, more sophisticated correction methods need to be employed. The adjustments introduced here are neither able to solve existing underestimated snowfall intensities and overestimated snowfall frequencies in RCMs satisfactorily nor do they improve inaccurate distribution patterns sufficiently (see Fig. 4.2, 4.3 and 4.4). For doing so, a quantile mapping (Rajczak et al., 2016) or a local intensity scaling of precipitation (Schmidli et al., 2006) might lead to more promising results. Yet, a comparison to simulated raw snowfall revealed that relative change signals are almost independent of the chosen correction approach (see Fig. 6.2). Notable differences only emerge for absolute changes. Thus, if the main interest focuses on analysing relative change signals, one might abstain from a time consuming and error prone bias correction approach.

3. Objective: Projections of different snowfall indices for the late 21st century

Climate change signals have been assessed by comparing variations of snowfall indices between the CTRL period 1981 - 2010 and SCEN period 2070 - 2099. Our results show that by the end of the 21st century, snowfall over the Alpine domain will be significantly reduced. Between September and May, mean snowfall is expected to decrease by approximately -45% under an RCP8.5 scenario. For the more moderate scenario, i.e., RCP4.5, projections show a decline of -25% (see Fig. 5.6). These results are in good agreement with previous studies (e.g. de Vries et al. (2014); Piazza et al. (2014)). Low lying areas experience the largest changes of up to -80% while the highest Alpine regions are only weakly affected. Variations of heavy snowfall, defined by the 99% all-day snowfall percentile, show an even more pronounced signal at lowermost altitudes. With increasing elevation, changes are generally smaller than for mean snowfall. Largest differences are observed between 500 m.a.s.l. and 1500 m.a.s.l. (see Fig. 5.5). O’Gorman (2014) found a very similar behaviour by analysing changes in mean and extreme snowfall over the Northern Hemisphere. He points out that heavy and extreme snowfall occur near an optimal temperature which seems to be independent on climate warming. In this thesis, we cannot answer conclusively whether contrasting responses between mean and heavy snowfall changes are driven by different physical processes. This feature might also partly be a statistical artefact generated by different dependencies of snowfall percentile variations on snowfall frequency changes (Frei et al., 2006).

In first approximation, the magnitude of future warming strongly influences the reduction of mean and heavy snowfall by modifying the snowfall frequency (see Fig. 5.9). Snowfall increases obtained at restricted climatologically cool and high-elevation regions, however, are not caused by frequency changes (see Fig. 5.7). At these locations, snowfall is assumed to increase due to more intense precipitation. With increasing temperatures, climatologically cool areas are shifted in a temperature interval which favours stronger snowfall intensities (see Fig. 5.10). Nevertheless, due to complex relationships between temperature, snowfall frequency and intensity, respectively, further research on this topic is desirable.

Future changes of winter precipitation over the Alps can lead to a variety of impacts in different sectors. With decreasing snowfall frequencies and the increase of the snowline (Steger et al., 2013), both associated to temperature changes, ski lift operators are looking into an uncertain future. A shorter snowfall season puts them under great financial pressure. Only for ski areas reaching up to high elevations, the climate change effects might be manageable. Even so they might start later into the ski season, the snow conditions into early spring, are expected to change less dramatically. Hence, it might be that the projected snowfall increase during the first months of the year allows them to extend their market share by offer additional ski touring packages in spring etc..

At lower altitudes, an intensification of winter precipitation, combined with smaller snowfall fractions (Serquet et al., 2013) increases the flood potential (Beniston, 2012). Snow can act as a buffer by releasing melt water constantly over a longer period of time. With climate warming, this storage capacity is lost, and heavy precipitation immediately drains into streams and rivers which might not be able to take up the vast amount of water fast enough. Less snowmelt in spring will also have impacts on hydro power generation and water management. So far, many Alpine regions are able to bypass dry periods by tapping melt water from the mountains. With reduced snow-packs, due to less snowfall, water shortage becomes a serious problem.

Regarding future socio-economic impacts caused by extreme snowfall events, conclusions based on the results presented in this study are difficult to draw. In our opinion, the 99% all-day snowfall percentile we used for defining heavy snowfalls, is not appropriate to speculate about future evolutions of (very) rare events (Schär et al., 2016). To do so, one might consider applying a generalized extreme value (GEV) analysis which is more suitable for answering questions related to extreme events.

Bibliography

- Abegg, S., B. Agrawala, F. Crick, and A. de Montfalcon. Climate change impacts and adaptation in winter tourism. In Agrawala, S., editor, *Climate change in the European Alps: adapting winter tourism and natural hazards management*, Book Section 2, pages 25–125. Organisation for Economic Cooperation and Development (OECD), Paris, France, 2007. doi: 10.1787/9789264031692-en.
- Agrawala, S. The European Alps: Location, Economy and Climate. In Agrawala, S., editor, *Climate change in the European Alps: adapting winter tourism and natural hazards management*, Book Section 1, pages 17–24. Organisation for Economic Cooperation and Development (OECD), Paris, France, 2007. doi: 10.1787/9789264031692-en.
- Allen, M. R. and W. J. Ingram. Constraints on future changes in climate and the hydrologic cycle. *Nature*, 419(6903):224–232, 2002. doi: 10.1038/nature01092.
- Ammann, W. J. Lawinen. In OccC, editor, *Extremereignisse und Klimaänderung*, Book Section 2.9, pages 77–80. Organe consultatif sur les changements climatiques (OccC), Bern, Switzerland, 2013.
- Beniston, M. Impacts of climatic change on water and associated economic activities in the Swiss Aps. *Journal of Hy*, 412, 2012. doi: 10.1016/j.jhydrol.2010.06.046.
- Collins, M., R. Knutti, J. Arblaster, J.-L. Dufresne, T. Fichfet, P. Friedlingstein, X. Gao, W. Gutowski, T. Johns, G. Krinner, M. Shongwe, C. Tebaldi, A. Weaver, and M. Wehner. Long-term Climate Change: Projections, Commitments and Irreversibility. In Stocker, T., D. Qin, G.-K. Plattner, M. Tignor, S. Allen, J. Boschung, A. Nauels, Y. Xia, V. Bex, and P. Midgley, editors, *Climate Change 2013: The Physical Science Basis. Contribution of Working Group I to the Fifth Assessment Report of the Intergovernmental Panel on Climate Change*, book section 12, pages 1029–1136. Cambridge University Press, Cambridge, United Kingdom and New York, NY, USA, 2013. doi: 10.1017/CBO9781107415324.024.
- Cubasch, U., D. Wuebbles, D. Chen, M. Facchini, D. Frame, N. Mahowald, and J.-G. Winther. Introduction. In Stocker, T., D. Qin, G.-K. Plattner, M. Tignor, S. Allen, J. Boschung, A. Nauels, Y. Xia, V. Bex, and P. Midgley, editors, *Climate Change 2013: The Physical Science Basis. Contribution of Working Group I to the Fifth Assessment Report of the Intergovernmental Panel on Climate Change*, book section 1, pages 119–158. Cambridge University Press, Cambridge, United Kingdom and New York, NY, USA, 2013. doi: 10.1017/CBO9781107415324.007.
- Dai, A. Precipitation characteristics in eighteen coupled climate models. *Journal of Climate*, 19(18):4605–4630, 2006. doi: 10.1175/JCLI3884.1.

- de Vries, H., G. Lenderink, and E. Meijgaard. Future snowfall in western and central Europe projected with a high-resolution regional climate model ensemble. *Geophysical Research Letters*, 41(12):4294–4299, 2014. doi: 10.1002/2014GL059724.
- Deller, M. Revisiting 21st century projections of extreme precipitation based on an ensemble of Euro-CORDEX RCM simulations. Master’s thesis, ETH Zurich, 2015.
- Elsasser, H. and P. Messerli. The vulnerability of the snow industry in the Swiss Alps. *Mountain research and development*, 21(4):335–339, 2001. doi: 10.1659/0276-4741(2001)021[0335:TVOTSI]2.0.CO;2.
- Frei, C. Interpolation of temperature in a mountainous region using nonlinear profiles and non-euclidean distances. *International Journal of Climatology*, 34(5):1585–1605, 2014. doi: 10.1002/joc.3786.
- Frei, C., J. H. Christensen, M. Déqué, D. Jacob, R. G. Jones, and P. L. Vidale. Daily precipitation statistics in regional climate models: Evaluation and intercomparison for the European Alps. *Journal of Geophysical Research*, 108(D3), 2003. doi: doi:10.1029/2002JD002287.
- Frei, C., R. Schöll, S. Fukutome, J. Schmidli, and P. L. Vidale. Future change of precipitation extremes in Europe: Intercomparison of scenarios from regional climate models. *Journal of Geophysical Research*, 111(D6), 2006. doi: 10.1029/2005JD005965.
- Frei, C. and C. Schär. A precipitation climatology of the alps from high-resolution rain-gauge observations. *International Journal of Climatology*, 18(8):873–900, 1998. doi: 10.1002/(SICI)1097-0088(19980630)18:8<873::AID-JOC255>3.0.CO;2-9.
- Giorgi, F. Regional climate modeling: Status and perspectives. *Journal de Physique IV (Proceedings)*, 139(1):101–118, 2006. doi: 10.1051/jp4:2006139008.
- Giorgi, F. Simulation of regional climate using a limited area model nested in a general circulation model. *Journal of Climate*, 3(9):941–963, 1990. doi: 10.1175/1520-0442(1990)003<0941:SORCUA>2.0.CO;2.
- Gobiet, A., S. Kotlarski, M. Beniston, G. Heinrich, J. Rajczak, and M. Stoffel. 21st century climate change in the European Alps: A review. *Science of the Total Environment*, 493: 1138–1151, 2014. doi: 10.1016/j.scitotenv.2013.07.050.
- Haechler, P. and D. Gerstgrasser. Early Warnings for extreme snowfall in the Swiss Alps. In *10th EMS Annual Meeting, 10th European Conference on Applications of Meteorology (ECAM) Abstracts, held Sept. 13-17, 2010 in Zürich, Switzerland*, volume 1, pages 353–355, 2009.

- Hawkins, E. and R. Sutton. The potential to narrow uncertainty in regional climate predictions. *Bulletin of the American Meteorological Society*, 90(8):1095–1107, 2009. doi: 10.1175/2009BAMS2607.1.
- Held, I. M. and B. J. Soden. Robust responses of the hydrological cycle to global warming. *Journal of Climate*, 19(21):5686–5699, 2006. doi: 10.1175/JCLI3990.1.
- IPCC. Summary for Policymakers: Emissions Scenarios. A Special Report of Working Group III of the Intergovernmental Panel on Climate Change. Technical report, Intergovernmental Panel on Climate Change (IPCC), 2000.
- IPCC. *Climate Change 2013: The Physical Science Basis. Contribution of Working Group I to the Fifth Assessment Report of the Intergovernmental Panel on Climate Change*. Cambridge University Press, Cambridge, United Kingdom and New York, NY, USA, 2013. doi: 10.1017/CBO9781107415324.
- Isotta, F. A., C. Frei, V. Weigluni, M. Perčec Tadić, P. Lassègues, B. Rudolf, V. Pavan, C. Cacciamani, G. Antolini, S. M. Ratto, M. Munari, S. Micheletti, V. Bonati, C. Lussana, C. Ronchi, E. Panettieri, G. Marigo, and G. Vertačnik. The climate of daily precipitation in the Alps: Development and analysis of a high-resolution grid dataset from pan-Alpine rain-gauge data. *International Journal of Climatology*, 34(5):1657–1675, 2014. doi: 10.1002/joc.3794.
- Jacob, D., J. Petersen, B. Eggert, A. Alias, O. Christensen, L. M. Bouwer, A. Braun, A. Colette, M. Déqué, G. Georgievski, E. Georgopoulou, A. Gobiet, L. Menut, G. Nikulin, A. Haensler, N. Hempelmann, C. Jones, K. Keuler, S. Kovats, N. Kröner, S. Kotlarski, A. Kriegsmann, E. Martin, E. van Meijgaard, C. Moseley, S. Pfeifer, S. Preuschmann, C. Radermacher, K. Radtke, D. Rechid, M. Rounsevell, P. Samuelsson, S. Somot, J. F. Soussana, C. Teichmann, R. Valentini, R. Vautard, B. Weber, and P. Yiou. EURO-CORDEX: New high-resolution climate change projections for European impact research. *Regional Environmental Change*, 14(2):563–578, 2013. doi: 10.1007/s10113-013-0499-2.
- Kendon, E. J., N. M. Roberts, C. A. Senior, and M. J. Roberts. Realism of rainfall in a very high-resolution regional climate model. *Journal of Climate*, 25(17):5791–5806, 2012. doi: 10.1175/JCLI-D-11-00562.1.
- Kessler, E. On the distribution and continuity of water substance in atmospheric circulation. *Meteorological Monographs*, 10(32):84, 1969.
- Kienzle, S. W. A new temperature based method to separate rain and snow. *Hydrological Processes*, 22(26):5067–5085, 2008. doi: 10.1002/hyp.7131.
- Koenig, U. and B. Abegg. Impacts of climate change on winter tourism in the swiss alps. *Journal of sustainable tourism*, 5(1):46–58, 1997. doi: 10.1080/09669589708667275.

- Konzelmann, T., B. Wehren, and Weingartner. Niederschlagsmessnetze, 2007. Hydrological Atlas of Switzerland, HADES, available from University of Bern, Plate 2.1.
- Kotlarski, S., K. Keuler, O. B. Christensen, a. Colette, M. Déqué, a. Gobiet, K. Goergen, D. Jacob, D. Lüthi, E. Van Meijgaard, G. Nikulin, C. Schär, C. Teichmann, R. Vautard, K. Warrach-Sagi, and V. Wulfmeyer. Regional climate modeling on European scales: A joint standard evaluation of the EURO-CORDEX RCM ensemble. *Geoscientific Model Development*, 7(4):1297–1333, 2014. doi: 10.5194/gmd-7-1297-2014.
- Laternser, M. and M. Schneebeli. Long-term snow climate trends of the Swiss Alps (1931–99). *International Journal of climatology*, 23(7):733–750, 2003. doi: 10.1002/joc.912.
- Lute, A. C., J. T. Abatzoglou, and K. C. Hegewisch. Projected changes in snowfall extremes and interannual variability of snowfall in the western United States. *Water Resources Research*, 51(2):960–972, 2015. doi: 10.1002/2014WR016267.
- Marty, C. Regime shift of snow days in Switzerland. *Geophysical Research Letters*, 35(12), 2008. doi: 10.1029/2008GL033998. L12501.
- Marty, C. and J. Blanchet. Long-term changes in annual maximum snow depth and snowfall in Switzerland based on extreme value statistics. *Climatic Change*, 111(3):705–721, 2011. doi: 10.1007/s10584-011-0159-9.
- McAfee, S. A., J. Walsh, and T. S. Rupp. Statistically downscaled projections of snow/rain partitioning for Alaska. *Hydrological Processes*, 28(12):3930–3946, 2014. doi: 10.1002/hyp.9934.
- MeteoSwiss. Daily Precipitation (final analysis): RhiresD, February 2013a. URL http://www.ifu.ethz.ch/hydrologie/research/research_data/proddocrhiresd.pdf. Date of query: 01.02.2016.
- MeteoSwiss. Daily Mean, Minimum and Maximum Temperature: TabsD, TminD ,TmaxD, February 2013b. URL http://www.ifu.ethz.ch/hydrologie/research/research_data/proddoctabsd.pdf. Date of query: 01.02.2016.
- Morrison, H. An overview of cloud and precipitation microphysics and its parametrization in models. In *WRF workshop*, Boulder, USA, November 2010. Presentation.
- Moss, R. H., J. A. Edmonds, K. A. Hibbard, M. R. Manning, S. K. Rose, D. P. Van Vuuren, T. R. Carter, S. Emori, M. Kainuma, T. Kram, et al. The next generation of scenarios for climate change research and assessment. *Nature*, 463(7282):747–756, 2010. doi: 10.1038/nature08823.
- Neff, E. How much rain does a rain gage gage? *Journal of Hydrology*, 35:213–220, 1977. doi: 10.1016/0022-1694(77)90001-4.

- O’Gorman, P. Contrasting responses of mean and extreme snowfall to climate change. *Nature*, 512(7515):416–418, 2014. doi: 10.1038/nature13625.
- Piazza, M., J. Boé, L. Terray, C. Pagé, E. Sanchez-Gomez, and M. Déqué. Projected 21st century snowfall changes over the French Alps and related uncertainties. *Climatic Change*, 122(4):583–594, 2014. doi: 10.1007/s10584-013-1017-8.
- Plaut, G., E. Schuepbach, and M. Doctor. Heavy precipitation events over a few Alpine sub-regions and the links with large-scale circulation, 1971-1995. *Climate Research*, 17(3): 285–302, 2001. doi: 10.3354/cr017285.
- Rajczak, J., P. Pall, and C. Schär. Projections of extreme precipitation events in regional climate simulations for Europe and the Alpine Region. *Journal of Geophysical Research: Atmospheres*, 118(9):3610–3626, 2013. doi: 10.1002/jgrd.50297.
- Rajczak, J., S. Kotlarski, and C. Schär. Does quantile mapping of simulated precipitation correct for biases in transition probabilities and spell-lengths? *Journal of Climate*, 29(5): 1605–1615, 2016. doi: 10.1175/JCLI-D-15-0162.1.
- Richards, F. J. A flexible growth function for empirical use. *Journal of Experimental Botany*, 10(2):290–301, 1959. doi: 10.1093/jxb/10.2.290.
- Rummukainen, M. State-of-the-art with regional climate models. *Wiley Interdisciplinary Reviews-Climate Change*, 1(1):82–96, 2010. doi: 10.1002/wcc.8.
- Rutledge, S. A. and P. V. Hobbs. The mesoscale and microscale structure and organization of clouds and precipitation in midlatitude cyclones. XII: A diagnostic modeling study of precipitation development in narrow cold-frontal rainbands. *Journal of the Atmospheric Sciences*, 41(20):2949–2972, 1984. doi: 10.1175/1520-0469(1984)041<2949:TMAMSA>2.0.CO;2.
- Schär, C., N. Ban, E. M. Fischer, J. Rajczak, J. Schmidli, C. Frei, F. Giorgi, T. R. Karl, E. J. Kendon, A. M. G. K. Tank, P. A. O’Gorman, J. Sillmann, X. Zhang, and F. W. Zwiers. Percentile indices for assessing changes in heavy precipitation events. *Climatic Change*, pages 1–16, 2016. doi: 10.1007/s10584-016-1669-2.
- Scherrer, S. C., C. Appenzeller, and M. Latarnser. Trends in Swiss Alpine snow days: The role of local-and large-scale climate variability. *Geophysical Research Letters*, 31(13), 2004. doi: 10.1029/2004GL020255. L13215.
- Schmidli, J., C. Frei, and P. L. Vidale. Downscaling from GCM precipitation: a benchmark for dynamical and statistical downscaling methods. *International Journal of Climatology*, 26(5):679–689, 2006. doi: 10.1002/joc.1287.

- Schmucki, E., C. Marty, C. Fierz, R. Weingartner, and M. Lehning. Impact of climate change in Switzerland on socioeconomic snow indices. *Theoretical and Applied Climatology*, pages 1–15, 2015. doi: 10.1007/s00704-015-1676-7.
- Seifert, A. and D. K. Beheng. A two-moment cloud microphysics parameterization for mixed-phase clouds. Part 1: Model description. *Meteorology and Atmospheric Physics*, 92(1): 45–66, 2005. ISSN 1436-5065. doi: 10.1007/s00703-005-0112-4.
- Serquet, G., C. Marty, and M. Rebetez. Monthly trends and the corresponding altitudinal shift in the snowfall/precipitation day ratio. *Theoretical and Applied Climatology*, 114 (3-4):437–444, 2013. doi: 10.1007/s00704-013-0847-7.
- Sevruk, B. Der Niederschlag in der Schweiz. Technical Report 31, Geographisches Institut der Eidgenössischen Technischen Hochschule in Zürich, Abteilung Hydrologie, Zurich, Switzerland, 1985.
- SFOE. Hydropower, August 2014. URL <http://www.bfe.admin.ch/themen/00490/00491/index.html?lang=en>. Date of query: 09.04.2015.
- SLF. Der Lawinenwinter 1999. Ereignisanalyse. Technical report, Eidgenössischen Institutes für Schnee-und Lawinenforschung (SLF), Davos, Switzerland, 2000.
- Soncini, A. and D. Bocchiola. Assessment of future snowfall regimes within the Italian Alps using general circulation models. *Cold Regions Science and Technology*, 68(3):113–123, 2011. doi: 10.1016/j.coldregions.2011.06.011.
- Steger, C., S. Kotlarski, T. Jonas, and C. Schär. Alpine snow cover in a changing climate: A regional climate model perspective. *Climate Dynamics*, 41(3-4):735–754, 2013. doi: 10.1007/s00382-012-1545-3.
- Straka, J. M. and E. R. Mansell. A bulk microphysics parameterization with multiple ice precipitation categories. *Journal of Applied Meteorology*, 44(4):445–466, 2005. doi: 10.1175/JAM2211.1.
- Van der Linden, P. and J. F. B. Mitchell. ENSEMBLES: Climate Change and its Impacts: Summary of research and results from the ENSEMBLES project. Summary Report 160, Met Office Hadley Centre, Exeter, UK, 2009.
- Vaughan, D., J. Comiso, I. Allison, J. Carrasco, G. Kaser, R. Kwok, P. Mote, T. Murray, F. Paul, J. Ren, E. Rignot, O. Solomina, K. Steffen, and T. Zhang. Observations: Cryosphere. In Stocker, T., D. Qin, G.-K. Plattner, M. Tignor, S. Allen, J. Boschung, A. Nauels, Y. Xia, V. Bex, and P. Midgley, editors, *Climate Change 2013: The Physical Science Basis. Contribution of Working Group I to the Fifth Assessment Report of*

the Intergovernmental Panel on Climate Change, book section 4, pages 317–382. Cambridge University Press, Cambridge, United Kingdom and New York, NY, USA, 2013. doi: 10.1017/CBO9781107415324.012.

Voigt, T., H.-M. Füßel, I. Gärtnerroer, C. Huggel, C. Marty, and M. Zemp. Impacts of climate change on snow, ice, and permafrost in Europe: Observed trends, future projections, and socio-economic relevance. Technical report, European Topic Centre on Air and Climate Change ETC/ACC, AH Bilthoven, Netherlands, 2010.

Wiesinger, T. and M. Adams. Schnee und Lawinen in den Schweizer Alpen Winter 1998/1999. Technical report, Eidgenössischen Institutes für Schnee-und Lawinenforschung (SLF), Davos, Switzerland, 2007.

Yang, D., E. Elomaa, A. Tuominen, A. Aaltonen, B. Goodison, T. Gunther, V. Golubev, B. Sevruk, H. Madsen, and J. Milkovic. Wind-induced Precipitation Undercatch of the Hellmann Gauges. *Hydrology Research*, 30(1):57–80, 1999.

Zubler, E. M., A. M. Fischer, M. A. Liniger, and T. Schlegel. Auftausalzverbrauch im Klimawandel. Fachbericht 253, MeteoSchweiz, Zurich, Switzerland, 2015.

Abbreviations

| | |
|-------------------|---|
| AR5 | Fifth Assessment Report of IPCC |
| CORDEX | Coordinated Downscaling Experiment |
| CTRL | Control period (1981-2010) |
| DJF | Winter months December, January, February |
| EVAL | Evaluation period (1971-2005) |
| GCM | Global Climate Model |
| GHG | Greenhouse Gas |
| IPCC | Intergovernmental Panel on Climate Change |
| IQR | Interquartile Range |
| JJA | Summer months June, July, August |
| MeteoSwiss | Swiss Federal Office of Meteorology and Climatology |
| PDF | probability density function |
| RCM | Regional Climate Model |
| RCP | Representative Concentration Pathway |
| SCEN | Scenario period (2070-2099) |
| SE | Standard Error |
| SFOE | Swiss Federal Office of Energy |
| SLF | WSL Institute for Snow and Avalanche Research |
| SWE | Snow Water Equivalent |
| WCRP | World Climate Research Program |
| WMO | World Meteorological Organisation |
| wrt. | with respect to |
| WSL | Swiss Federal Institute for Forest, Snow and Landscape Research |

Acronyms

| | | |
|-------------------------|--|----|
| Δ | Absolute change signal | - |
| δ | Relative change signal | - |
| A | Curve fitting parameter for Slope snow fractionation method | - |
| B | Curve fitting parameter for Slope snow fractionation method | - |
| C | Curve fitting parameter for Richards snow fractionation method | - |
| CSD | Consecutive snowfall days | d |
| D | Curve fitting parameter for Richards snow fractionation method | - |
| E | Curve fitting parameter for Richards snow fractionation method | - |
| F | Curve fitting parameter for Richards snow fractionation method | - |
| i | High resolution grid point number | - |
| k | Coarse grid point number | - |
| n | Total number of high resolution grid points which will account for new coarse grid point | - |
| P | Daily precipitation on coarse grid | mm |
| P_{AF} | Total precipitation adjustment factor | - |
| P_{corr} | Bias corrected daily precipitation | mm |
| P' | Daily precipitation on high resolution grid | mm |
| S | Daily snowfall amount on coarse grid | mm |
| S_{10d} | Maximal 10 day snowfall amount (derived by averaging the corresponding seasonal maximum amounts) | mm |
| S_{3d} | Maximal 3 day snowfall amount (derived by averaging the corresponding seasonal maximum amounts) | mm |
| S_{BI} | Daily snowfall amount on coarse grid derived with Binary snow fractionation method | mm |

| | | |
|-----------------------------|--|------------|
| S_{freq} | Snowfall frequency (days with snowfall >1 mm divided by total number of days within the considered period) | % |
| S_{int} | Snowfall intensity (daily mean snowfall amount at days with snowfall >1 mm) | mm/d |
| S_{mean} | (Spatio-) temporally-averaged snowfall amount | mm or mm/d |
| S_{q99} | Seasonal heavy snowfall amount (defined by 99% all-day snowfall percentile) | mm/d |
| S_{q99} | Monthly heavy snowfall amount (defined by 99% all-day snowfall percentile) | mm/d |
| S_{q99,frac} | Heavy snowfall fraction (derived by calculating the percentage of heavy snowfall sum ($S > S_{q99}$) and total snowfall sum (S_{tot})) | |
| S_{RI} | Daily snowfall amount on coarse grid derived with Richards snow fractionation method | mm |
| S_{SG} | Daily snowfall amount on coarse grid derived with Subgrid snow fractionation method | mm |
| S_{SL} | Daily snowfall amount on coarse grid derived with Sope snow fractionation method | mm |
| S_{tot} | Total snowfall amount over a specific period (and area) | mm |
| S' | Daily snowfall amount on high resolution grid | mm |
| sf | Snow fraction | - |
| sf_{BI} | Snow fraction derived with Binary snow fractionation method | - |
| sf_{RI} | Snow fraction derived with Richards snow fractionation method | - |
| sf_{SG} | Snow fraction derived with Subgrid snow fractionation method | - |
| sf_{SL} | Snow fraction derived with Slope snow fractionation method | - |
| slope | Parameter for deriving snow fraction with Slope snow fractionation method | - |

| | | |
|--------------------------|--|----------|
| T' | Daily mean temperature on high resolution grid | °C |
| T' | Daily mean temperature on coarse grid | °C |
| T* | Snow fractionation temperature | °C |
| T* | Adjusted snow fractionation temperature | °C |
| T*_{a,BI} | Adjusted snow fractionation temperature for Binary snow fractionation method | °C |
| T*_{a,RI} | Adjusted snow fractionation temperature for Richards snow fractionation method | °C |
| T_{2m} | Temperature 2 m above ground | °C |
| topo | Topography | m.a.s.l. |
| topo_{sd} | Topographical standard deviation | m |

Appendix

A Additional information data and methods

A.1 Analysed data sets

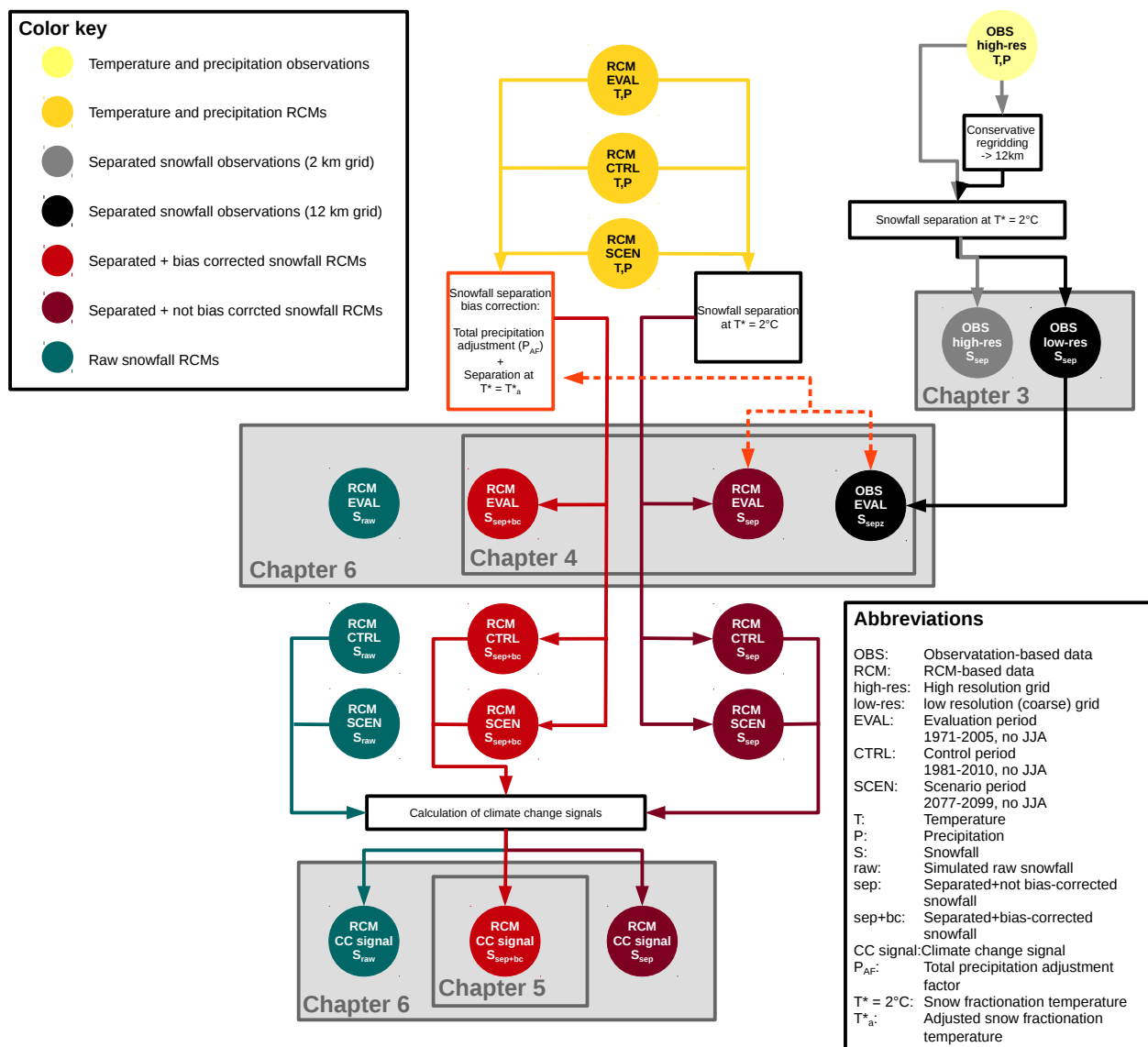


Fig. A.1: Overview of all analysed data sets within this thesis. Colored circles denote the different types of data (see color key). Grey boxes show data analysed and compared with each other in the corresponding chapter. The white framed boxes denote the applied procedures to derive the data.

A.2 Simulation data

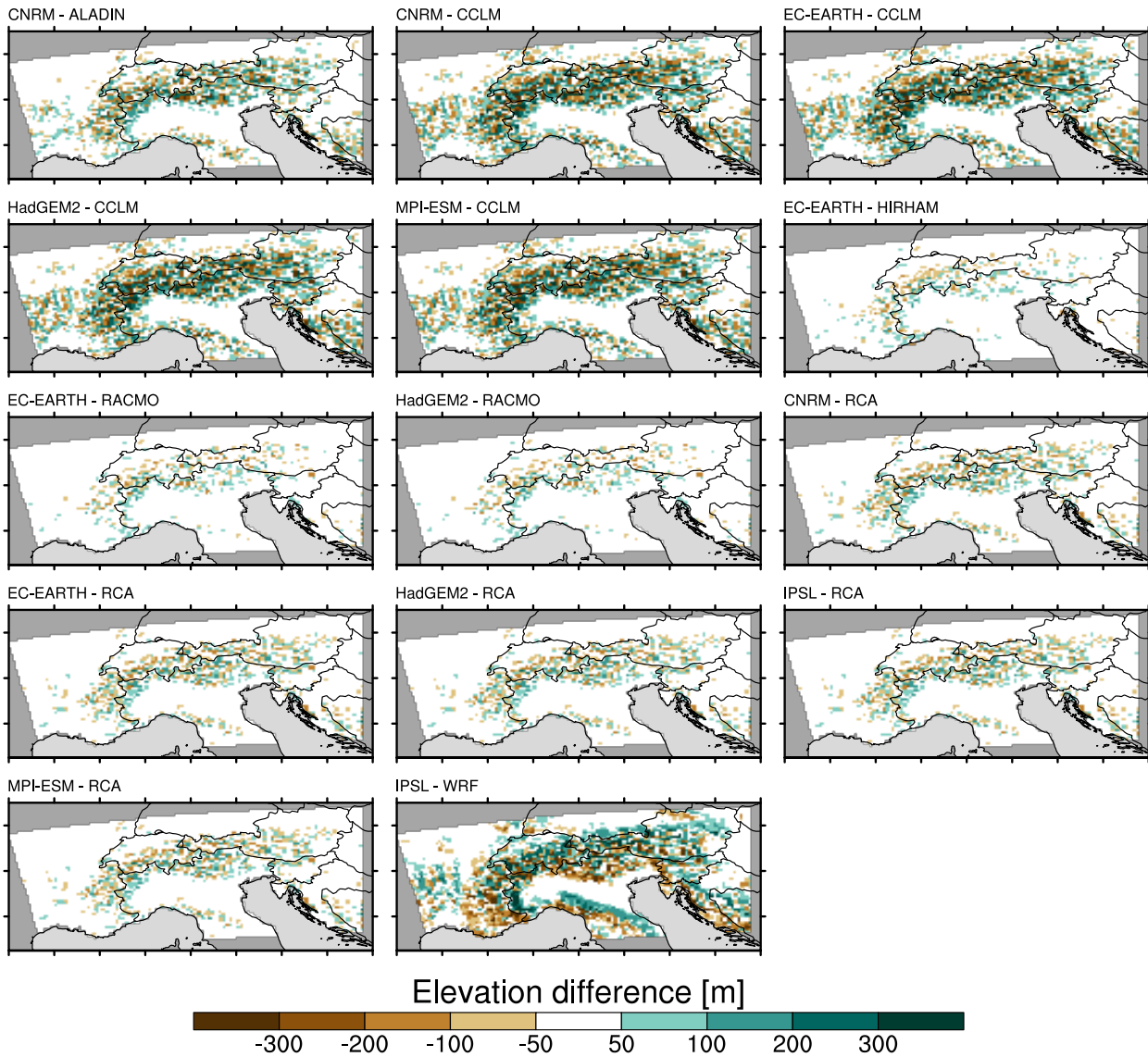


Fig. A.2: Elevation differences of the 14 RCM simulations wrt. to the observation-based topography file.

A.3 Station data

Tab. A.1: Geographical information of the 29 Swiss stations used for the comparison to raw snowfall outputs of six EURO-CORDEX simulations. The last column (S_{mean}) summarises the mean September to May snowfall in the period 1971 - 2005. Primary station measurements were converted from cm/d to mm (SWE)/d by assuming a ratio of 10:1, i.e., a mean snow density of 100 kg/m³.

| Station ID | Name | Lat [°N] | Lon [°E] | Elevation [m.a.s.l.] | S_{mean} [mm] |
|------------|----------------------|-------------|-------------|-------------------------|---------------------------|
| MAG | Magadino / Cadenazzo | 8.93 | 46.16 | 203 | 38 |
| LUG | Lugano | 8.96 | 46 | 273 | 24 |
| BAS | Basel / Binningen | 7.58 | 47.54 | 316 | 32 |
| OTL | Locarno / Monti | 8.79 | 46.17 | 367 | 51 |
| GVE | Genève-Cointrin | 6.13 | 46.25 | 412 | 31 |
| KLO | Zürich / Kloten | 8.54 | 47.48 | 426 | 57 |
| ALT | Altdorf | 8.62 | 46.89 | 438 | 64 |
| LUZ | Luzern | 8.3 | 47.04 | 454 | 58 |
| SIO | Sion | 7.33 | 46.22 | 482 | 48 |
| NEU | Neuchâtel | 6.95 | 47 | 485 | 42 |
| PAY | Payerne | 6.94 | 46.81 | 490 | 36 |
| TAE | Aadorf / Tänikon | 8.9 | 47.48 | 539 | 80 |
| BER | Bern / Zollikofen | 7.46 | 46.99 | 553 | 53 |
| SMA | Zürich / Fluntern | 8.57 | 47.38 | 556 | 85 |
| CHU | Chur | 9.53 | 46.87 | 556 | 113 |
| FAH | Fahy | 6.94 | 47.42 | 596 | 74 |
| STG | St. Gallen | 9.4 | 47.43 | 776 | 192 |
| CDF | La Chaux-de-Fonds | 6.79 | 47.08 | 1018 | 284 |
| ENG | Engelberg | 8.41 | 46.82 | 1036 | 431 |
| ROB | Poschiavo / Robbia | 10.06 | 46.35 | 1078 | 142 |
| DIS | Disentis / Sedrun | 8.85 | 46.71 | 1197 | 389 |
| ABO | Adelboden | 7.56 | 46.49 | 1327 | 447 |
| MVE | Montana | 7.46 | 46.3 | 1427 | 414 |
| DAV | Davos | 9.84 | 46.81 | 1594 | 488 |
| ZER | Zermatt | 7.75 | 46.03 | 1638 | 279 |
| SBE | S. Bernardino | 9.18 | 46.46 | 1639 | 561 |
| GRH | Grimsel Hospiz | 8.33 | 46.57 | 1980 | 1277 |
| SAE | Säntis | 9.34 | 47.25 | 2502 | 1089 |
| WFJ | Weissfluhjoch | 9.81 | 46.83 | 2691 | 924 |

A.4 Calculation procedure for relative and absolute change signals

Relative and absolute change signals were derived according to the following procedures:

1. The CTRL and SCEN period fields of a specific snowfall index X were computed separately.
2. For the CTRL period field, all grid-points with values smaller as or equal to the snowfall index dependent threshold were masked (see Tab. A.2).
3. Masked out grid points in the CTRL period field were also not considered in the SCEN period field.
4. For a specific elevation interval, corresponding grid points were extracted and averaged separately for the two periods.
5. In a last steps relative and absolute for the specific interval have been calculated according to Equations 2.19 and 2.18, respectively.

Tab. A.2: Table showing the applied threshold values for various snowfall indices before relative and absolute change signals were calculated. The cutoff values were applied to the CTRL period fields by masking out the corresponding grid point values. In a second step, Masked out grid points were left out in the SCEN period fields as well (see procedure above). The threshold values for seasonal (September to May) and monthly snowfall indices might differ.

| Snowfall index | Name | Unit | seasonal threshold | monthly threshold |
|---------------------------------------|--|------|----------------------------|----------------------------|
| S_{tot} | Snowfall over entire period ^a | mm | 10 | 10/9=1.11 |
| $S_{\text{q99}}/S_{\text{q99,month}}$ | Heavy snowfall | mm/d | 1 | 1 |
| S_{freq} | Snowfall frequency | % | 1 | 1 |
| S_{int} | Snowfall intensity ^b | mm/d | $S_{\text{freq}} \leq 1\%$ | $S_{\text{freq}} \leq 1\%$ |
| S_{q99frac} | Heavy snowfall fraction | % | 1 | not calc. |
| S_{3d} | Max. 3 day snowfall | mm | 1 | not calc. |
| S_{10d} | Max. 10 day snowfall | mm | 1 | not calc. |
| CSD | Consecutive snowfall days | d | 2 | not calc. |

^aSeasonal mean snowfall (S_{mean}) from September to May was derived by dividing S_{tot} by the total number of years within the considered period. Monthly mean snowfall was derived by dividing S_{tot} by the total number of days within the considered period and month, respectively.

^bWhenever S_{freq} was masked out, so was the corresponding grid point value of S_{int} .

B Additional information grid coarsening

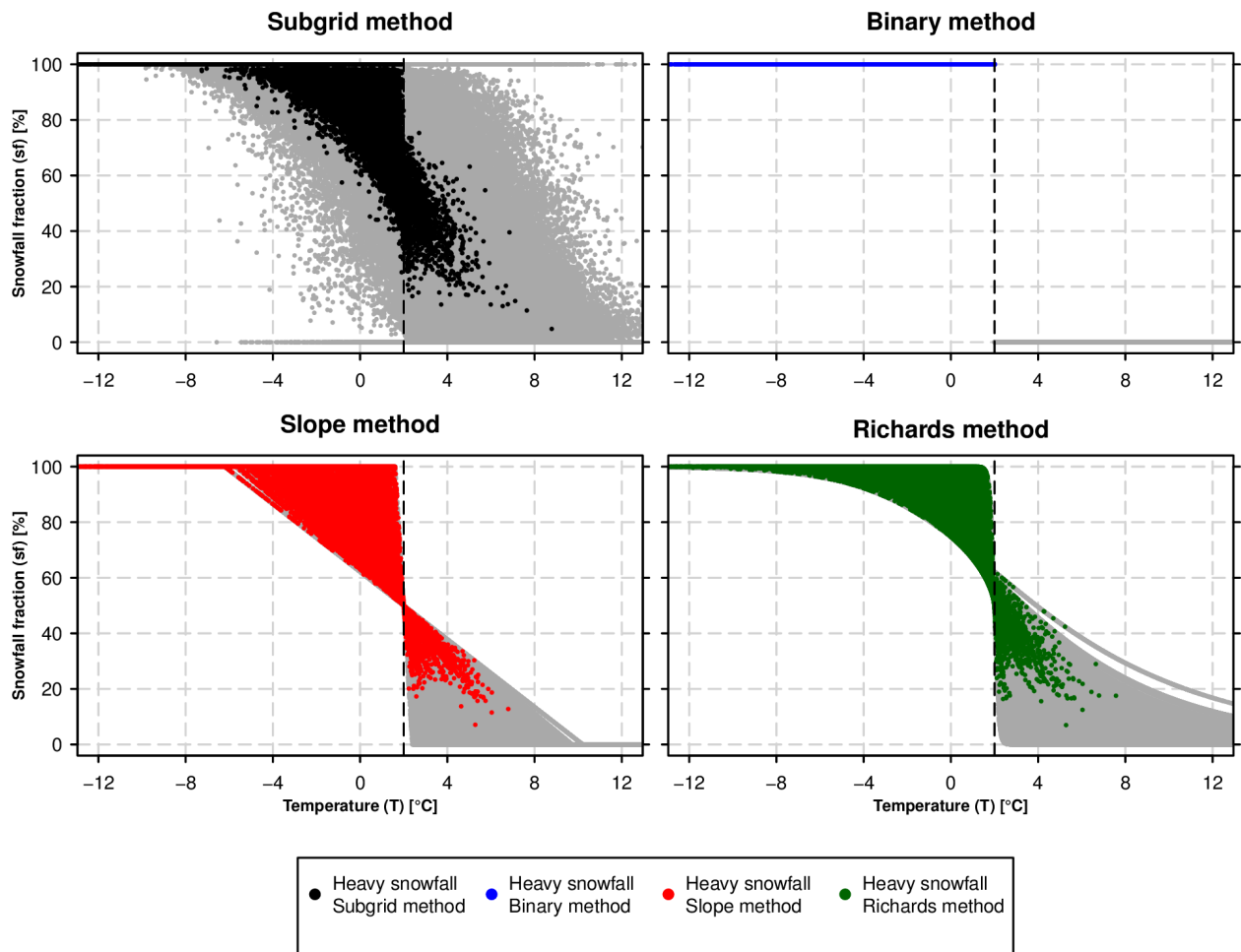


Fig. B.1: Daily mean temperature vs. snow fraction for the Subgrid high resolution snow fraction method (top-left) and the three coarse grid snow fractionation methods Binary (top-right), Richards (bottom-left) and Richards method (bottom-right). The grey dots show the temperature vs. snow fraction relationship for all snowfalls between 1971 - 2005 over the Swiss domain. In black, blue, red and green, all snowfall events which exceed the grid point-based S_{q99} are shown. Note that S_{q99} might differ among the snow fractionation methods.

C Additional information bias correction and evaluation

C.1 Bias correction factors

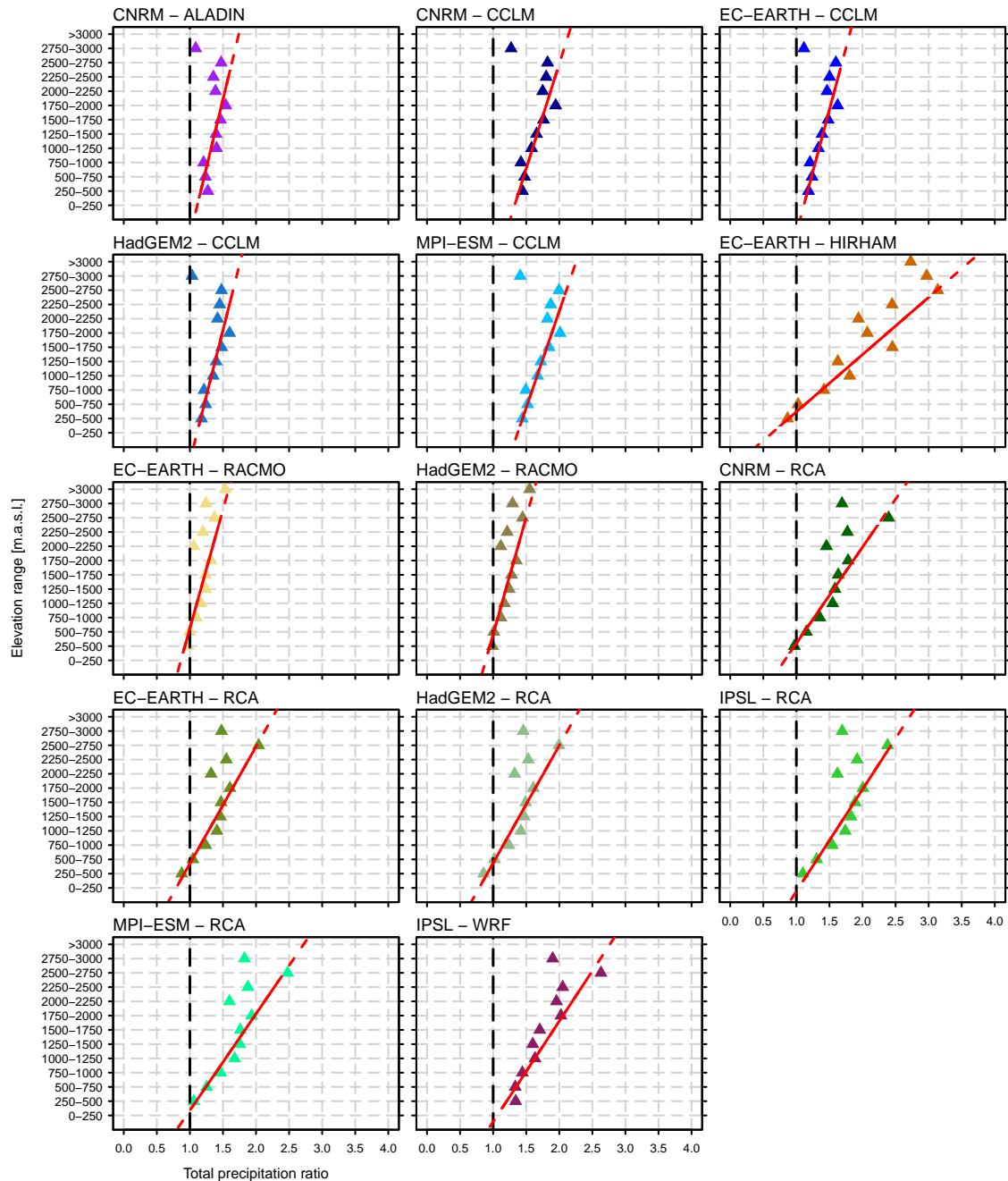


Fig. C.1: Ratios (RCM simulation wrt. observational analysis) of total precipitation sums from September to May 1971 - 2005 vs. 250 m elevation intervals for the Swiss domain. The linear regression line, applied to the ratios for elevations intervals between 250 m.a.s.l. and 2750 m.a.s.l., is represented by the red line.

Tab. C.1: Table showing the linear regression parameters intercept and slope (see Eq. 2.16) with corresponding adjustment factors for total precipitation (calculated for an elevation of 1000 m.a.s.l.) $P_{AF,1000}$ and adjusted snow fractionation temperatures $T^*_{BI,a}$ (Binary method) and $T^*_{RI,a}$ (Richards method) for the 14 RCM simulations. For both snow fractionation methods, i.e., Binary and Richard method, the initial snow fractionation temperature is $T^* = 2^\circ\text{C}$ (see Eq. 2.5 and 2.12).

| Model Simulation | intercept | slope | $P_{AF,1000}$ | $T^*_{BI,a}$ [$^\circ\text{C}$] | $T^*_{RI,a}$ [$^\circ\text{C}$] |
|-------------------|-----------|---------|---------------|-----------------------------------|-----------------------------------|
| CNRM – ALADIN | -5067.79 | 4781.78 | 0.79 | 0 | -0.1 |
| CNRM – CCLM | -4619.94 | 3674.04 | 0.65 | 0.3 | 0.3 |
| EC-EARTH – CCLM | -4579.45 | 4336.49 | 0.78 | 0.4 | 0.4 |
| HadGEM2 – CCLM | -4842.11 | 4593.99 | 0.79 | 0.1 | 0.2 |
| MPI-ESM – CCLM | -4399.22 | 3391.01 | 0.63 | 0.9 | 1.1 |
| EC-EARTH – HIRHAM | -386.79 | 1004.09 | 0.72 | 0.1 | 0.2 |
| EC-EARTH – RACMO | -3342.35 | 4155.57 | 0.96 | -1.5 | -1.5 |
| HadGEM2 – RACMO | -3394.57 | 4100.7 | 0.93 | -0.2 | -0.3 |
| CNRM – RCA | -1137.53 | 1685.74 | 0.79 | 0.5 | 0.4 |
| EC-EARTH – RCA | -1376.89 | 2052.25 | 0.86 | 0.4 | 0.3 |
| HadGEM2 – RCA | -1376.68 | 2061.67 | 0.87 | 0.7 | 0.7 |
| IPSL – RCA | -1598.78 | 1787.93 | 0.69 | 0.5 | 0.4 |
| MPI-ESM – RCA | -1354.13 | 1692.82 | 0.72 | 1.3 | 1.4 |
| IPSL – WRF | -1621.73 | 1761.84 | 0.67 | -0.4 | -0.5 |

C.2 Evaluation: Binary snow fractionation method

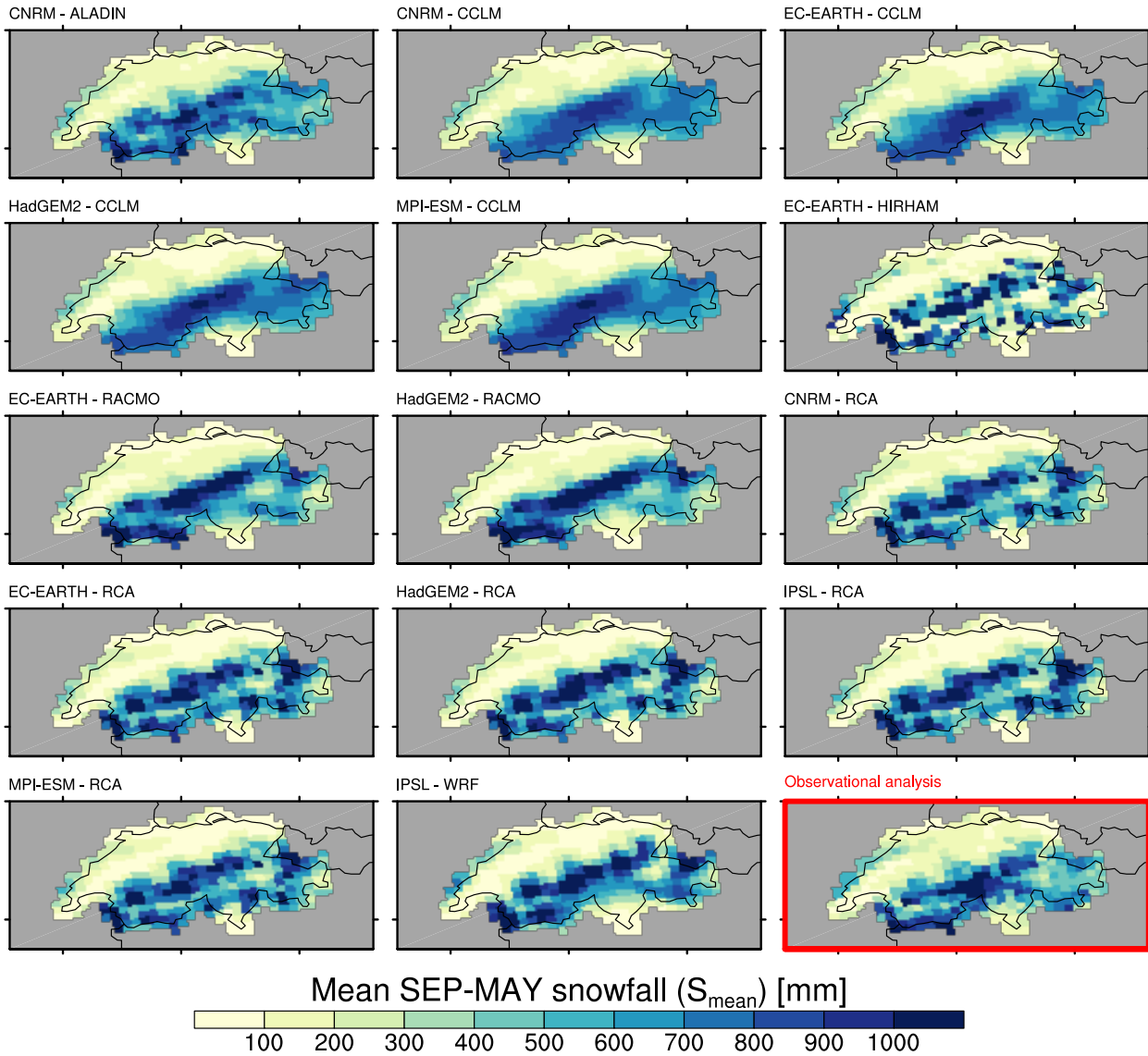


Fig. C.2: Spatial distribution of mean September to May snowfall (S_{mean}) in the period 1971 - 2005 and for the 14 RCM simulations after applying the bias correction and fractionating the snowfall with the Binary method. In the lower right panel, the horizontal map of the observation-based estimate is shown (snow fractionation with Binary method at $T^* = 2 \text{ }^\circ\text{C}$, see Eq. 2.5).

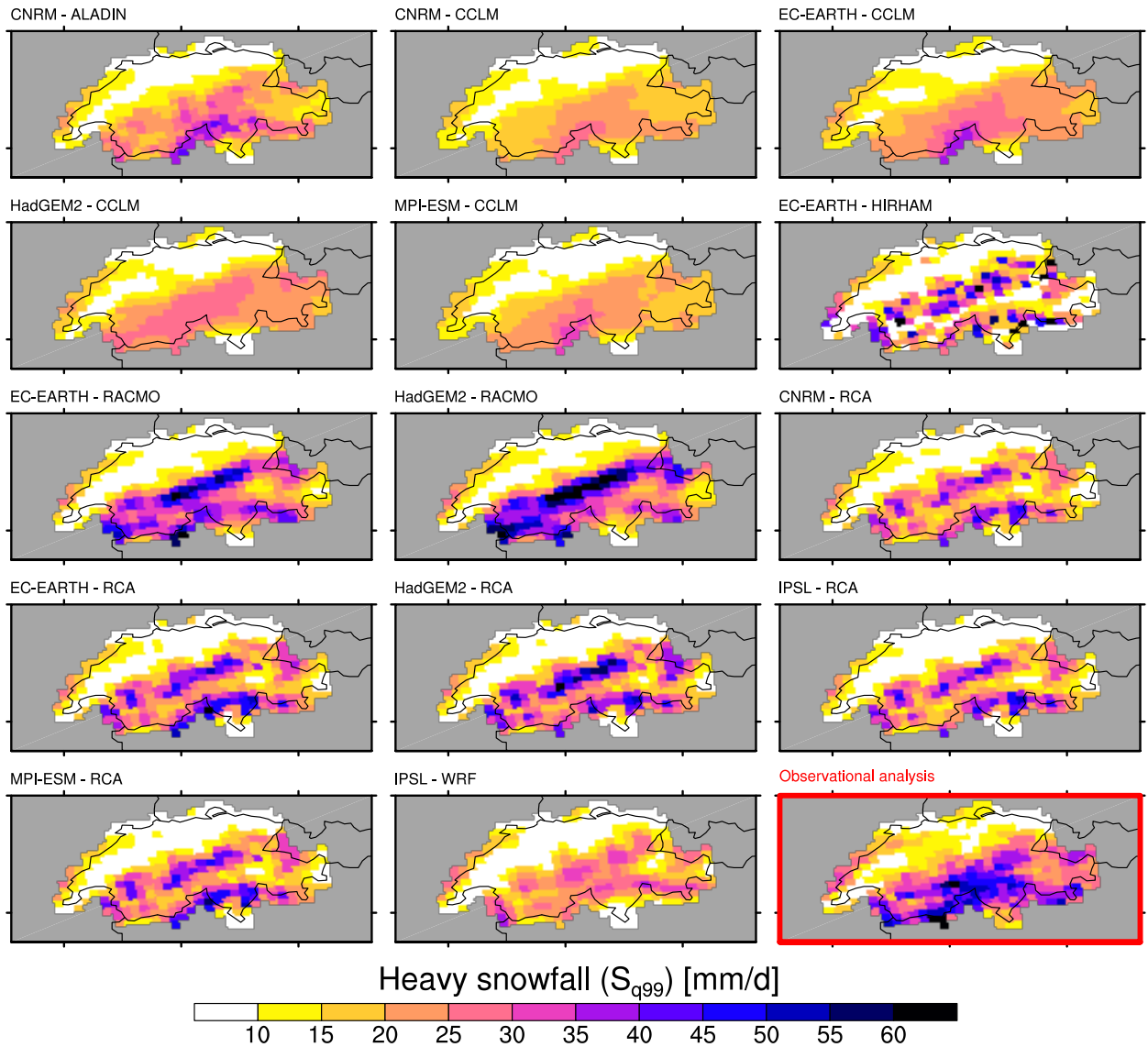


Fig. C.3: Spatial distribution of heavy snowfall (S_{q99}) between September and May in the period 1971 - 2005 and for the 14 RCM simulations after applying the bias correction and fractionating the snowfall with the Binary method. In the lower right panel, the horizontal map of the observation-based estimate is shown (snow fractionation with Binary method at $T^* = 2^\circ\text{C}$, see. Eq. 2.5).

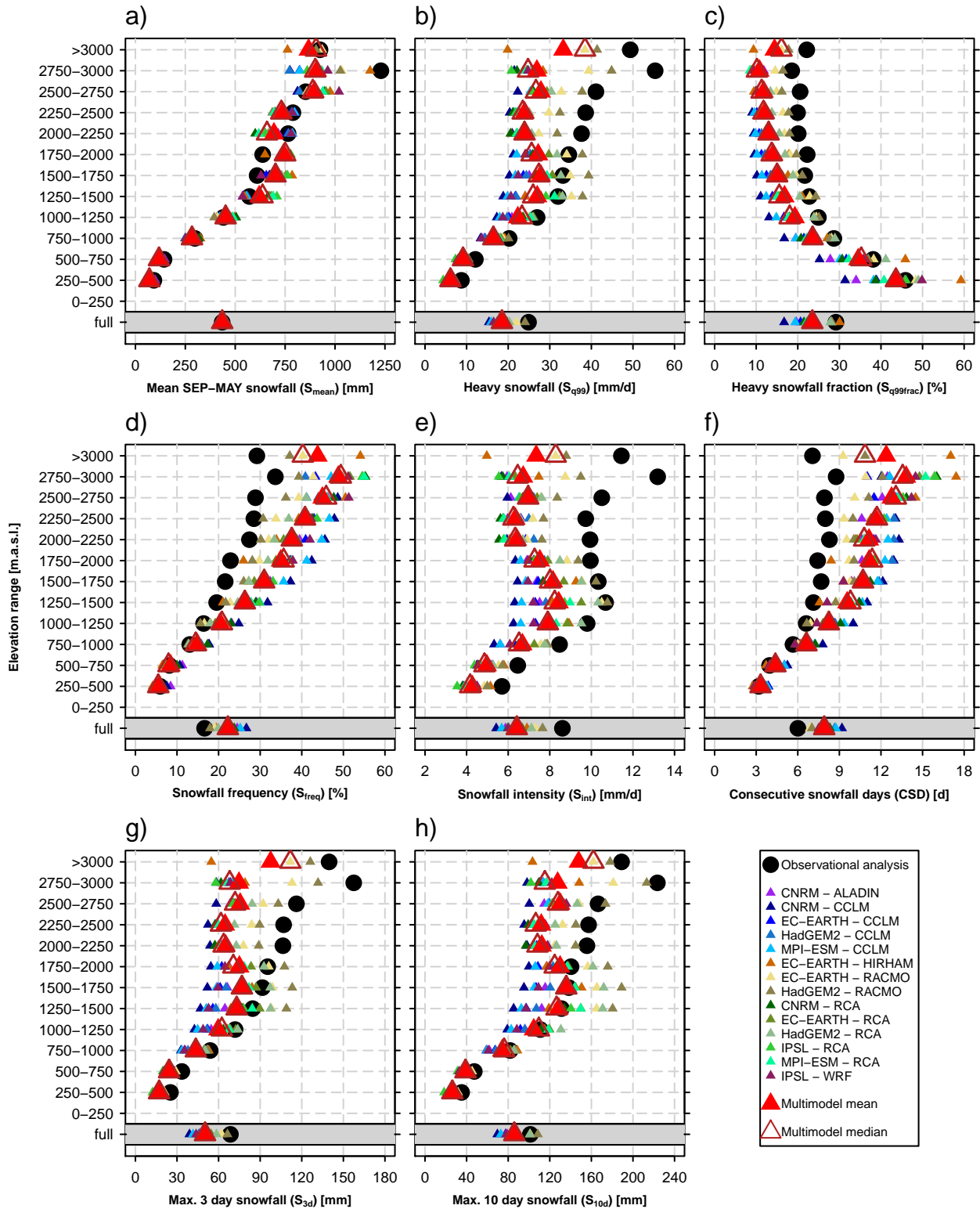


Fig. C.4: Evaluation of seasonal (September to May) snowfall indices in the period 1971 - 2005 after applying the bias correction and separating the snowfall with the Binary method. The black circles represent the values of the observation-based analysis. Small triangles show the individual RCM simulations whereas the large triangles denote the multimodel mean (red, filled) and multimodel median (brown, open).

C.3 Evaluation: Binary snow fractionation method - Comparison of separated + bias corrected and separated + not bias-corrected snowfall

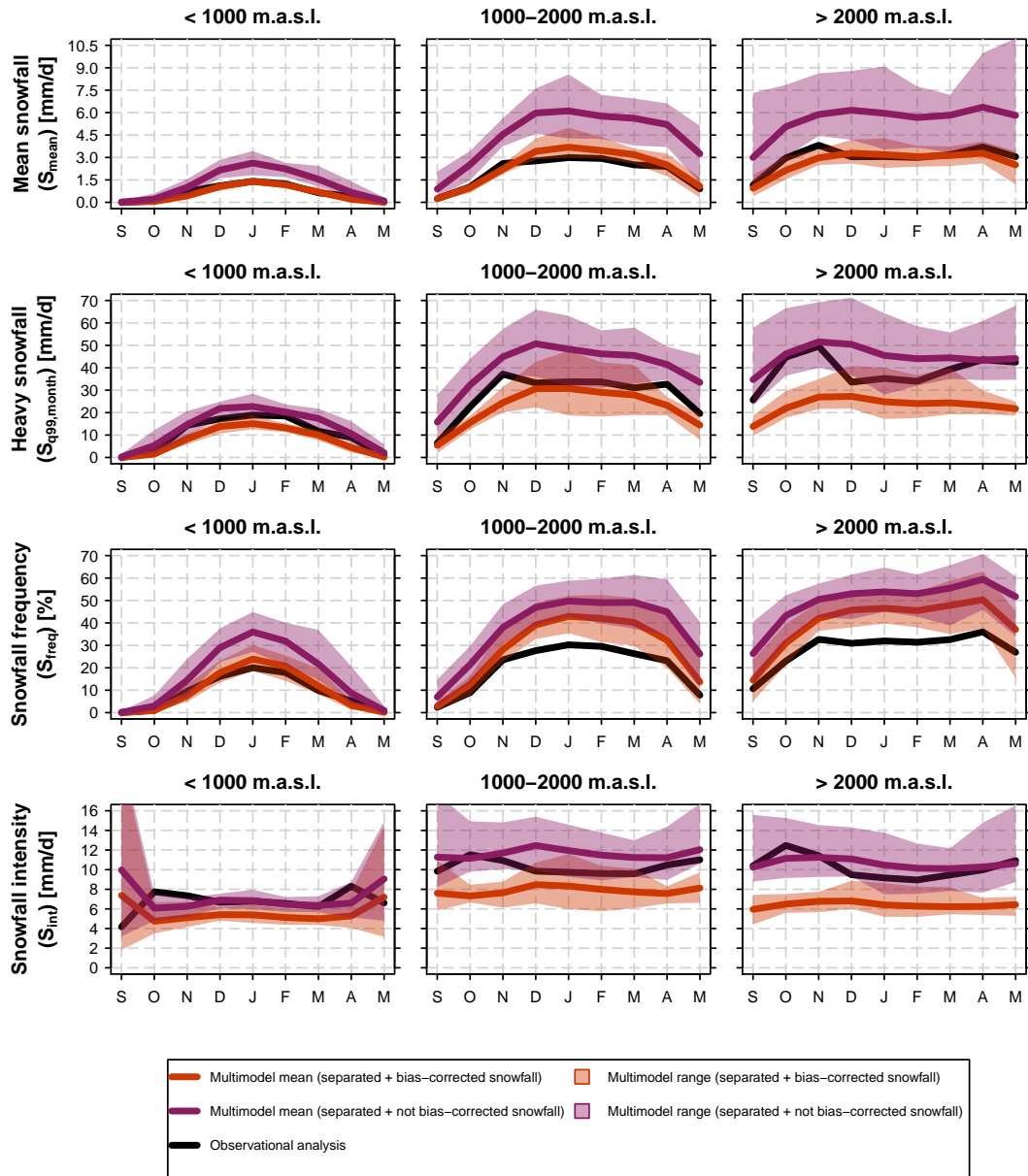


Fig. C.5: Evaluation of monthly (September to May) snowfall indices in the period 1971 - 2005. Black lines depict the observation-based analysis (snow fractionation with Binary method at $T^* = 2^\circ\text{C}$, see Eq. 2.5). The red line displays the seasonal cycle of the multimodel mean based on the separated + bias-corrected snowfall of the 14 RCM simulations (snow fractionation with Binary method at $T^*_{a,BI}$, see Tab. C.1). Seasonal cycles of the multimodel mean based on the separated + not bias-corrected snowfall are shown in violet (snow fractionation with Binary method at $T^* = 2^\circ\text{C}$). The shading represents the corresponding multimodel range. The columns represent the three elevation intervals below 1000 m.a.s.l., between 1000 m.a.s.l. and 2000 m.a.s.l. and above 2000 m.a.s.l..

D Additional information snowfall projections

D.1 Projections: Richards snow fractionation method, RCP4.5

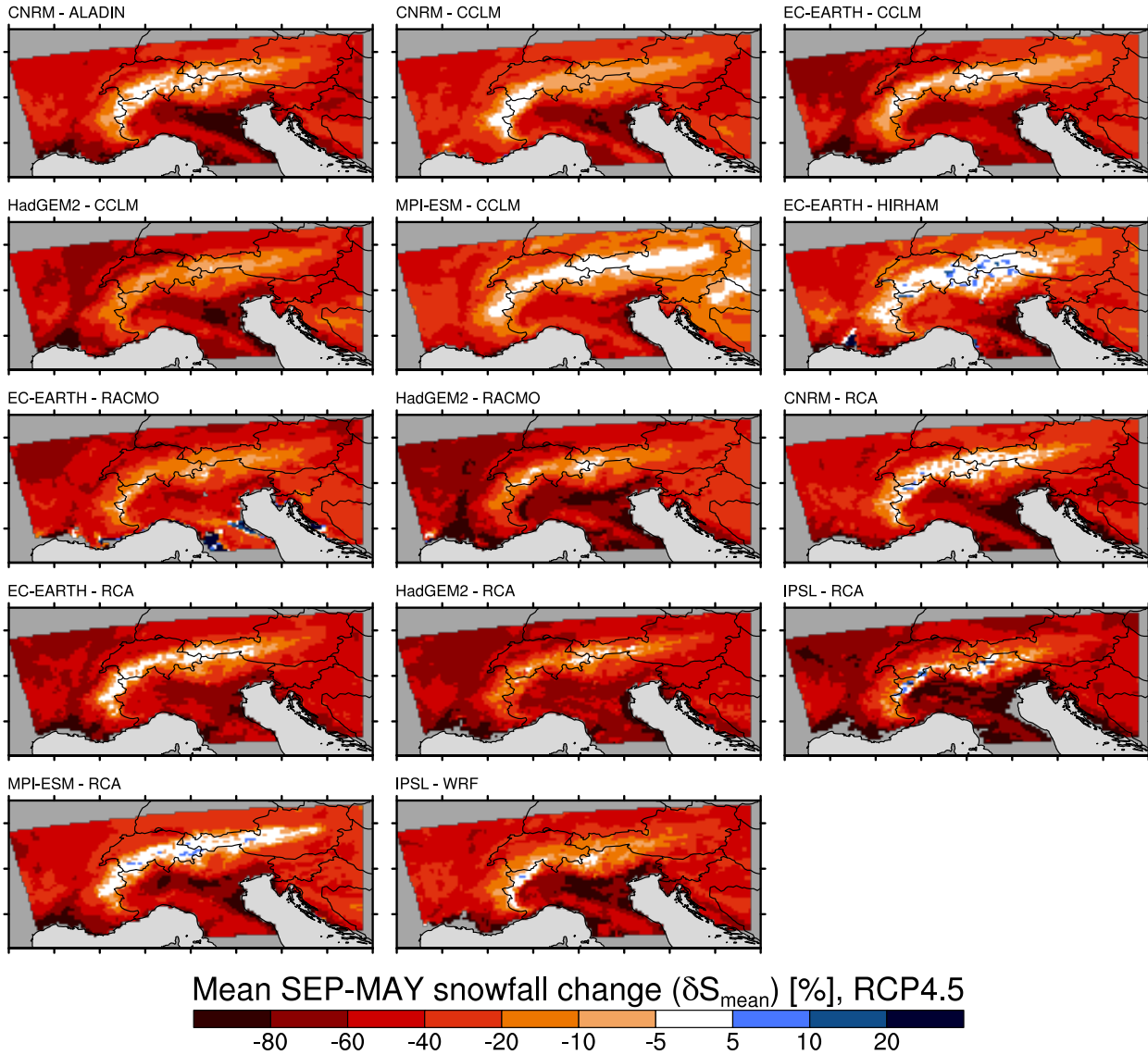
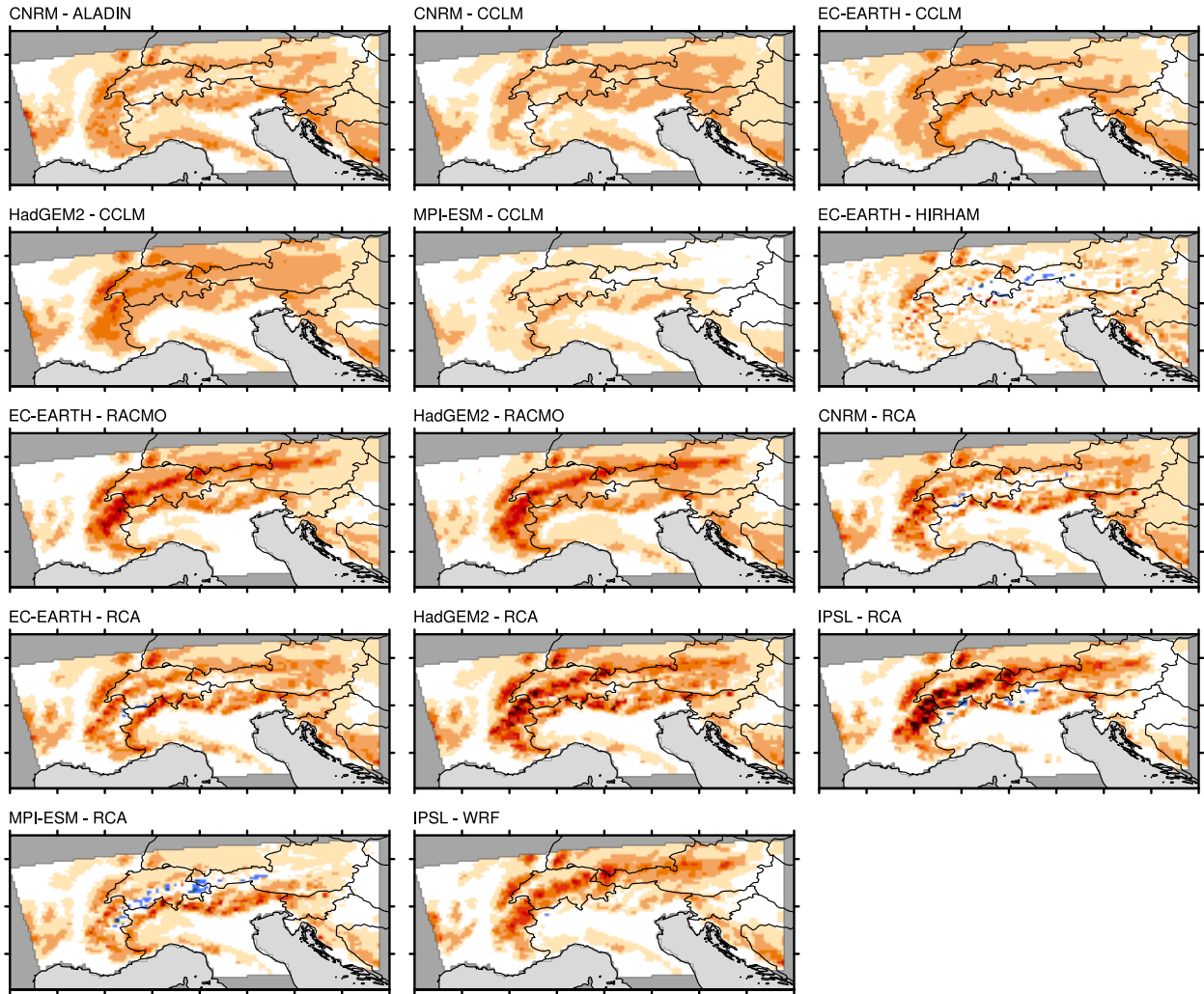


Fig. D.1: Spatial distribution of relative changes (SCEN 2070 - 2099 wrt. CTRL 1981 - 2010) in mean September to May snowfall (δS_{mean}) for RCP4.5 and for the 14 RCM simulations after applying the bias correction and fractionating the snowfall with the Richards method.



Mean SEP-MAY snowfall change (ΔS_{mean}) [mm], RCP4.5

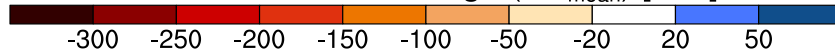


Fig. D.2: Spatial distribution of absolute changes (SCEN 2070 - 2099 wrt. CTRL 1981 - 2010) in mean September to May snowfall (ΔS_{mean}) for RCP4.5 and for the 14 RCM simulations after applying the bias correction and fractionating the snowfall with the Richards method.

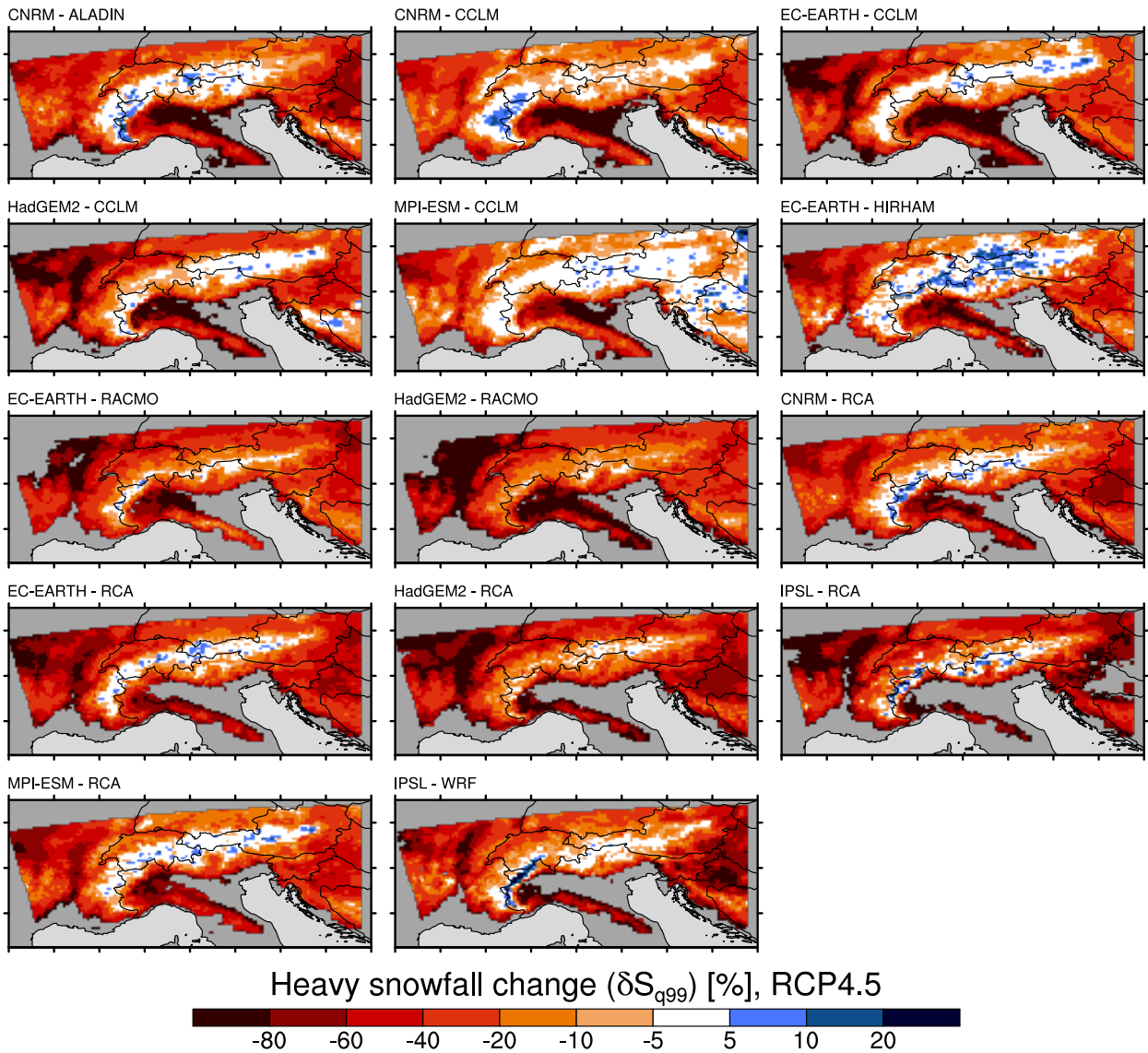


Fig. D.3: Spatial distribution of relative changes (September to May, SCEN 2070 - 2099 wrt. CTRL 1981 - 2010) in heavy snowfall (δS_{q99}) for RCP4.5 and for the 14 RCM simulations after applying the bias correction and fractionating the snowfall with the Richards method.

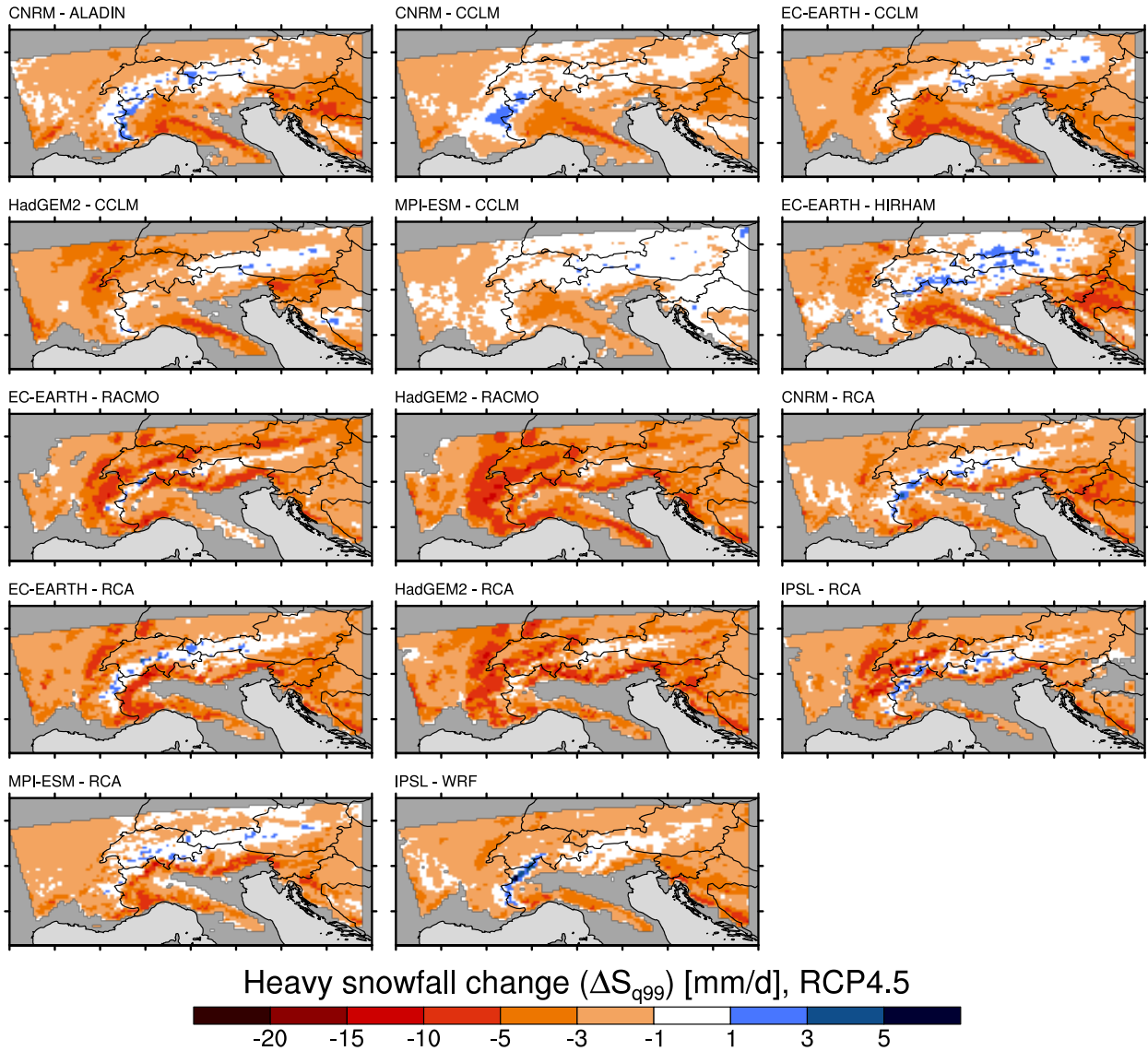


Fig. D.4: Spatial distribution of absolute changes (September to May, SCEN 2070 - 2099 wrt. CTRL 1981 - 2010) in heavy snowfall (ΔS_{q99}) for RCP4.5 and for the 14 RCM simulations after applying the bias correction and fractionating the snowfall with the Richards method.

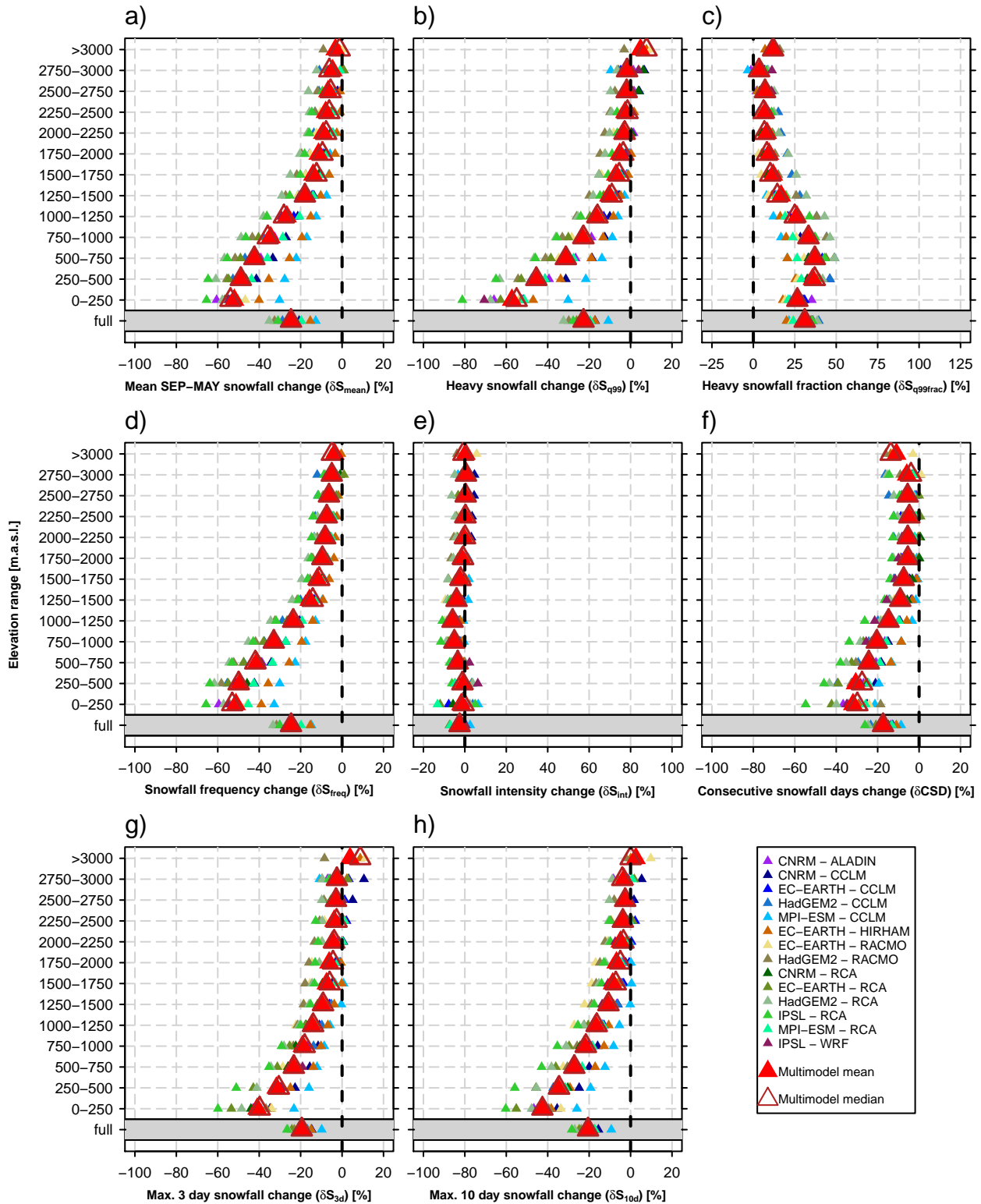


Fig. D.5: Relative changes (SCEN 2070 - 2099 wrt. CTRL 1981 - 2010) of seasonal (September to May) snowfall indices for RCP4.5 after applying the bias correction to the 14 RCM simulations and separating the snowfall with the Richards method. Small triangles show the individual RCM simulations whereas the large triangles denote the multimodel mean (red, filled) and multimodel median (brown, open).

D.2 Projections: Richards snow fractionation method, RCP8.5

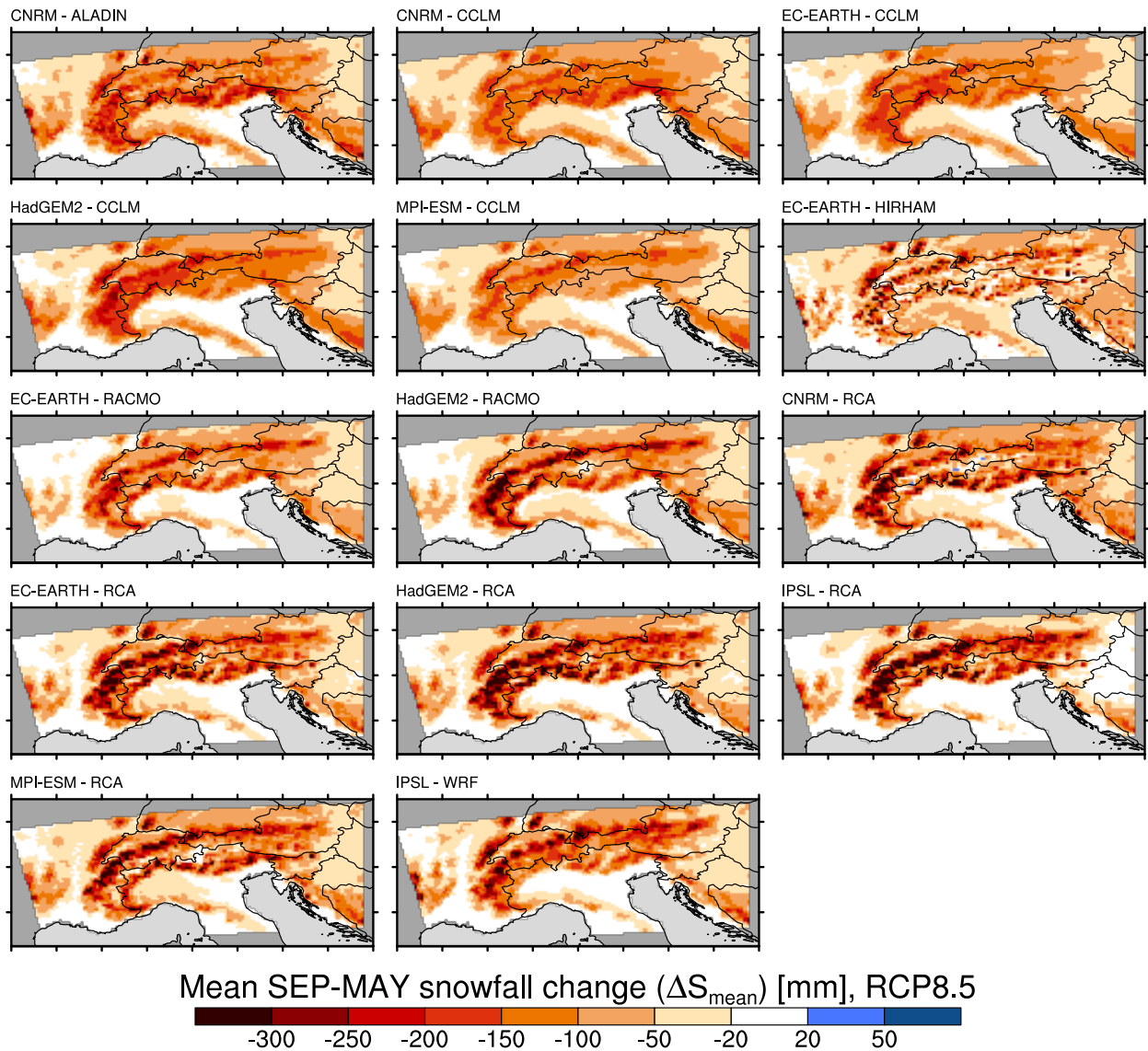


Fig. D.6: Spatial distribution of absolute changes (SCEN 2070 - 2099 wrt. CTRL 1981 - 2010) in mean September to May snowfall (ΔS_{mean}) for RCP8.5 and for the 14 RCM simulations after applying the bias correction and fractionating the snowfall with the Richards method.

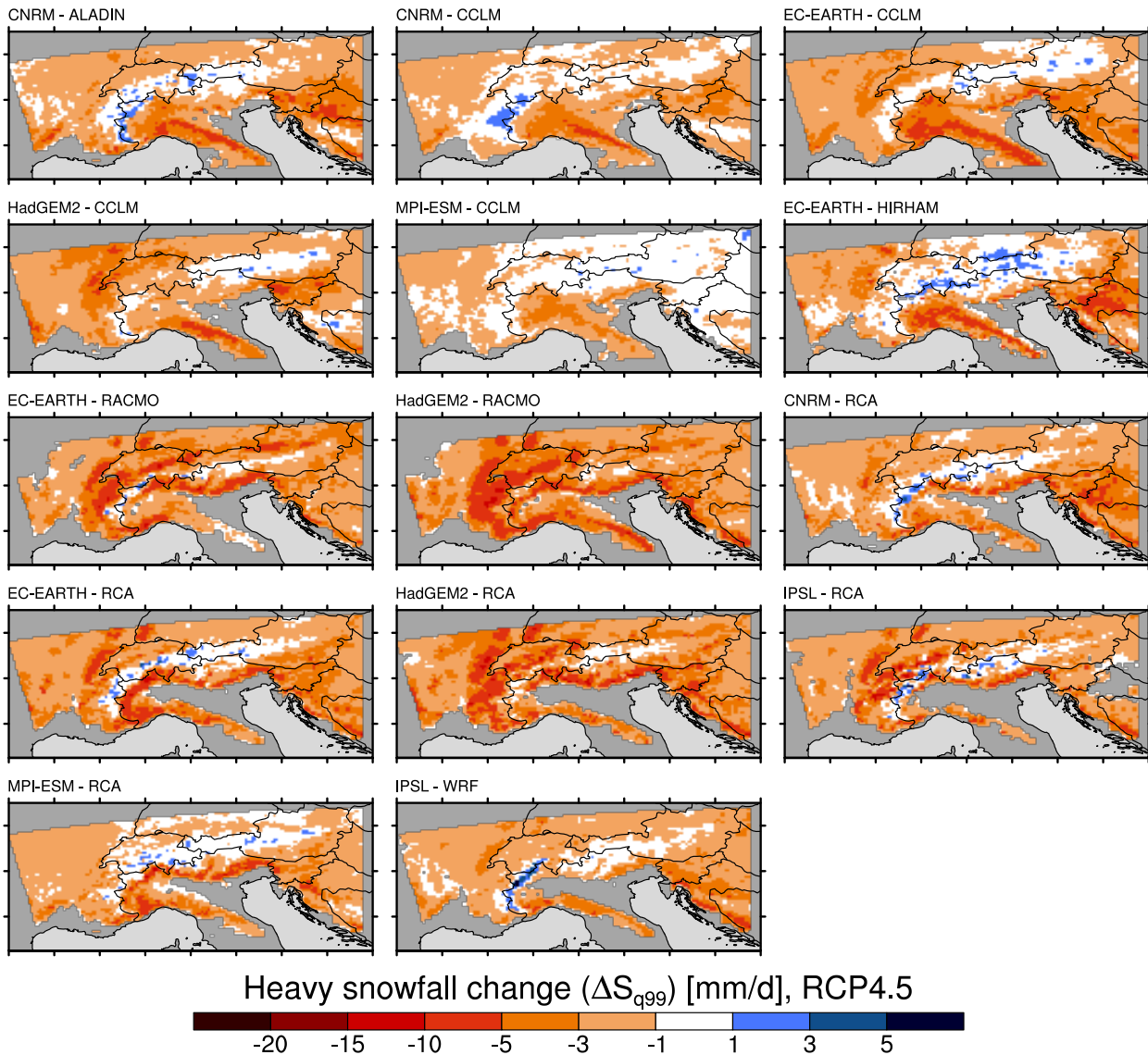


Fig. D.7: Spatial distribution of absolute changes (September to May, SCEN 2070 - 2099 wrt. CTRL 1981 - 2010) in heavy snowfall (ΔS_{q99}) for RCP8.5 and for the 14 RCM simulations after applying the bias correction and fractionating the snowfall with the Richards method.

D.3 Projections: Binary snow fractionation method, RCP4.5

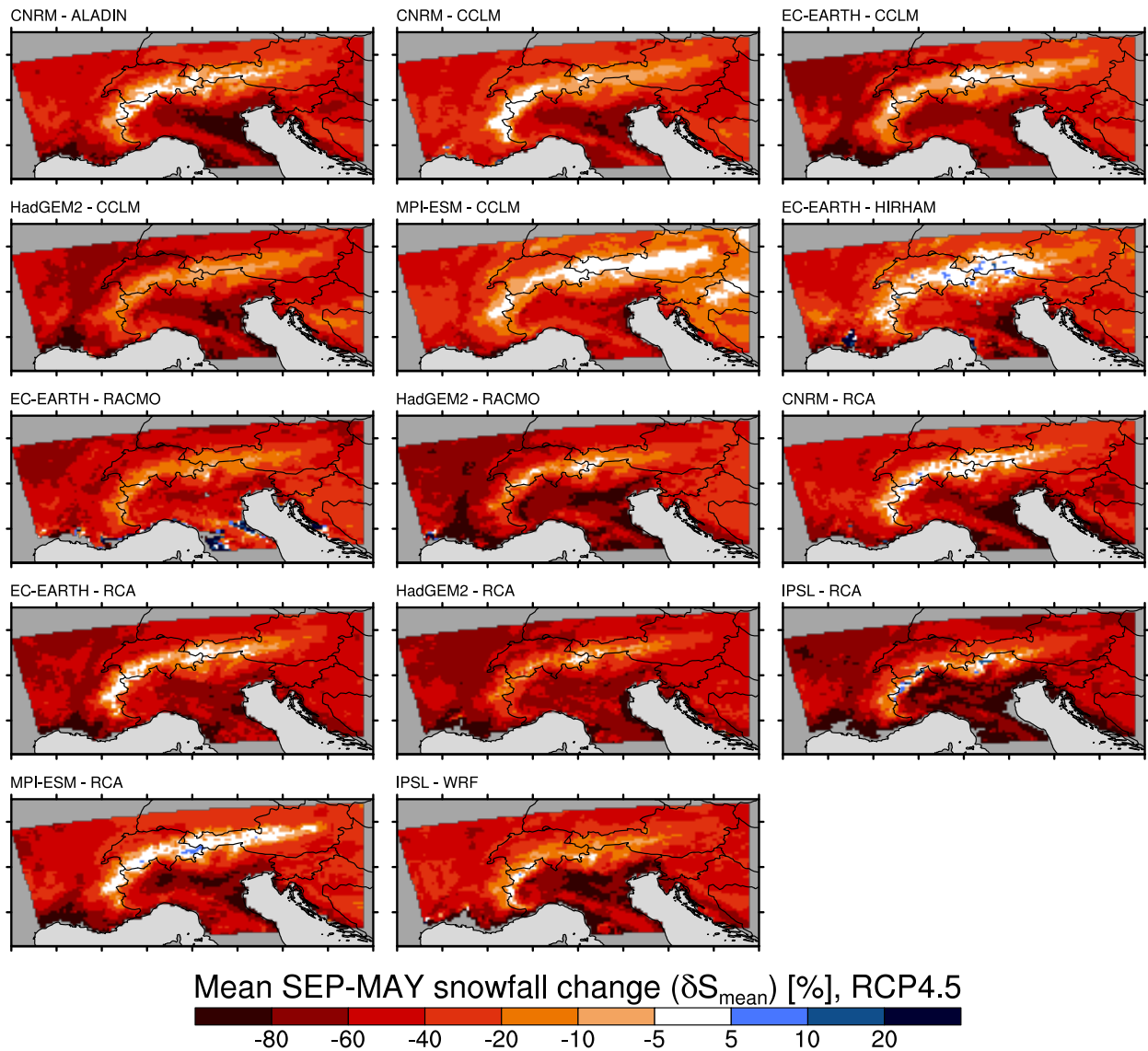


Fig. D.8: Spatial distribution of relative changes (SCEN 2070 - 2099 wrt. CTRL 1981 - 2010) in mean September to May snowfall (δS_{mean}) for RCP4.5 and for the 14 RCM simulations after applying the bias correction and fractionating the snowfall with the Binary method.

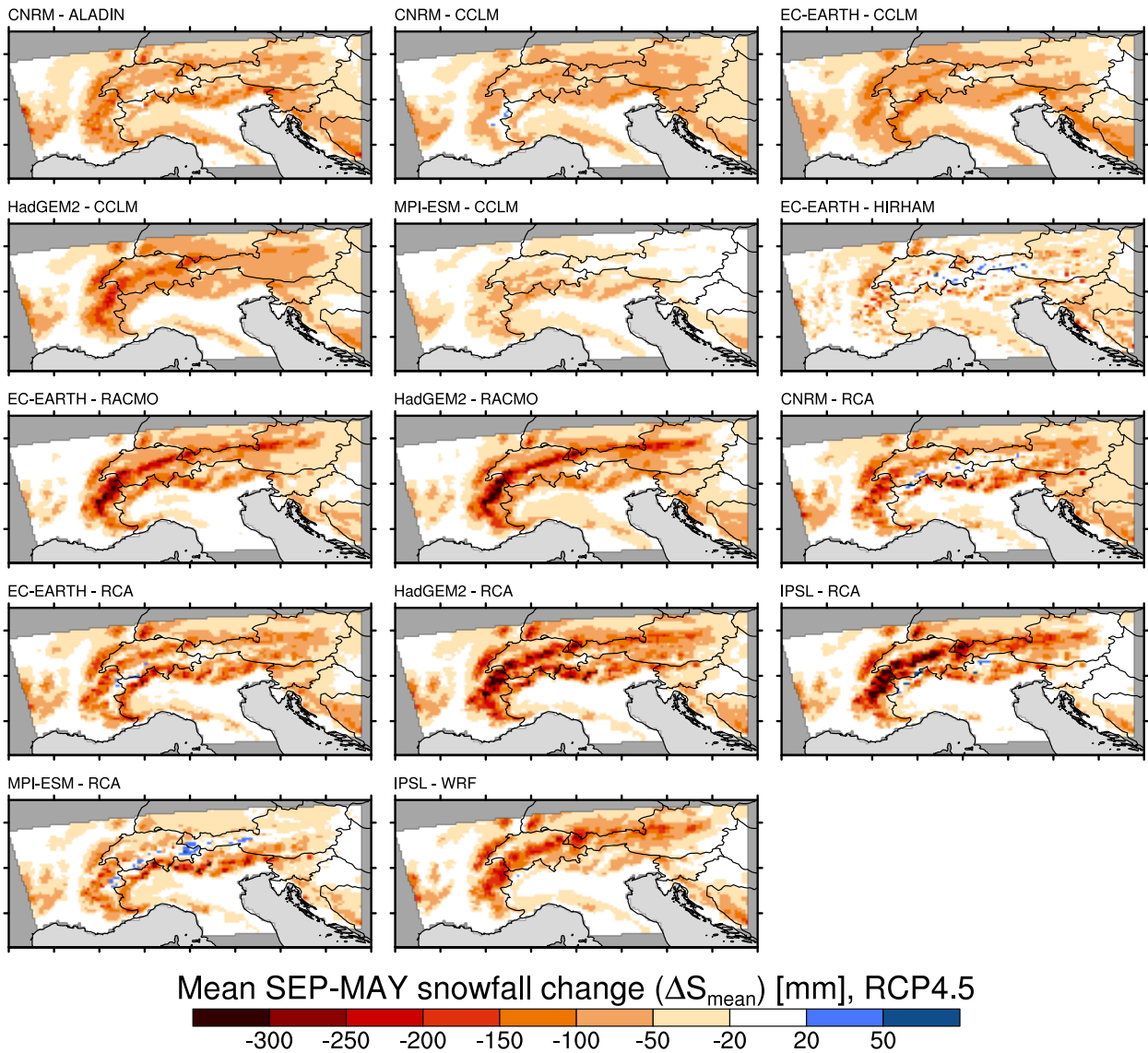


Fig. D.9: Spatial distribution of absolute changes (SCEN 2070 - 2099 wrt. CTRL 1981 - 2010) in mean September to May snowfall (ΔS_{mean}) for RCP4.5 and for the 14 RCM simulations after applying the bias correction and fractionating the snowfall with the Binary method.

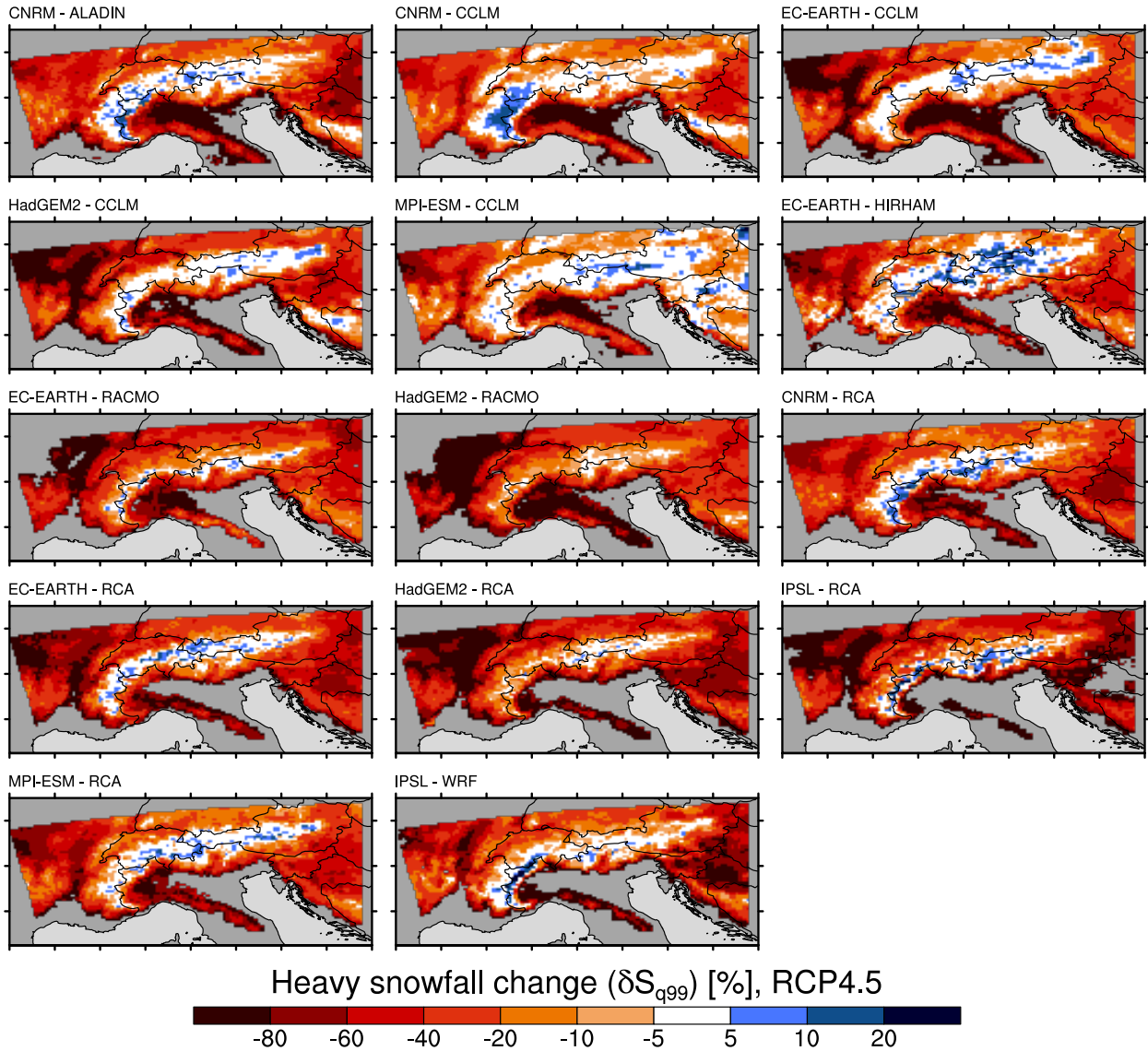


Fig. D.10: Spatial distribution of relative changes (September to May, SCEN 2070 - 2099 wrt. CTRL 1981 - 2010) in heavy snowfall (δS_{q99}) for RCP4.5 and for the 14 RCM simulations after applying the bias correction and fractionating the snowfall with the Binary method.

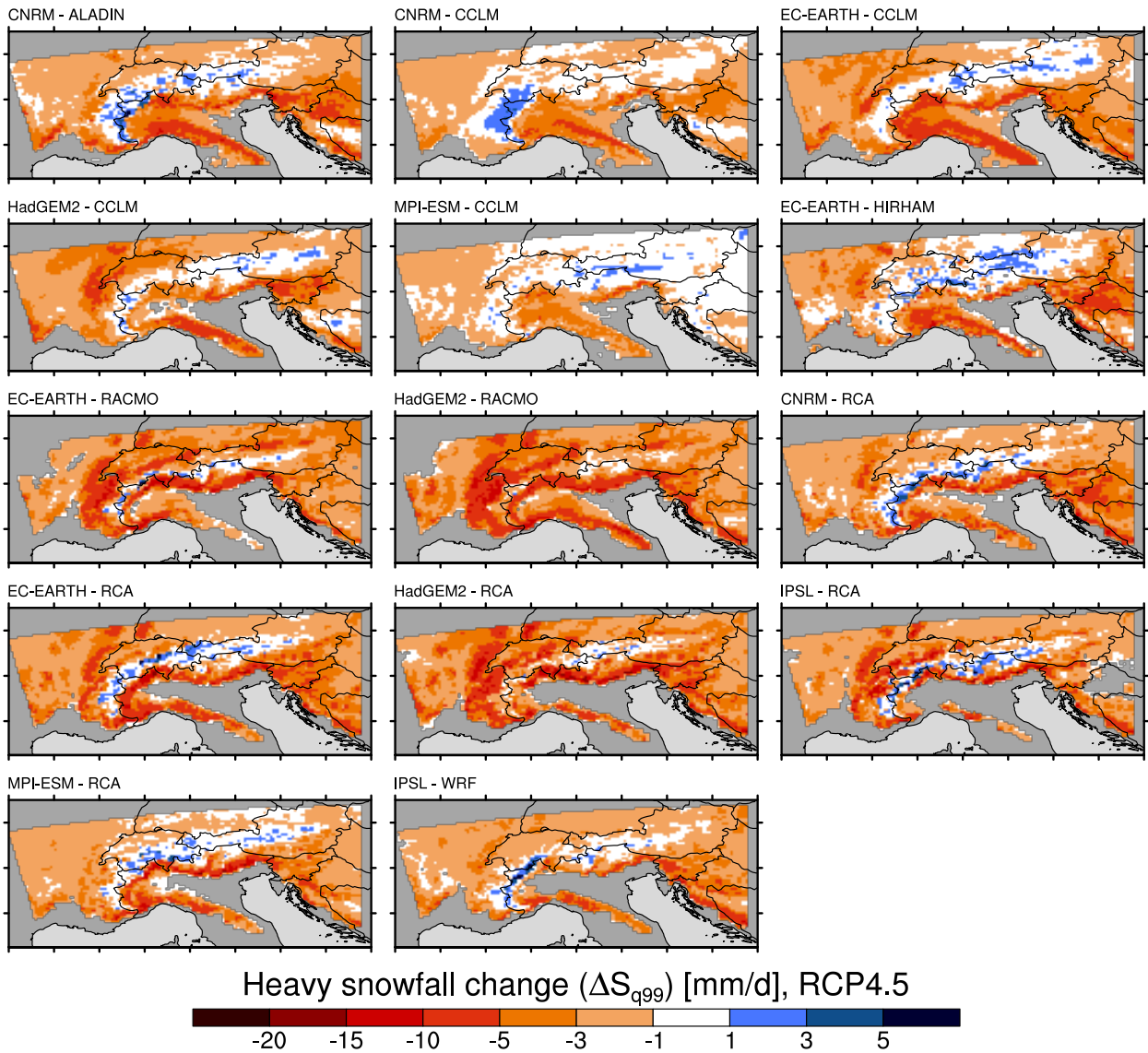


Fig. D.11: Spatial distribution of absolute changes (September to May, SCEN 2070 - 2099 wrt. CTRL 1981 - 2010) in heavy snowfall (ΔS_{q99}) for RCP4.5 and for the 14 RCM simulations after applying the bias correction and fractionating the snowfall with the Binary method.

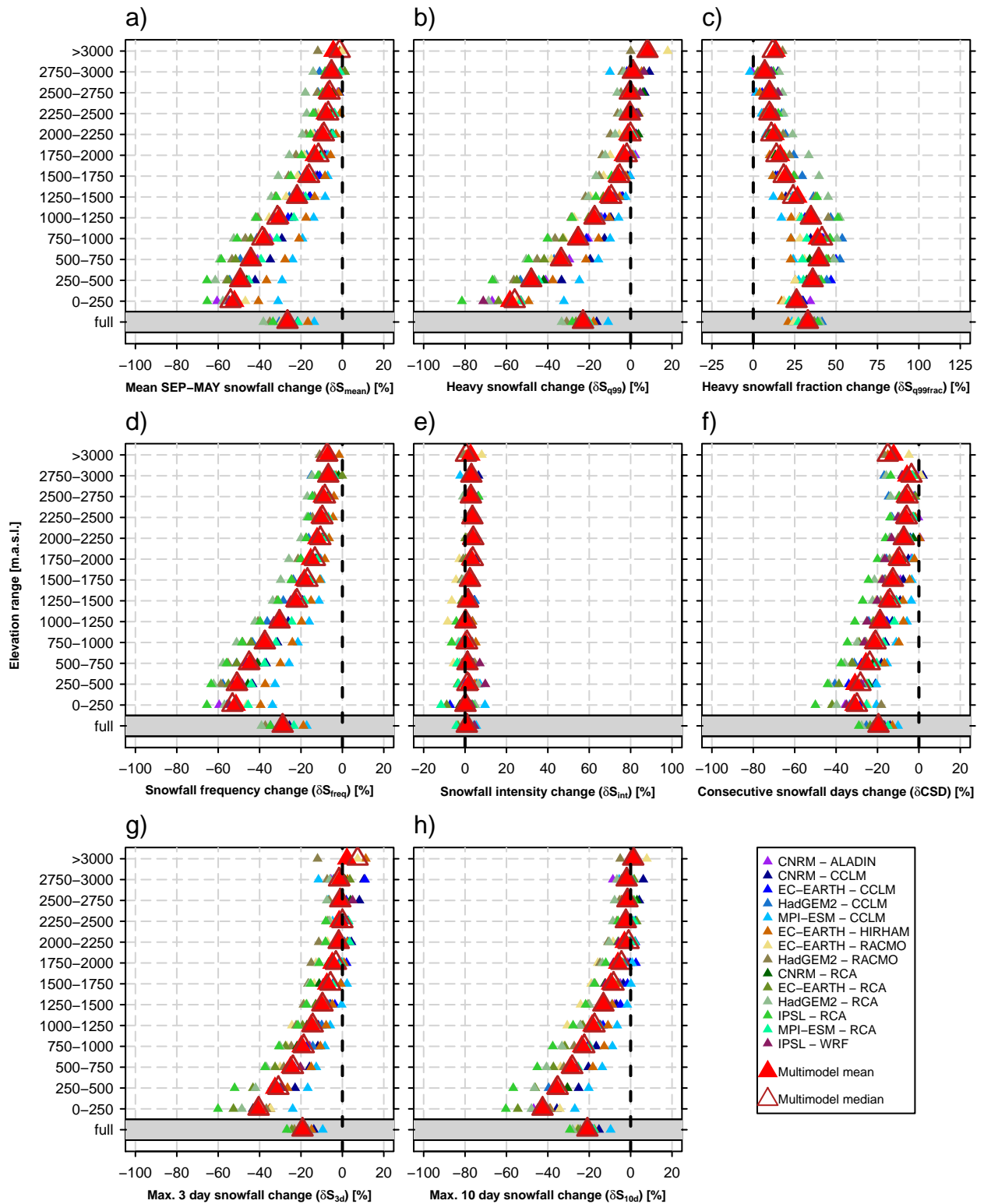


Fig. D.12: Relative changes (SCEN 2070 - 2099 wrt. CTRL 1981 - 2010) of seasonal (September to May) snowfall indices for RCP4.5 after applying the bias correction to the 14 RCM simulations and separating the snowfall with the Binary method. Small triangles show the individual RCM simulations whereas the large triangles denote the multimodel mean (red, filled) and multimodel median (brown, open).

D.4 Projections: Binary snow fractionation method, RCP8.5

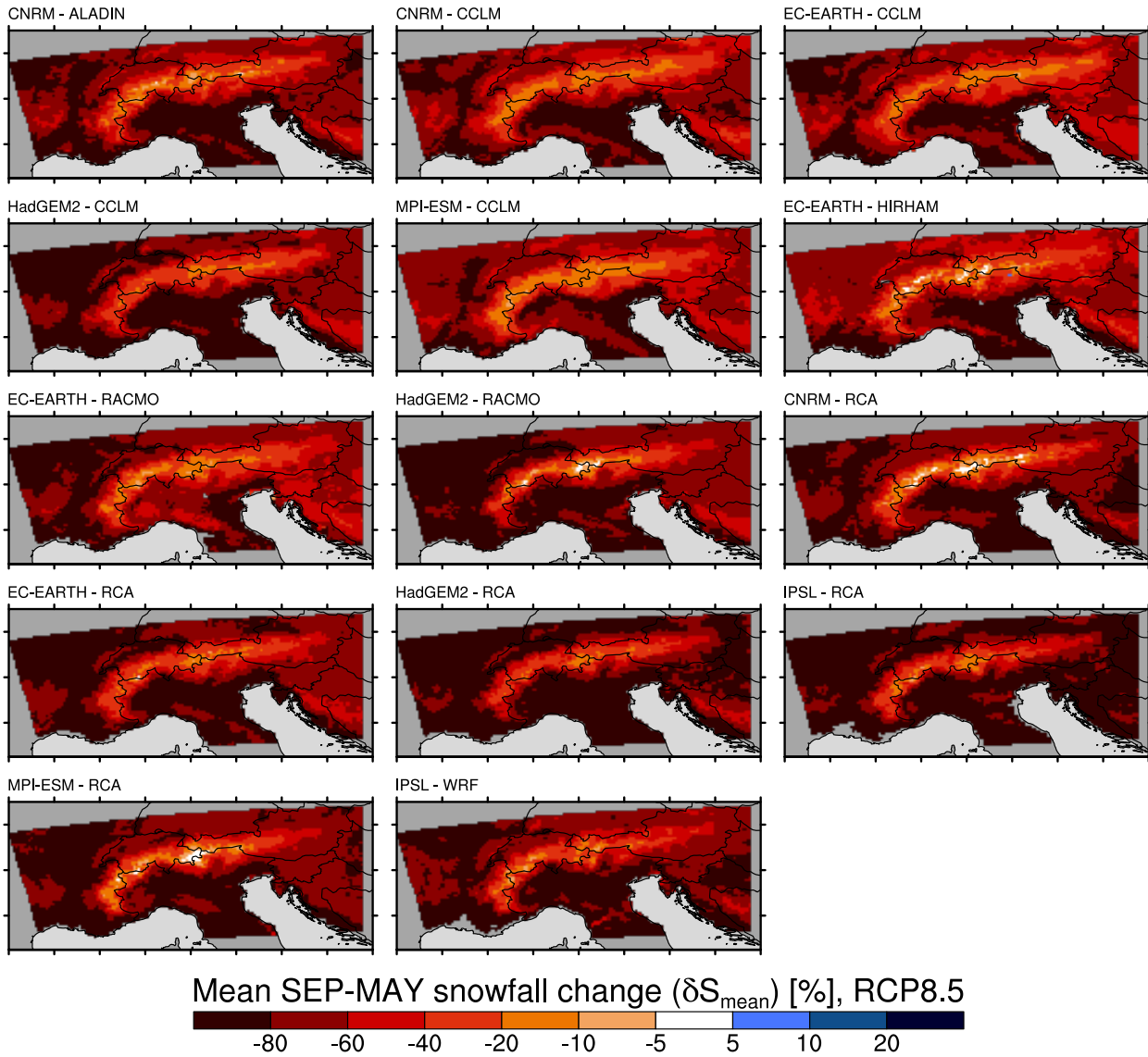


Fig. D.13: Spatial distribution of relative changes (SCEN 2070 - 2099 wrt. CTRL 1981 - 2010) in mean September to May snowfall (δS_{mean}) for RCP8.5 and for the 14 RCM simulations after applying the bias correction and fractionating the snowfall with the Binary method.

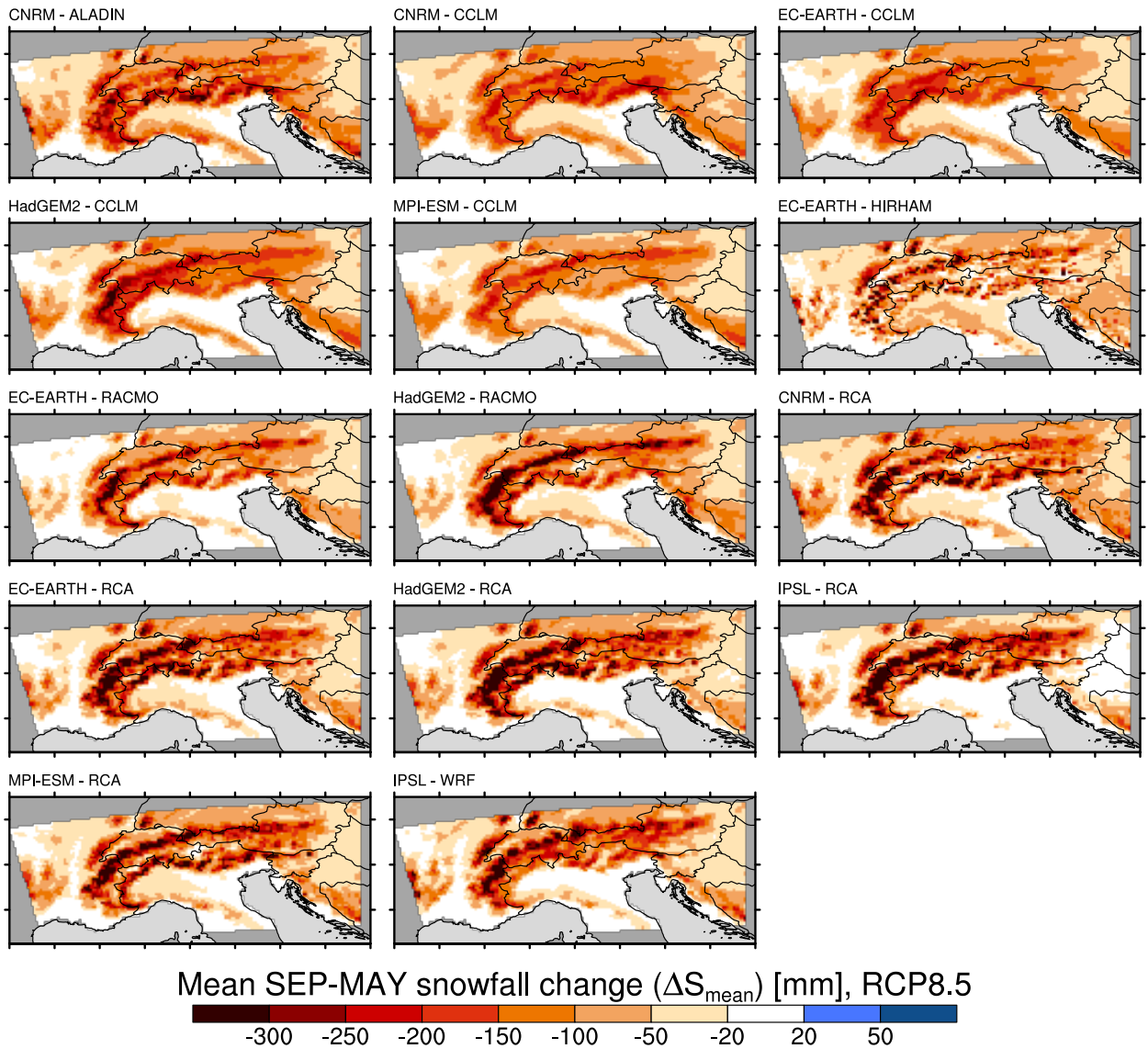


Fig. D.14: Spatial distribution of absolute changes (SCEN 2070 - 2099 wrt. CTRL 1981 - 2010) in mean September to May snowfall (δS_{mean}) for RCP8.5 and for the 14 RCM simulations after applying the bias correction and fractionating the snowfall with the Binary method.

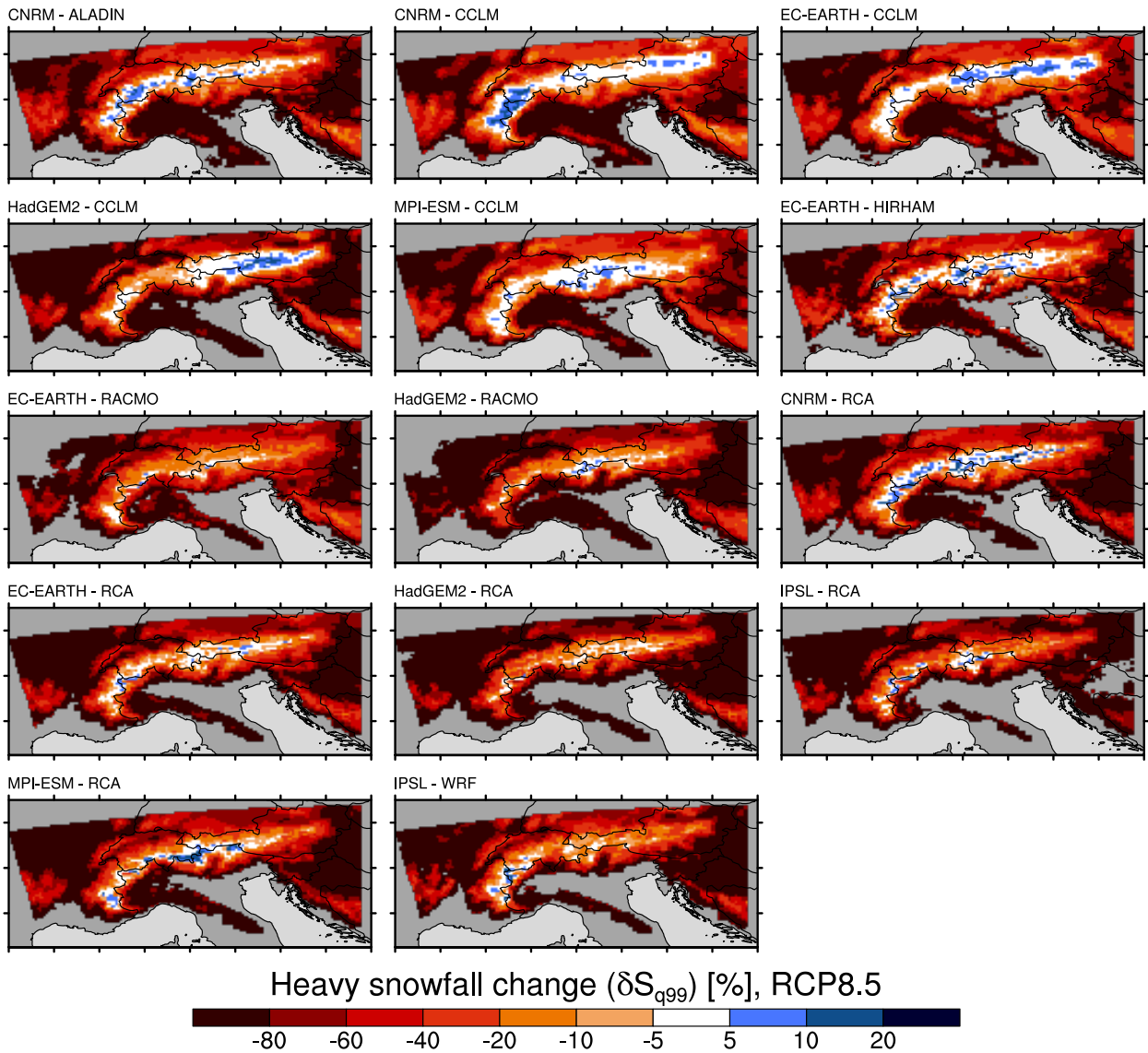


Fig. D.15: Spatial distribution of relative changes (September to May, SCEN 2070 - 2099 wrt. CTRL 1981 - 2010) in heavy snowfall (δS_{q99}) for RCP8.5 and for the 14 RCM simulations after applying the bias corrections and fractionating the snowfall with the Binary method.

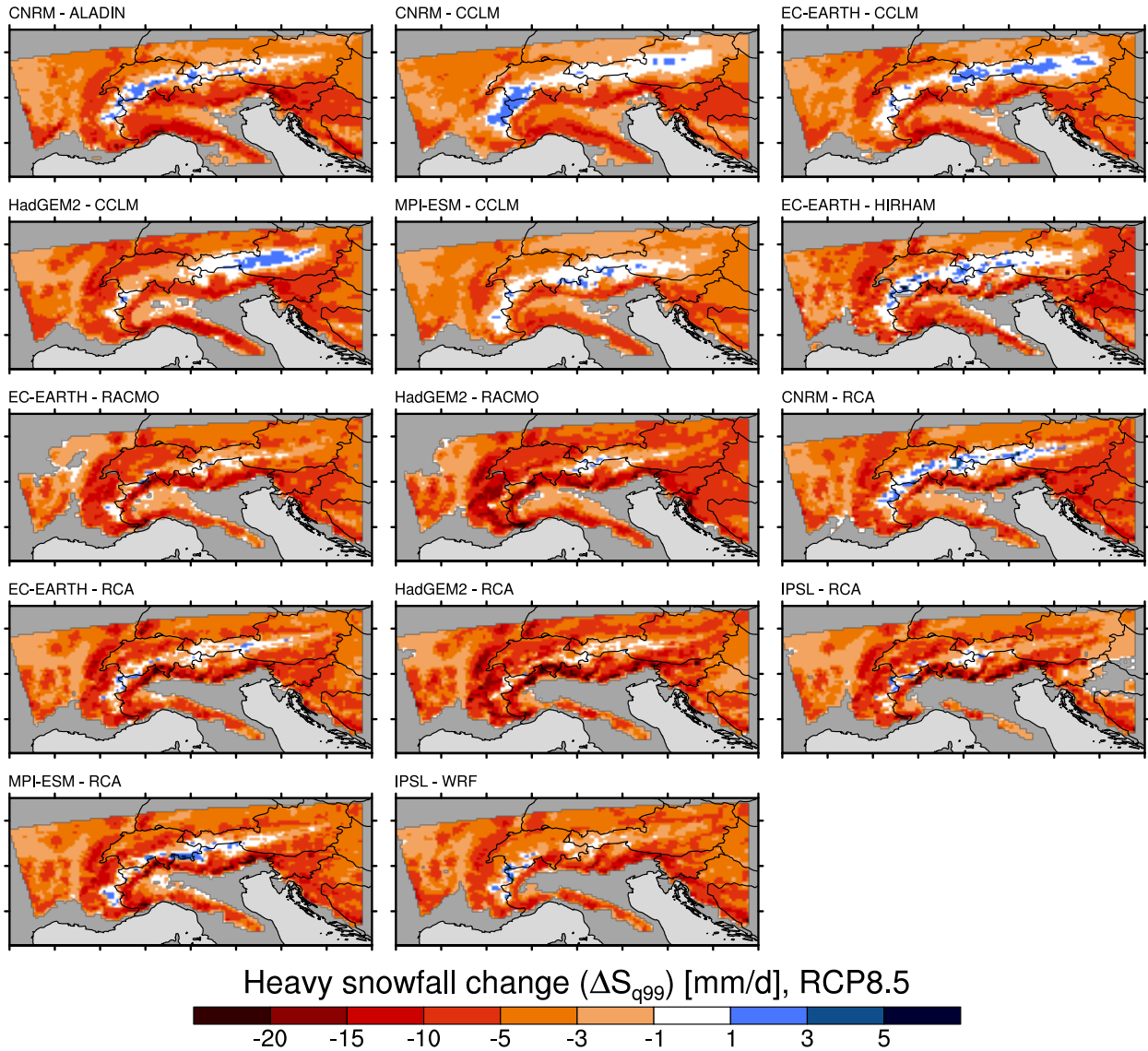


Fig. D.16: Spatial distribution of absolute changes (September to May, SCEN 2070 - 2099 wrt. CTRL 1981 - 2010) in heavy snowfall (δS_{q99}) for RCP8.5 and for the 14 RCM simulations after applying the bias correction and fractionating the snowfall with the Binary method.

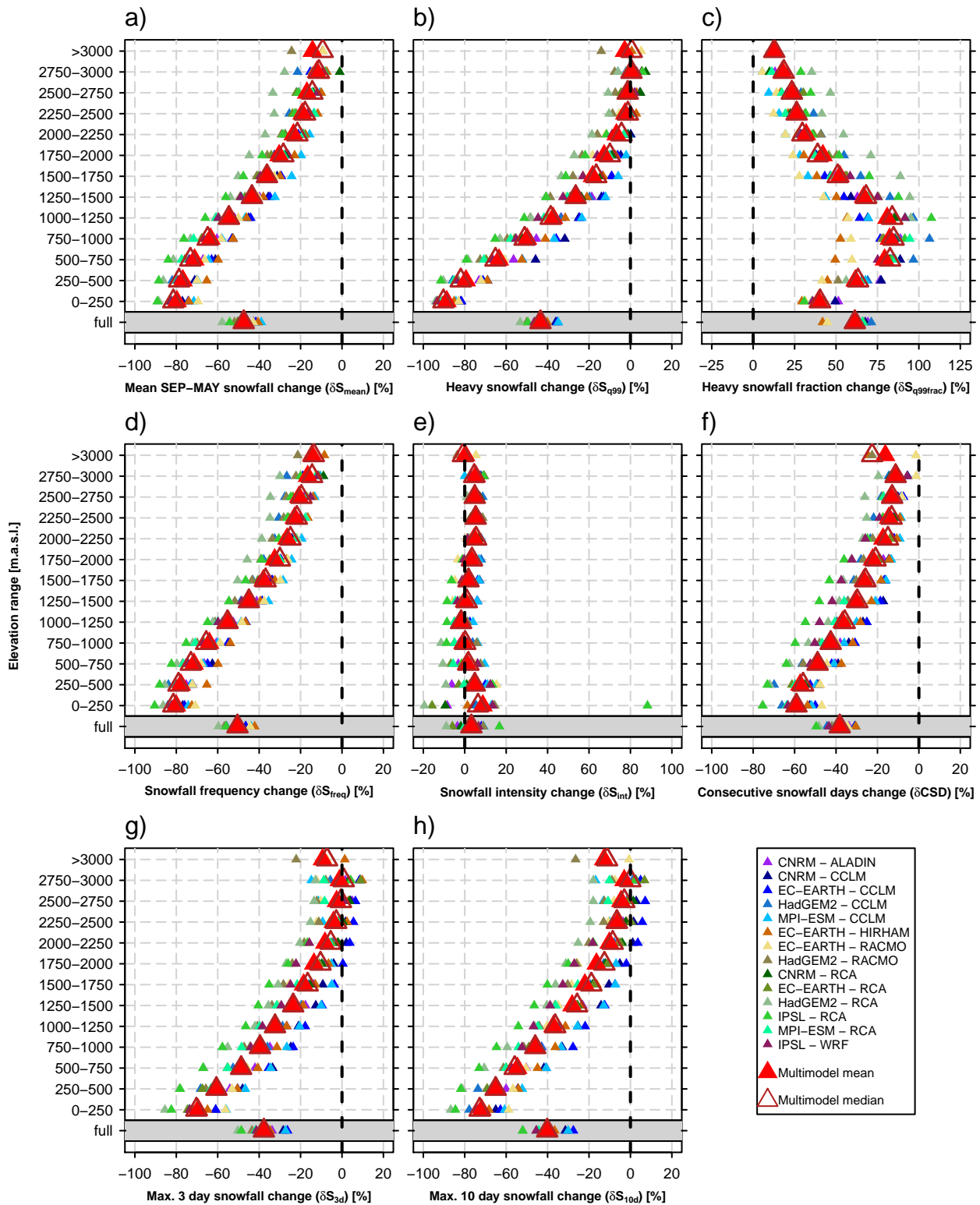


Fig. D.17: Relative changes (SCEN 2070 - 2099 wrt. CTRL 1981 - 2010) of seasonal (September to May) snowfall indices for RCP8.5 after applying the bias correction to the 14 RCM simulations and separating the snowfall with the Binary method. Small triangles show the individual RCM simulations whereas the large triangles denote the multimodel mean (red, filled) and multimodel median (brown, open).

D.5 Projections: Binary snow fractionation method - Comparison of RCP4.5 and RCP8.5

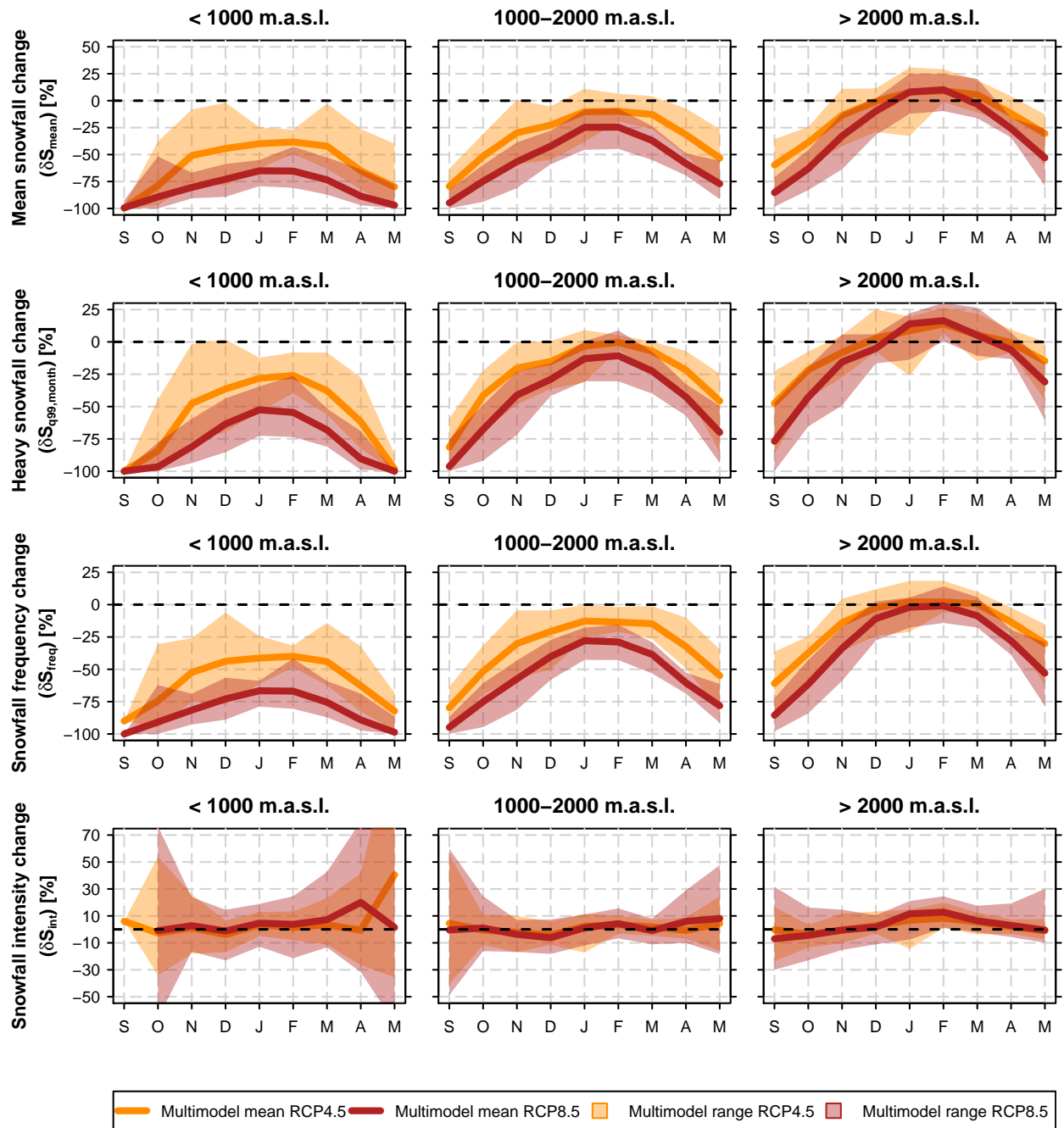


Fig. D.18: Relative changes (SCEN 2070 - 2099 wrt. CTRL 1981 - 2010) of monthly (September to May) snowfall indices for RCP4.5 (orange) and RCP8.5 (red) after applying the bias correction to the 14 RCM simulations and separating the snowfall with the Binary method. The lines show the seasonal cycle of the multimodel mean according to the respective RCP scenario. The shading represents the multimodel range. The columns represent the three elevations intervals below 1000 m.a.s.l., between 1000 m.a.s.l. and 2000 m.a.s.l. and above 2000 m.a.s.l.

E Additional information simulated raw snowfall

E.1 Raw snowfall: Comparison of separated + not bias corrected and simulated raw snowfall

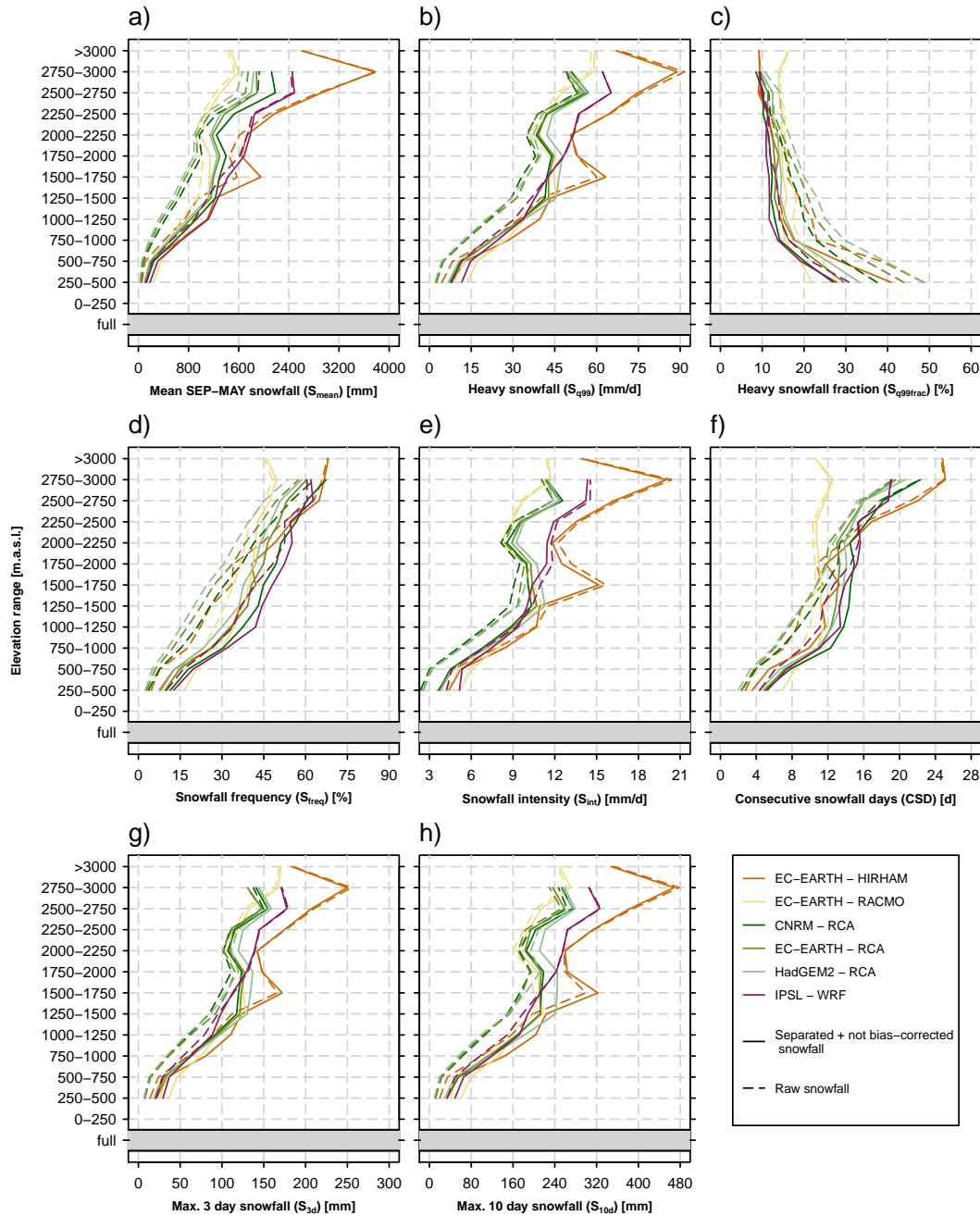


Fig. E.1: Seasonal (September to May) snowfall indices in the period 1971 - 2005 for a subset of six EURO-CORDEX simulations. Outputs of separated + not bias-corrected snowfall are denoted by solid lines (snow fractionation with Richards method at $T^* = 2^\circ\text{C}$). Results based on simulated raw snowfall outputs are represented by dashed lines. The analysis is constrained to the Swiss domain (see Sec. 2.3).



Eidgenössische Technische Hochschule Zürich
Swiss Federal Institute of Technology Zurich

Declaration of originality

The signed declaration of originality is a component of every semester paper, Bachelor's thesis, Master's thesis and any other degree paper undertaken during the course of studies, including the respective electronic versions.

Lecturers may also require a declaration of originality for other written papers compiled for their courses.

I hereby confirm that I am the sole author of the written work here enclosed and that I have compiled it in my own words. Parts excepted are corrections of form and content by the supervisor.

Title of work (in block letters):

SNOWFALL IN THE ALPS: EVALUATION AND PROJECTIONS BASED ON THE EURO-CORDEX REGIONAL CLIMATE MODELS

Authored by (in block letters):

For papers written by groups the names of all authors are required.

Name(s):

FREI

First name(s):

PRISCO

With my signature I confirm that

- I have committed none of the forms of plagiarism described in the 'Citation etiquette' information sheet.
- I have documented all methods, data and processes truthfully.
- I have not manipulated any data.
- I have mentioned all persons who were significant facilitators of the work.

I am aware that the work may be screened electronically for plagiarism.

Place, date

Aadorf, 2nd May 2016

Signature(s)

For papers written by groups the names of all authors are required. Their signatures collectively guarantee the entire content of the written paper.

